UNIVERSITÀ DEGLI STUDI DI PADOVA

Dipartimento di Fisica e Astronomia "Galileo Galilei"

Master Degree in Physics

Final Dissertation

Generalisations of the Sachdev-Ye-Kitaev model

Thesis supervisor

Prof. Luca Dell'Anna

Candidate

Michele Cappellesso

Academic Year 2022/2023

Contents

Introduction

In recent years, more precisely since 2016, a lot of research effort has been focused towards the study of the Sachdev-Ye-Kitaev (SYK) model. There are multiple reasons behind the sudden interest in a model that in practice appeared in the literature in 1993, but they can be summed up into three main properties (the meaning of which will become more clear later): the solvability at strong coupling, the saturation of the chaos bound, and the emergent conformal symmetry. All these properties are actually tied together by *quantum holography*, a tantalising theory that connects two areas of physics that were previously thought to be incompatible with each other: quantum field theory and general relativity. Although it is still at the conjecture level, holography has been proven to give new insights in many areas of physics, and it is one of the most promising paths into the mysterious world of quantum gravity. We will briefly address the holographic duality in chapter 4, but it is sufficient to know that it connects a conformal field theory with a large number of degrees of freedom in a flat space to another field theory in a curved space described by *classical* general relativity. The problem is that finding a holographic model which is simple enough to be solvable and that still maintains non-trivial properties is a very difficult task. For this reason, the SYK model was born as a "toy-model" of holography during A. Kitaev's research on the black hole information paradox. With the aim of studying holography in a thermal setting, he simplified the previous version developed by Sachdev and Ye in '93, keeping only necessary characteristics for the properties that we previously mentioned. The most interesting characteristic of the model is that its connection through black holes passes through *quantum chaos*, which is diagnosed by an exponential growth of the so-called "out-of-time-ordered correlators" (OTOCs for short). The exponent of such growth, the quantum analogue of the Lyapunov exponent, is subject to the upper bound $2\pi/\beta$, and the most notable objects that saturate this bound are black holes. In fact, the gravity dual of the SYK model at finite temperature contains a black hole in an anti-de Sitter space, and so this model constitutes a benchmark for studying black holes through holography.

Since its proposal in 2016, many generalisations of the model have been proposed, and later, despite its "abstractness", the first proposals for the experimental realisation started to appear. The main difficulty was the large number $\binom{N}{4} \sim N^4$ of interaction terms, which was relieved by introduction of a variant called "sparse SYK", that was first implemented experimentally on a quantum processor in November 2022 [22]. Furthermore, by creating two exact replicas of the system, it has been possible to measure a transfer of information between the two systems which corresponds, in the gravitational dual, to a passage through a wormhole. There is still much room for improvement on the experimental side, and many unanswered questions on the theoretical ones, but it is clear that this model has proved to be an interesting challenge for many physics areas.

The original model consists in a large number N of Majorana fermions with only one time dimension and zero spatial dimensions, and they all interact with each other through a quartic interaction, but the couplings that mediate this interaction are random variables following a zero-mean gaussian distribution. These couplings are to be considered as fixed for each realisation of the model (this is the so-called *quenched disorder*), which leads to technical difficulties, but it is also an essential characteristic of the model. The average over this disorder, in fact, together with the large N limit, leads to a particularly organised set of Feynman diagrams: the two-point function is composed by the sum of diagrams where one recursively inserts a melonic diagram in any propagator of the previous diagram, thus forming a sort of fractal structure. The analytic form of the Schwinger-Dyson equations

is then particularly simple, and they can be solved numerically at any temperature, but in the strong coupling limit they become even simpler, since they acquire a time-reparametrisation symmetry and they can be solved analytically. This equations can be derived with two different methods: either diagrammatically, by analising the structure of Feynman diagrams, or through dynamical mean field theory, where one approaches the quenched disorder with a replica trick. This last method produces an effective action of two bilocal fields, and in this action the role which is usually played by $\hbar$ is given instead by the parameter $1/N$. Therefore, in the limit of N going to infinity, one is allowed to consider only the solutions of the saddle-point equations of this bilocal action.

The aim of this thesis is to review the basic properties of this model (focusing on the field-theoretical side), in particular the the two-point and four-point functions, the emergent conformal symmetry, and the structure of the next-to-leading order corrections in the large-N limit expansion. We also review some of the most notable generalisations of the model, and introduce a new variation by considering small correlations in the probability distributions of the couplings. The results suggests that the properties of the model remains essentially the same for whatever generalisation one may introduce, provided that one preserves a few essential characteristics. These are the fermionic nature and large number of the degrees of freedom, their O(N) symmetry[1] (which becomes apparent after the average over the disorder), and the zero-average of the couplings.

Outline of the thesis

- In chapter 1 we review the basics of the model, starting from its definition and its relation to quantum disorder. we derive the Schwinger-Dyson equations with two different methods, the diagrammatic approach and dynamical mean-field theory. We discuss the limit of strong coupling, where the equations are solvable analytically, and the conformal symmetry. At the end of this chapter, for convenience, we introduce straightforward generalisation of the model to a q-body interaction.
- In chapter 2 we give a brief review of the fast scrambling phenomenon and its relation to out-of-time-ordered correlators.
- The discussion on the four-point function is presented separately in chapter 3 because of its bulkiness. We review the general procedure for the derivation in the conformal limit, where the function is divided in two contributions. The first one is a finite contribution made up from the sum of conformal blocks, which are related to the mass of the primary operators of the gravitational dual. The second one is divergent in the conformal limit, and one must consider a first-order deviation from it, which produces a parametrically large contribution.
- In chapter 4 we give a brief introduction to the concept of quantum holography, so that the reader is able to appreciate the connection between the SYK model and general relativity, which is the main reason why the model was developed in the first place. We only give a glimpse of the mathematical formalism, as to enter in its details would require a whole course, but it should be enough to understand the principles behind this duality and what its applications could be.
- In chapter 5 we discuss the diagrammatic structure of the next-to-leading order corrections, mainly by generalising the approach of reference [12]. The order in $1/N$ of the diagrams turns out to be governed by simple rules, but when going at higher orders the number of diagrams becomes large very fast.
- Chapter 6 generalises the probability distribution of the couplings, while keeping them uncorrelated between each other. It has been proved [19] that, as long as the average and variance of

[1] In some variations of the model the symmetry is a bit different: in the model with f flavours of fermions proposed by Gross and Rosenhaus [13] the symmetry is $O(N_1) \times \ldots, O(N_f)$; in the Gurau-Witten model, which, at leading order, reproduces the same properties of SYK, there is only one fixed coupling, but the fields are rank-three tensors and the full symmetry of the model is $O(N^6)$.

the couplings stays the same, the model remains the same at leading order in the large N limit. We show this explicitly by considering the case of a uniform distribution. We introduce small correlations in the couplings, and show that the model still retains its characteristics. Of course, if the correlations become too large, one should expect to obtain significantly different physics, since we would not have enough information to define its behaviour.

- Finally in chapter 7 we give a review of the sparse SYK model, showing that, with few requirements, it maintains the same chaotic behaviour as the original model but with a much smaller number of interactions.

Chapter 1

The model

The first proposal of the Sachdev-Ye-Kitaev model considered a quartic interaction, with hamiltonian of the form

$$H = \frac{1}{4!} \sum_{i,j,k,l=1}^{N} J_{ijkl}\, \chi_i \chi_j \chi_k \chi_l \tag{1.1}$$

where the $\chi_i = \chi_i(t)$, $i = 1, \ldots, N$, are Majorana fermions, which satisfy

$$\chi_i^\dagger = \chi_i\,, \qquad \{\chi_i, \chi_j\} = \delta_{ij} \tag{1.2}$$

and they are placed in a space with one time dimension and zero spatial dimensions (one can think of them as N fermionic sites with an infinite-ranged interaction). The couplings J_{ijkl} are identically distributed random variables which are totally antisymmetric in the indices $ijkl$ (since any symmetric part would give zero contribution to the hamiltonian due to the anticommutation of the fields), and we assume them to follow a gaussian distribution

$$P(J_{ijkl}) \propto \exp\left(-\frac{N^3 J_{ijkl}^2}{12\, J^2}\right)\,, \tag{1.3}$$

which leads to

$$\overline{J_{ijkl}} \equiv \int dJ_{ijkl} P(J_{ijkl}) = 0 \tag{1.4}$$

$$\overline{J_{ijkl}^2} = \frac{6!\, J^2}{N^3} \tag{1.5}$$

The numerical prefactor in (1.5) is a matter of convention, while the power of N in the denominator is crucial for the free energy to scale like N (as we will see later on, the leading order vacuum diagrams are proportional to N). The parameter J sets the energy scale of the interaction (while the fields χ_i are dimensionless). From the hamiltonian we can use coherent states path integral formalism to build the partition function [1] $\mathcal{Z} = \int D\chi_i\, \mathrm{e}^{-S[\chi_i]}$, with

$$S[\chi_i] = \int d\tau \left(\frac{1}{2}\sum_{i=1}^{N} \chi_i(\tau)\frac{d}{d\tau}\chi_i(\tau) + \frac{1}{4!}\sum_{i,j,k,l=1}^{N} J_{ijkl}\, \chi_i \chi_j \chi_k \chi_l\right) \tag{1.6}$$

where we notice the appearance of the usual kinetic term. Before proceeding with the discussion of the interacting case, notice that in the non-interacting case the hamiltonian is exactly zero, so the operators are constant even in the Heisenberg picture. The two-point function, then, follows

[1] We will mainly work in euclidean time, using a Wick rotation $\tau = it$ and set $\hbar = 1$.

immediately from the anticommutation rules (1.2) (which imply $\chi_i^2 = \frac{1}{2}$)[2]:

$$G_0(\tau)_{ij} \equiv -\langle T(\chi_i(\tau)\chi_j(0))\rangle = -\theta(\tau)\langle\chi_i\chi_j\rangle + \theta(-\tau)\langle\chi_j\chi_i\rangle = -\frac{1}{2}\,\mathrm{sgn}(\tau)\delta_{ij} \tag{1.7}$$

$$G_0(i\omega)_{ij} = \frac{1}{i\omega}\,\delta_{ij} \tag{1.8}$$

which is antisymmetric in τ, and it is also valid at finite-temperature for $\tau \in [-\frac{\beta}{2}, \frac{\beta}{2})$.

1.1 Quenched disorder

An important aspect of the SYK model is that it involves quenched disorder. This means that, when computing quantities, one should consider fixed realisations of the random couplings J_{ijkl}, so in principle each observable of the model should be a function of this couplings, so one could expect to obtain different results for each individual realisation. Thankfully, however, if these random parameters are identically distributed, many of the quantities (e.g. the free energy) of quenched-disordered many-body systems are *self-averaging*, which means that in the limit of large N they do not depend on the single realisation of this couplings:

$$\lim_{N\to\infty} F_N(\beta, \mathbf{J}) = F_\infty(\beta) \tag{1.9}$$

(for brevity we denote by $\mathbf{J}$ the set of all couplings, not to be confused with the energy scale J). Clearly, the average over the disorder of a quantity is equal to its $\mathbf{J}$-independent value:

$$F = -\lim_{N\to\infty}\frac{1}{\beta N}\overline{\log \mathcal{Z}(\mathbf{J})} = -\lim_{N\to\infty}\frac{1}{\beta N}\int D\mathbf{J}\,\log\int D\chi_i\, e^{-S[\chi_i,\mathbf{J}]} = F_\infty(\beta) \tag{1.10}$$

where we defined the measure $D\mathbf{J} = \prod_{i<j<k<l} dJ_{ijkl}P(J_{ijkl})$. This means that, when computing the free energy, we have to take the expectation value *after* taking the logarithm of the partition function, and this is in general complicated. It is much easier, instead, to compute the *annealed* free energy

$$F_{annealed} = -\lim_{N\to\infty}\frac{1}{\beta N}\log\int D\mathbf{J}\,D\chi_i\, e^{-S[\chi_i,\mathbf{J}]} \tag{1.11}$$

which contains a much simpler gaussian integral in the couplings. Here, the fields χ_i and the couplings J_{ijkl} are put on the same footing, which is appropriate if the two are varying with the same timescale (which is not our case, since we assumed the J_{ijkl} to be fixed). In general, these two types of free energy are not equivalent, but one can simplify the calculations in the quenched case by exploiting the *replica trick*, which is based on the identity $\overline{\log\mathcal{Z}} = \lim_{n\to 0}\frac{1}{n}\log\overline{\mathcal{Z}^n}$. To apply this method one has to consider n exact replicas of the system (with the same realisation of the couplings), and average over the disorder[3]:

$$\overline{\mathcal{Z}^n} = \int D\chi_i^1 \dots D\chi_i^n \overline{e^{-S(\chi_i^1)\cdots - S(\chi_i^n)}} \tag{1.12}$$

If the result is an explicit function of n, we just take the limit[4] $n \to 0$ and compute the observables with our new effective action. An alternative formulation of this method is, for any observable O,

$$\overline{\langle O\rangle} = \overline{\frac{1}{\mathcal{Z}}\int D\chi\, O(\chi)e^{-S(\chi)}} = \lim_{n\to 0}\overline{\mathcal{Z}^{n-1}\int D\chi\, O(\chi)e^{-S(\chi)}} = \lim_{n\to 0}\int D\chi^1\dots D\chi^n O(\chi^1)\overline{e^{-S(\chi^1)\cdots - S(\chi^n)}} \tag{1.13}$$

[2]Otherwise, one can (as usual) just Fourier-transform the free action together with a source term, from which we obtaining the Green's function in the frequency-space. In appendix A.1 we derive the free propagator in a more rigorous way, which requires N to be even.

[3]The superscript on the fields is the replica index and not an exponent.

[4]It may seem nonsensical to take this limit for an integer variable (after all, we are integrating on a number of variable proportional to n), and the mathematical subtleties behind this method, appear in the systems called "spin-glasses". There are cases, in fact, where the system exhibits replica symmetry breaking, which means that the systems has many ground states. In our case, however, we will not have to worry about this subtleties, at least for any reasonable temperature.

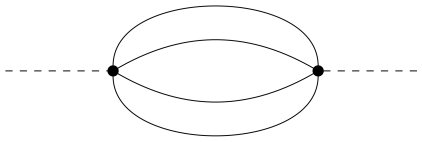

Figure 1.1: Diagram corresponding to the first order correction if one were to treat the couplings J_{ijkl} as a quantum field. The solid lines correspond to the propagator of the fermionic fields and the solid ones to the scalar ones.

and of course the result must be independent of the replica index. In practice, as mentioned in [20], since many of the quantities are self-averaging, the disorder-average can be seen as a way to perform the calculations analytically without having to consider the dependence on the individual realisations of the couplings. An alternative point of view on the annealed disorder [10], consists in considering the J_{ijkl} as a static scalar field with a two-point function equal to $\langle J_{ijkl}J_{ijkl}\rangle_{LO} = \frac{6!\,J^2}{N^3}$. This would produce additional quantum corrections, the first of which is represented in figure 1.1. We can see, however, that this contribution contains two scalar propagators, so it is suppressed by a factor of N^3, and at leading order in $1/N$ annealed and quenched disorder coincide.

1.2 The Schwinger-Dyson equations

There are two equivalent ways of deriving the Schwinger-Dyson equations for the SYK model: one follows a diagrammatic approach, while the other employs dynamical mean-field theory via the replica trick to produce an effective action of bilocal fields. In both cases the disorder average, the anti-commutation of the fermions, and the large N limit will contribute to produce equations that are simple enough to be solved numerically for general temperature and analytically in the low temperature/strong coupling limit $\beta J \gg 1$. We will then focus on this particular limit and study the properties of the solutions, in particular their conformal symmetry.

1.2.1 The diagrammatic approach

We start this approach by considering the high-temperature diagrammatic expansion. The Feynman rules in this case are given by:

- For each free propagator include $\frac{1}{2}\text{sgn}(\tau)$, or $-\frac{1}{i\omega}$ in Fourier-space.
- For each vertex include a factor of J_{ijkl}.
- Connect all vertices pairwise (there must be an even number) with a dashed line, and average the related couplings.
- Symmetry factors and integrations as usual.

The average over the couplings forces the fermion indices attached to each couple of vertices to be equal in pairs, and produces a factor of $\frac{3!J^2}{N^3}$ for each disorder-average. This also forces each correlator to contain an even number of fermionic fields, and the indices of this fields to be equal in pairs. When building Feynman diagrams for the two-point function, the only ones that survive in the large N limit are the ones made of so-called *melonic* diagrams (also called *sunset* diagrams), as the one in figure 1.2. We will prove this more rigorously in chapter 5, but one can see it intuitively by noticing that, if the disorder average line is "in parallel" with the maximum number of fermionic lines (in this case three), we have the maximum number of fermion indices that we can sum over. If not, the disorder average (which forces the indices attached to the vertices to be equal in pairs) would produce additional constraints on the indices, which would diminish the final power of N related to the diagram. For example, cross-diagrams (such as the one in figure 1.4) are instead suppressed in the large N limit by

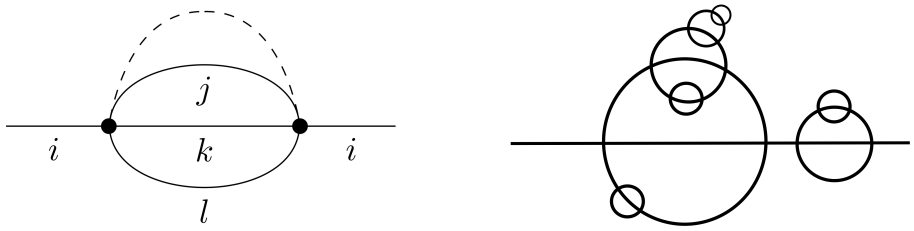

Figure 1.2: Melonic diagram (left) for the model with a quartic fermion interaction. This is the first high-temperature contribution to the two-point correlator $G(\tau,\tau') = \frac{1}{N}\sum_{i=1}^{N}\langle T\,\chi_i(\tau)\chi_i(\tau')\rangle$. On the right we have depicted (schematically) one of the leading-order in N contributions to the two point function, made by the composition of many melonic diagrams.

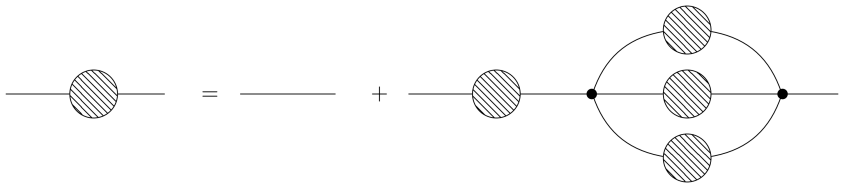

Figure 1.3: Diagrammatic representation of the Schwinger-Dyson equations. The bare line corresponds to the free propagator G_0, the "blob" corresponds to the self-energy Σ, so the bare line together with the blob form the full propagator G.

a factor of N^2. One can then insert such melonic diagram at every point of every propagator, since the factors of N^3 and $\frac{1}{N^3}$ will cancel, and, at leading order, the two-point function is independent of N.

The insertion of melonic diagrams can then be implemented recursively, and one obtains the following set of equations for the two-point function and the self-energy Σ (the first of which we wrote in Fourier space using a single frequency thanks to the time-translation invariance of the system):

$$G(i\omega)^{-1} = i\omega - \Sigma(i\omega) \tag{1.14}$$

$$\Sigma(\tau_1,\tau_2) = J^2\,G(\tau_1,\tau_2)^3 \tag{1.15}$$

They are represented diagrammatically by figure 1.3.

1.2.2 The mean field approach

In this section we derive the Schwinger-Dyson equations by implementing the replica trick that we mentioned in section 1.1 (a similar derivation for a generalisation of this model can be found in [13]). We start by considering M replicas of the same system and average the total partition function over

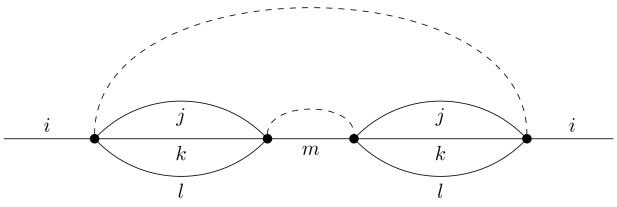

Figure 1.4: Example of cross diagram: the disorder average constrains the indices of the different melons and the diagram is of order $1/N^2$.

the disorder:

$$\begin{aligned}\overline{\mathcal{Z}^M} &= \int d\mathbf{J}\, P(\mathbf{J})\mathcal{Z}[\mathbf{J}]^M \\ &= \int D\chi_i d\mathbf{J} \exp\left[-\frac{N^3}{12J^2}\sum_{i,j,k,l} J_{ijkl}^2 - \sum_{\alpha=1}^{M}\int d\tau \left(\frac{1}{2}\sum_{i=1}^{N}\chi_i^\alpha \frac{d}{d\tau}\chi_i^\alpha + \frac{1}{4!}\sum_{i,j,k,l} J_{ijkl}\chi_i^\alpha\chi_j^\alpha\chi_k^\alpha\chi_l^\alpha\right)\right] \\ &= \int D\chi_i \exp\left[-\frac{1}{2}\sum_{\alpha=1}^{M}\sum_{i=1}^{N}\chi_i^\alpha\frac{d}{d\tau}\chi_i^\alpha + \frac{J^2}{8N^3}\sum_{i,j,k,l}\left(\sum_{\alpha=1}^{M}\int d\tau\, \chi_i^\alpha\chi_j^\alpha\chi_k^\alpha\chi_l^\alpha\right)^2\right] \\ &= \int D\chi_i \exp\left[-\frac{1}{2}\sum_{\alpha=1}^{M}\sum_{i=1}^{N}\int d\tau\chi_i^\alpha\frac{d}{d\tau}\chi_i^\alpha + \frac{NJ^2}{8}\int d\tau_1 d\tau_2 \sum_{\alpha,\beta}\left(\frac{1}{N}\sum_{i=1}^{N}\chi_i^\alpha(\tau_1)\chi_i^\beta(\tau_2)\right)^4\right]\end{aligned} \tag{1.16}$$

where α, β are the replica indices. We now introduce the collective field

$$\tilde{G}^{\alpha\beta}(\tau_1,\tau_2) = \frac{1}{N}\sum_{i=1}^{N}\chi_i^\alpha(\tau_1)\chi_i^\beta(\tau_2) \tag{1.17}$$

by inserting a delta function

$$\begin{aligned}&\delta\left(\tilde{G}^{\alpha\beta}(\tau_1,\tau_2) - \frac{1}{N}\sum_{i=1}^{N}\chi_i^\alpha(\tau_1)\chi_i^\beta(\tau_2)\right) \propto \\ &\propto \int D\tilde{\Sigma}^{\alpha\beta}(\tau_1,\tau_2)\exp\left[-\frac{N}{2}\tilde{\Sigma}^{\alpha\beta}(\tau_1,\tau_2)\left(\tilde{G}^{\alpha\beta}(\tau_1,\tau_2) - \frac{1}{N}\sum_{i=1}^{N}\chi_i^\alpha(\tau_1)\chi_i^\beta(\tau_2)\right)\right]\end{aligned} \tag{1.18}$$

We use the tildes to distinguish these fields from the respective solutions of the saddle-point equations, which coincide with the two-point correlator and the self-energy in the large N limit. The total partition function then becomes

$$\begin{aligned}\overline{\mathcal{Z}^M} = \int D\chi_i D\tilde{G}^{\alpha\beta}D\tilde{\Sigma}^{\alpha\beta}\exp\Bigg[&-\frac{1}{2}\sum_{\alpha,\beta}\sum_{i=1}^{N}\int d\tau_1 d\tau_2\, \chi_i^\alpha(\tau_1)\left(\delta_{\alpha\beta}\delta(\tau_{12})\frac{d}{d\tau_2} - \tilde{\Sigma}^{\alpha\beta}(\tau_1,\tau_2)\right)\chi_i^\beta(\tau_2) \\ &- \frac{N}{2}\sum_{\alpha,\beta}\int d\tau_1 d\tau_2\, \left(\tilde{\Sigma}^{\alpha\beta}(\tau_1,\tau_2)\tilde{G}^{\alpha\beta}(\tau_1,\tau_2) - \frac{J^2}{4}\tilde{G}^{\alpha\beta}(\tau_1,\tau_2)^4\right)\Bigg]\end{aligned} \tag{1.19}$$

(we denote for brevity $\tau_{ij} \equiv \tau_i - \tau_j$, and we will use this notation also in the remainder of this work). We assume a replica-diagonal saddle point[5],

$$\tilde{G}^{\alpha\beta} = \tilde{G}\,\delta_{\alpha\beta} \qquad \tilde{\Sigma}^{\alpha\beta} = \tilde{\Sigma}\,\delta_{\alpha\beta} \tag{1.20}$$

and integrate over the fermionic degrees of freedom, so that we are left with an effective action of these bilocal fields

$$\begin{aligned}\overline{\mathcal{Z}^M} &= \int D\tilde{G}D\tilde{\Sigma}\exp[-MS_{eff,rep}] \\ S_{eff,rep} &\equiv -\frac{N}{2}\log\det\left(\partial_\tau - \tilde{\Sigma}\right) + \frac{N}{2}\int d\tau_1 d\tau_2\, \left(\tilde{\Sigma}(\tau_1,\tau_2)\tilde{G}(\tau_1,\tau_2) - \frac{J^2}{4}\tilde{G}(\tau_1,\tau_2)^4\right)\end{aligned} \tag{1.21}$$

Having isolated the replica-dependence, we can now take the limit $M \to 0$ and obtain the partition function for the bilocal fields:

$$\begin{aligned}\overline{\mathcal{Z}} &= \int D\tilde{G}D\tilde{\Sigma}\exp[-S_{eff}] \\ \frac{S_{eff}}{N} &\equiv -\frac{1}{2}\operatorname{tr}\log\left(\partial_\tau - \tilde{\Sigma}\right) + \frac{1}{2}\int d\tau_1 d\tau_2\, \left(\tilde{\Sigma}(\tau_1,\tau_2)\tilde{G}(\tau_1,\tau_2) - \frac{J^2}{4}\tilde{G}(\tau_1,\tau_2)^4\right)\end{aligned} \tag{1.22}$$

[5] In appendix A.2 we argue why replica non-diagonal contribution are subleading in the large N limit

In the limit of $N \to \infty$ the action is dominated by the saddle point. To derive the saddle point equations we take the variation of the action with respect to $\tilde{\Sigma}$ and $\tilde{G}$. The variation of $\tilde{\Sigma}$ gives

$$\begin{aligned}\delta_{\tilde{\Sigma}} S_{eff} &= -\frac{1}{2}\,\mathrm{tr}\left[(\underbrace{\partial_\tau}_{G_0^{-1}} - \tilde{\Sigma})^{-1}\delta\tilde{\Sigma}\right] + \frac{1}{2}\int d\tau_1 d\tau_2\, \tilde{G}(\tau_1,\tau_2)\,\delta\tilde{\Sigma}(\tau_1,\tau_2) \\ &= \frac{1}{2}\int d\tau_1 d\tau_2 \left((G_0^{-1}(\tau_1,\tau_2) - \tilde{\Sigma}(\tau_1,\tau_2))^{-1}\delta\tilde{\Sigma}(\tau_2,\tau_1) - \tilde{G}(\tau_1,\tau_2)\,\delta\tilde{\Sigma}(\tau_1,\tau_2)\right) \\ &= \frac{1}{2}\int d\tau_1 d\tau_2 \left(-(G_0^{-1}(\tau_1,\tau_2) - \tilde{\Sigma}(\tau_1,\tau_2))^{-1} - \tilde{G}(\tau_1,\tau_2)\right)\delta\tilde{\Sigma}(\tau_1,\tau_2)\end{aligned} \tag{1.23}$$

where in the last line we have used the antisymmetry $\tilde{\Sigma}(\tau_1,\tau_2) = -\tilde{\Sigma}(\tau_2,\tau_1)$. Using the translational invariance of the system to write $\tilde{\Sigma}(\tau_1,\tau_2) = \tilde{\Sigma}(\tau_1-\tau_2) \equiv \tilde{\Sigma}(\tau)$ and going to Fourier space we obtain the saddle-point equation

$$i\omega - \tilde{\Sigma}(\omega) = \tilde{G}(\omega)^{-1}\,. \tag{1.24}$$

Taking the variation with respect to $\tilde{G}$, instead, we obtain

$$\delta_{\tilde{G}} S_{eff} = \frac{1}{2}\int d\tau_1 d\tau_2 \left(\tilde{\Sigma}(\tau_1,\tau_2) - J^2\tilde{G}(\tau_1,\tau_2)^3\right)\delta\tilde{G}(\tau_1,\tau_2) \tag{1.25}$$

which gives

$$\tilde{\Sigma}(\tau) = J^2\tilde{G}(\tau)^3\,. \tag{1.26}$$

These are exactly the Schwinger-Dyson equations that we obtained through the diagrammatic approach. Notice, also, that in the action (1.22) the role usually played by $\hbar$ is substituted by the parameter $1/N$. This is a common characteristic of large N models, where the large number of degrees of freedom allows one to rearrange the diagrammatic expansion in a different way: we were able to sum diagrams with an infinite number of loops, but we kept only those who survived in the limit of $N \to \infty$.

1.2.3 Solutions at strong coupling

In the low energy limit one can drop the first term in the r.h.s of equation (1.14) and the equations can be solved analytically, since one obtains

$$\int dt\, G(t_1,t)\Sigma(t,t_2) = -\delta(t_1-t_2) \tag{1.27}$$

$$\Sigma(t_1,t_2) = J^2 G(t_1,t_2)^3 \tag{1.28}$$

which can be put together to form

$$J^2\int \mathrm{d}t\, G(t_1,t)G(t,t_2)^3 = -\delta(t_1-t_2) \tag{1.29}$$

This equation is solved by

$$G(t) = -\left(\frac{1}{4\pi J^2}\right)^{1/4}\frac{\mathrm{sgn}(t)}{\sqrt{|t|}} \tag{1.30}$$

where we used time-translation invariance to write $G(t,0) \equiv G(t)$. We can check this ansatz by substituting it in the l.h.s of (1.29). After relabelling for convenience $t_1 - t \to t$ and $t_1 - t_2 \equiv t_{12}$, we get

$$I \equiv \frac{1}{4\pi}\int_{-\infty}^{\infty}\mathrm{d}t\,\frac{\mathrm{sgn}(t)}{\sqrt{|t|}}\frac{\mathrm{sgn}(t_{12}-t)}{\sqrt{|t_{12}-t|^3}} \overset{!}{=} 0 \tag{1.31}$$

Using the Fourier transforms

$$\int \frac{\mathrm{d}t}{\sqrt{2\pi}} \frac{\mathrm{sgn}(t)}{\sqrt{|t|}} e^{i\omega t} = i\frac{\mathrm{sgn}(\omega)}{\sqrt{|\omega|}} \tag{1.32}$$

$$\int \frac{\mathrm{d}t}{\sqrt{2\pi}} \frac{\mathrm{sgn}(t)}{\sqrt{|t|^3}} e^{i\omega t} = 2i\,\mathrm{sgn}(\omega)\sqrt{|\omega|} \tag{1.33}$$

and substituting in I, we obtain:

$$\begin{aligned} I &= \int \frac{\mathrm{d}t}{4\pi} \int \frac{\mathrm{d}\omega}{\sqrt{2\pi}} \int \frac{\mathrm{d}\omega'}{\sqrt{2\pi}} \left(i\frac{\mathrm{sgn}(\omega)}{\sqrt{|\omega|}} \right) \left(2i\,\mathrm{sgn}(\omega')\sqrt{|\omega'|} \right) e^{-i\omega t} e^{-i\omega'(t_{12}-t)} \\ &= -\frac{1}{(2\pi)} \int \mathrm{d}\omega \int \mathrm{d}\omega'\, e^{-i\omega t_{12}} \left(\frac{\mathrm{sgn}(\omega)}{\sqrt{|\omega|}} \right) \left(\mathrm{sgn}(\omega')\sqrt{|\omega'|} \right) \underbrace{\int \frac{\mathrm{d}t}{2\pi} e^{-it(\omega-\omega')}}_{\delta(\omega-\omega')} \\ &= -\int \frac{\mathrm{d}\omega}{2\pi}\, e^{-i\omega t_{12}} = -\delta(t_{12}) \end{aligned} \tag{1.34}$$

as we wanted. We see then from (1.30) that in the infrared the fields acquire an anomalous dimension $\Delta = 1/4$.

1.3 The reparametrisation symmetry

In the low energy limit the S.D. equations become:

$$J^2 \int \mathrm{d}t\, G(t_1,t)\Sigma(t,t_2) = -\delta(t_1-t_2) \tag{1.35}$$

$$\Sigma(t_1,t_2) = J^2\, G(t_1,t_2)^3 \tag{1.36}$$

In this form they are invariant under time representations $t \to f(t)$ ($f(t)$ must preserve time-orientation) provided that

$$\begin{aligned} G(t_1,t_2) &\to [f'(t_1)f'(t_2)]^{1/4} G(f(t_1),f(t_2)) \\ \Sigma(t_1,t_2) &\to [f'(t_1)f'(t_2)]^{3/4} \Sigma(f(t_1),f(t_2)) \end{aligned} \tag{1.37}$$

In fact, if we consider equation (1.35) on variables $\sigma_i = f(t_i)$, by applying this transformation we get

$$\begin{aligned} &J^2 \int \mathrm{d}\sigma\, G(\sigma_1,\sigma)\Sigma(\sigma,\sigma_2) = -\delta(\sigma_1-\sigma_2) \\ &J^2 \int \mathrm{d}t |f'(t)|\, \frac{G(t_1,t)}{[f'(t_1)f'(t)]^{1/4}} \frac{\Sigma(t,t_2)}{[f'(t)f'(t_2)]^{3/4}} = -\frac{\delta(t_1-t_2)}{|f'(t_1)|} \\ &J^2 \int \mathrm{d}t\, G(t_1,t)\Sigma(t,t_2) = -\delta(t_1-t_2) \end{aligned} \tag{1.38}$$

where the powers of $f'(t_1)$ and $f'(t_2)$ cancel against the r.h.s thanks to the delta function (and the modulus can be removed because f must be monotonically increasing). We can exploit this transformation property to pass from the zero temperature Green's function to the finite temperature one by using a circular map $t \to f(t) = \mathrm{e}^{2\pi i t/\beta}$ (or alternatively $\tan\left(\frac{\pi t}{\beta}\right)$), where β is the inverse of the temperature. In this case, by applying (1.37), we get

$$\frac{1}{\sqrt{t_1-t_2}} \to \sqrt{\frac{2\pi i}{\beta}} \frac{1}{\sqrt{\mathrm{e}^{2\pi i t_1/\beta} - \mathrm{e}^{2\pi i t_2/\beta}}} \tag{1.39}$$

Without loss of generality we can define the time interval $t = t_1 - t_2$, defining $t_1 = t/2$ and $t_2 = -t/2$ so that

$$\sqrt{\frac{1}{t}} \to \sqrt{\frac{\pi}{\beta}} \frac{1}{\sqrt{\sin(\pi t/\beta)}} \tag{1.40}$$

We can then Wick-rotate back to real time, $t = -it_r$, thus obtaining the finite temperature Green's function

$$G_{T>0}(t_r) = -\frac{\pi^{1/4}}{\sqrt{2\beta J}} \frac{1}{\sqrt{\sinh(\pi t_r/\beta)}} \tag{1.41}$$

We also mention that in the literature there is an ambiguity in the name of the symmetry (1.37), which is sometimes referred as "conformal" symmetry, whereas sometimes the term "conformal" only refers to the symmetry group SL(2,R). This is because the term conformal group is by definition [1] "the subgroup of coordinate transformations that leave the metric invariant up to a scale change"

$$x_\mu \to x'_\mu \quad \text{s.t} \quad g'_{\mu\nu}(x') = \Lambda(x) g_{\mu\nu}(x) \ , \tag{1.42}$$

in other words all the coordinate transformations that preserve the angles. In $d \leq 2$ dimensions these coincide with the set of differentiable transformations, which have an infinite dimensional local Lie algebra described by the generators

$$\begin{aligned} L_n &= -t^{n+1}\partial_t \, , \quad n \in \mathbb{Z} \\ [L_m, L_n] &= (m-n) L_{m+n} \end{aligned} \tag{1.43}$$

The transformations generated by this group, however, are not globally well-defined, since $t^{n+1}\partial_t$ is divergent for $t \to 0$ unless we require $n \geq -1$. After the change of variable $t = -1/w$, the same generators become $\left(-\frac{1}{w}\right)^{n+1} \left(\frac{dz}{dw}\right)^{-1} \partial_w = \left(-\frac{1}{w}\right)^{n-1} \partial_w$, which is well-defined only for $n \leq 1$. Only the subgroup generated by L_{-1}, L_0, L_{+1} is then defined globally (including infinity), and this are precisely the generator of the algebra SL(2,R). The term "conformal algebra", then, usually refers only to this subgroup.

1.4 q-body interaction

Everything done so far can be easily generalised to the case of a q-body interaction (sometimes called SYK_q), where q is an even number [6]. Here we will focus on the case $q \geq 4$, since the case $q = 2$ is significantly different, though it can be completely solved by using random matrix theory [9] [13]. The hamiltonian is now

$$H = \frac{i^{\frac{q}{2}}}{q!} \sum_{i_1,\dots,i_q=1}^{N} J_{i_1 \dots i_q} \chi_{i_1} \cdots \chi_{i_q} \tag{1.44}$$

with a disorder average of

$$\overline{J_{i_1 \dots i_q}} = 0 \tag{1.45}$$

$$\overline{J^2_{i_1 \dots i_q}} = \frac{(q-1)!\, J^2}{N^{q-1}} \tag{1.46}$$

The two-point function is now made by melonic diagrams with $q-1$ fermionic lines in parallel with the disorder average. The self energy is simply given by $\Sigma(t_1, t_2) = J^2\, G(t_1, t_2)^{q-1}$, and the solution of the S.D equation can be found with a similar ansatz as the previous one:

$$G(t) = \frac{b}{|t|^{2\Delta}} \text{sgn}(t) \ , \qquad \Delta \equiv \frac{1}{q} \tag{1.47}$$

[6] So that the hamiltonian is a bosonic operator.

To find the value of b it is convenient to go to Fourier space as before, using

$$\int_{-\infty}^{+\infty} \mathrm{d}t\, \mathrm{e}^{i\omega t} \frac{\mathrm{sgn}(t)}{|t|^{2\Delta}} = i\, 2^{1-2\Delta}\sqrt{\pi}\frac{\Gamma(1-\Delta)}{\frac{1}{2}+\Delta}|\omega|^{2\Delta-1}\mathrm{sgn}(\omega) \tag{1.48}$$

and we obtain

$$J^2 b^q \pi = \left(\frac{1}{2} - \Delta\right)\tan(\pi\Delta) \tag{1.49}$$

As a side note, one could also consider a model that contains an interaction term for each q, but no interesting application of this has been found [9].

Chapter 2

Fast scrambling and OTOCs

Before looking at the computation of the four-point function, we discuss in this chapter the connection between the SYK model and chaos.

2.1 From classical to quantum chaos

Let's start by recalling classical chaos, which does not have a universal definition, but it is usually characterised by the sensitivity to the initial conditions (sometimes called "butterfly effect"). Consider a vector $\mathbf{X}$ in an N-dimensional phase space, obeying the equations of motion

$$\dot{X}^i(t) = F^i[\mathbf{X}(t)] \,, \quad i = 1, \dots, N \tag{2.1}$$

where F is a smooth vector function. Given a norm $\|\cdot\|$ in the phase space, we linearise F around a fixed point $\mathbf{X}_0$,

$$\delta\dot{X}^i(t) = \sum_j A^i_j \delta X^j + B^i(\delta\mathbf{X}) \tag{2.2}$$

where $\delta\mathbf{X} \equiv \mathbf{X} - \mathbf{X}_0$, $A^i_j \equiv \frac{\partial F^i}{\partial X^j}|_{\delta\mathbf{X}=0}$, and B is a smooth function such that $\|B(\delta\mathbf{X})\| \longrightarrow 0$ as $\|\delta\mathbf{X}\| \to 0$. After diagonalizing A, the solution of (2.2) is straightforward, and we have

$$\delta\mathbf{X} = \sum_{j=1}^{N} c_j \mathbf{v}_j \, e^{\lambda_j t} \tag{2.3}$$

where $\mathbf{v}_j$ and λ_j are respectively the eigenvectors and eigenvalues of A, and the c_j are simply the integration constants. For sufficiently large time and sufficiently small $\mathbf{X}_0$ (such that (2.2) remains linear), the solution (2.3) will evolve exponentially like $\approx e^{\lambda_{max} t}$, where λ_{max} is the largest eigenvalue of A. If λ_{max} is positive, then, the the trajectories will rapidly diverge: an infinitesimal change in the initial condition will result in completely different trajectories. The exponent λ_{max} is referred to as the "Lyapunov exponent", and can be defined more formally as

$$\lambda_L \equiv \lim_{t\to\infty} \lim_{\|\delta\mathbf{X}\|\to 0} \sup \left(\frac{1}{t} \log \frac{\|\delta\mathbf{X}(t)\|}{\|\delta\mathbf{X}(0)\|} \right) \tag{2.4}$$

If we take as norm $\|\mathbf{X}\| = \sum_{i=1}^{N} |X^i|$, we can get the Lyapunov exponent from the Poisson brackets

$$\left|\left\{q^i(t), p^j(0)\right\}_{PB}\right| = \left| \sum_{k=1}^{N} \frac{\partial q^i(t)}{\partial q^k(0)} \frac{\partial p^j(0)}{\partial p^k(0)} - \frac{\partial p^j(0)}{\partial q^k(0)} \frac{\partial q^i(t)}{\partial p^k(0)} \right| = \left| \frac{\partial q^i(t)}{\partial q^j(0)} \right| \sim \exp(\lambda_L t) \tag{2.5}$$

Naively, one would generalise this to the quantum case by exploiting the fact that $|\{q^i(t), p^j(0)\}_{PB}| \sim \frac{1}{\hbar}|\big[q^i(t), p^j(0)\big]|$ as $\hbar \to 0$, and take the expectation value of some initial and final states as

$$\langle \text{out}| \, |\big[q^i(t), p^j(0)\big]| \, |\text{in}\rangle \tag{2.6}$$

However, this expression strongly depends on the initial and final states chosen, so we sum over final states and instead of the initial one we average over the thermal ensemble:

$$C(t) = \sum_n \sum_{\text{out}} \frac{1}{\mathcal{Z}} e^{-\beta E_n} \langle n| \left[q^i(t), p^j(0)\right]^\dagger |\text{out}\rangle \langle \text{out}| \left[q^i(t), p^j(0)\right] |n\rangle = -\langle \left[q^i(t), p^j(0)\right]^2 \rangle_\beta \tag{2.7}$$

For small times this correlator will grow exponentially like $C(t) \sim \hbar^2 e^{2\lambda_L t}$, until we reach the time $t_* \sim \frac{1}{\lambda_L} \log\big(\frac{1}{\hbar}\big)$, which in this context is called the "Ehrenfest time", and after that it approaches some constant value. In large N systems, where the role of $\hbar$ is substituted by $1/N$, we have instead $t_* \sim \frac{1}{\lambda_L} \log(N)$.

2.2 Out-of-time-ordered correlators

For quantum systems with a large number N of degrees of freedom, the quantity (2.7) can be generalised to

$$C(t) = -\langle [V(t), W(0)]^2 \rangle_\beta \tag{2.8}$$

where V and W are hermitian operators with $\mathcal{O}(1)$ degrees of freedom and a vanishing one-point function, $\langle V \rangle_\beta = \langle V \rangle_\beta = 0$ (in the SYK model we can use the Majorana fermions χ_i). The system is then called *chaotic*[1] if (2.8) grows exponentially for all possible pairs of V and W. The time at which $C(t)$ saturates is called the "scrambling time". There is also another relevant time for the correlator (2.8), the "dissipation time": this is the timescale t_d for the exponential decay of two-point functions like $\langle V(t)V(0)\rangle$. For the SYK model we can see from (1.41) that we have $t_d \sim \beta$, which is a typical behaviour for strongly coupled systems, and for chaotic systems one generally has $t_d \sim \frac{1}{\lambda_L}$. Notice that this time is parametrically smaller than the Ehrenfest time $t_* \sim \frac{1}{\lambda_L} \log\big(\frac{1}{\hbar}\big)$, where the small parameter in this case is $\hbar$.

If the system is not already UV regulated, like lattice systems, the correlator (2.8) could be divergent, and the common prescription in this context is to consider instead

$$-\operatorname{tr}\left[y^2 [W(t), V] y^2 [W(t), V]\right] \tag{2.9}$$

with y defined by

$$y^4 = \frac{1}{\mathcal{Z}} e^{-\beta H} \tag{2.10}$$

and V is just $V(0)$. This moves one of the two commutators in (2.8) halfway around the thermal circle. A similar function, which is key in understanding the decomposition of the correlator (2.8), is

$$F(t) = \operatorname{tr}\left[yVyW(t)yVyW(t)\right] \tag{2.11}$$

where the operators are evenly spaced around the thermal circle, and are not in the usual time order. This function, as shown in figure 2.1, is analytic in a strip of vertical width $\beta/2$ in the complex time plane. Noticing that $F(t - i\frac{\beta}{4}) = \operatorname{tr}\left[y^2 V W(t) y^2 V W(t)\right]$, the correlator (2.9) can then be written as

$$\begin{aligned} -\operatorname{tr}\left[y^2 [W(t), V] y^2 [W(t), V]\right] = \operatorname{tr}\left[y^2 W(t) V y^2 V W(t)\right] + \operatorname{tr}\left[y^2 V W(t) y^2 W(t) V\right] \\ - F(t + i\frac{\beta}{4}) - F(t - i\frac{\beta}{4}) \end{aligned} \tag{2.12}$$

[1] Actually, the definition of "quantum chaos" is still ambiguous, and there are other possible approaches, for example observing the level statistics of the system

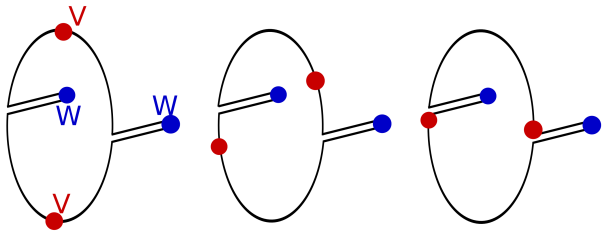

Figure 2.1: Pictorial representation of the time-contour of the operators in (2.11). The circle represents the evolution in imaginary time, so that at $F(t+i\tau)$ corresponds to a rotation of $2\pi\tau/\beta$ along the circle. The folds of the W operators (which are to be thought as orthogonal to the circle) represent ordinary real-time evolution. On the left we have $\tau = 0$, $F(t)$, the central one is for $|\tau| < \beta/4$, and on the right $\tau = \beta/4$. Figure taken from [8].

Near the decomposition time t_d, when the two-point functions decay exponentially as $\langle V(t)V\rangle \sim \langle W(t)W\rangle \sim \langle W(t)V\rangle \sim e^{-t/t_d}$, all the terms in (2.12) are almost equal (by Wick's theorem) and they cancel against each other. Since the first two terms can be written as a norm of states (as we discuss in the next section), they remain of order one even at later times, and then the late-time exponential growth of the correlator is due to the rapid decrease of $F(t \pm i\frac{\beta}{4})$. Intuitively, these behaviour is given by the fact that, for large time t, all operators are well separated along the contour of figure 2.1, so the terms arranged as $VW(t)VW(t)$ decay, while the ones as $VVW(t)W(t)$ do not, independently of τ.

2.3 The thermofield double interpretation

Another useful representation of the quantities quantities in this context is given by the thermofield double state, which is defined by

$$|\text{TFD}\rangle \equiv \frac{1}{\mathcal{Z}^{\frac{1}{2}}} \sum_n e^{-\beta E_n/2} |\overline{n}\rangle_L |n\rangle_R \tag{2.13}$$

which is an entangled state in the Hilbert space of two copies of the same system, called "left" and "right", so that the traced-out density matrix of each copy is $\rho_L = \rho_R = \frac{1}{\mathcal{Z}^{1/2}} \sum_n e^{-\beta E_n} |n\rangle \langle n|$. Notice that the terms on the first line of (2.12) can be written as the norm of the state $yW(t)Vy^{-1}|\text{TFD}\rangle$. For any operator O of the original system, we define the operators acting on the left and right systems as $O_R = 1 \otimes O$ and $O_L = O^T \otimes 1$. Notice that, because of the high correlation between L and R components in $|\text{TFD}\rangle$, an expectation value like $\langle \text{TFD}| V_L V_R |\text{TFD}\rangle$ is large. Finally, we connect with the previous discussion by noticing that

$$F(t) = \langle \Psi| V_L V_R |\Psi\rangle \tag{2.14}$$

$$|\Psi\rangle \equiv \frac{1}{\mathcal{Z}^{\frac{1}{2}}} \sum_{m,n} e^{-\beta(E_m+E_n)/4} W(t)_{n\overline{m}} |\overline{m}\rangle_L |n\rangle_R \tag{2.15}$$

The behaviour of $F(t)$ is then explained by the fact that, for t small, the perturbation induced by W will not change significantly the correlations between the two systems, so that F remains large. For larger t, instead, the out-of-sync evolution of L and R will completely destroy their entanglement, and F decreases rapidly. This is the quantum analogue of the butterfly effect. Let us also mention that, in the holographic dual of this model the left and right systems correspond to the two identical sides of a traversable wormhole, and this used in [22] to study the related dynamic of information transfer between two identical subsystems.

2.4 Fast scrambling

To understand the meaning of "scrambling", let's consider the argument of [4], where the "fast scrambling" conjecture was first proposed. One can consider a complex and chaotic quantum system with N degrees of freedom and prepare it in a pure state $|\Psi\rangle$. After a long enough time, the system will have *thermalise*, i.e. the entanglement entropy of every subsystem of size m, with $m < N/2$, will approach its maximum value, even though the state of the whole system has remained pure, due to unitary evolution. Let us recall that, given a subsystem L and its complement R, the entanglement entropy of the first is

$$S_L = -\operatorname{tr}(\rho_L \log \rho_L) \ , \quad \text{with } \ \rho_L \equiv \operatorname{tr}_R |\Psi\rangle \langle\Psi| \tag{2.16}$$

where tr_R denotes the trace over the subsystem R. This means the initial information gets "scrambled" across the system, and one can recover it only by measuring $\mathcal{O}(N)$ degrees of freedom. If one perturbs the system, after a certain amount of time, this perturbation will also get smeared across the whole system. The fast scrambling conjecture, then, states that the time in which this happens cannot be shorter than $t_* \sim \beta \log N$; the systems that saturate this bound are called "fast scramblers", and the most notable example are black holes. Actually, if the N degrees of freedom are arranged in a d dimensional lattice, this time becomes $t_* \sim \beta N^{\frac{1}{d}}$, since the linear dimension of the system is $\propto N^{\frac{1}{d}}$. In this sense black holes and the SYK model can be thought as infinite dimensional systems. A few years later, Maldacena, Shenker, and Stanford [8] developed an analogue of this conjecture for OTOCs, and proved mathematically (under a few reasonable assumptions) the rate at which (2.11) decreases is bounded by

$$\frac{d}{dt}(F_d - F(t)) \leq \frac{2\pi}{\beta}(F_d - F(t)) \tag{2.17}$$

where F_d is the constant value approached by F after the dissipation time. This equivalent to saying that the Lyapunov exponent must satisfy

$$\lambda_L \leq \frac{2\pi}{\beta} \tag{2.18}$$

At the end of the next chapter we will see that the SYK model saturates this bound.

Chapter 3

The four-point function

We will now study the four-point function in the general q case, mainly by following the derivation contained in [9]. Since the disorder average matches the indices between couples of vertices, we cannot have correlation functions with an odd number of points, and the indices of the fields in the correlator must be equal in pairs. That said, the four-point correlator is

$$\frac{1}{N^2}\sum_{i,j=1}^{N}\langle T(\chi_i(\tau_1)\chi_i(\tau_2)\chi_j(\tau_3)\chi_j(\tau_4))\rangle = G(\tau_{12})G(\tau_{34}) + \frac{1}{N}\mathcal{F}(\tau_1,\tau_2,\tau_3,\tau_4) + O(\frac{1}{N^2}) \tag{3.1}$$

where we remind that $\tau_{ij} \equiv \tau_i - \tau_j$ (from now on this notation will be considered implicit for time differences). The first term is a disconnected piece given by the contraction of the two couples of fields with the same index while the second contains the connected part at leading order in 1/N, plus a disconnected term that is of order $1/N$ because it sets $i = j$. We have already factored out the expected dependency on N from $\mathcal{F}$, in fact one can obtain any 2p-point diagrams by cutting p edges of vacuum graphs, which at leading order are proportional to N. Since each cut lowers the power of N by one (because we add a constraint on the particle index of each couple of external legs) we expect 2-point functions to be independent of N (as confirmed by section 1.2), 4-point functions proportional to 1/N and so on.

The connected diagrams at L.O. are ladder diagrams [5] [9] [11] with a number $n \geq 1$ of rungs (as in figure 3.1), and each rung is made by $q-2$ propagators plus a disorder average line, so that

$$\mathcal{F}(\tau_1,\tau_2,\tau_3,\tau_4) = \sum_{n=0}^{\infty}\mathcal{F}_n(\tau_1,\tau_2,\tau_3,\tau_4) \tag{3.2}$$

where $\mathcal{F}_n$ is a ladder diagram with n rungs. The first term $\mathcal{F}_0$ is the previously mentioned disconnected piece, which is just a couple of dressed propagators:

$$\mathcal{F}_0(\tau_1,\tau_2,\tau_3,\tau_4) = -G(\tau_{13})G(\tau_{24}) + G(\tau_{14})G(\tau_{23}) \tag{3.3}$$

All the following terms can then be constructed through the application of a kernel (represented in figure 3.2)

$$K(\tau_1,\tau_2;\tau_3,\tau_4) \equiv -(q-1)J^2 G(\tau_{13})G(\tau_{24})G(\tau_{34})^{q-2} \tag{3.4}$$

that contains a rung of the ladder. It is meant to be applied as a "matrix" to each ladder $\mathcal{F}_n$, so that $\mathcal{F}_{n+1} = K\mathcal{F}_n$ in the sense that

$$\mathcal{F}_{n+1}(\tau_1,\tau_2,\tau_3,\tau_4) = \int \mathrm{d}\tau_a\,\mathrm{d}\tau_b\, K(\tau_1,\tau_2;\tau_a,\tau_b)\,\mathcal{F}_n(\tau_a,\tau_b,\tau_3,\tau_4) \tag{3.5}$$

In this way we can write $\mathcal{F}$ as a geometric series, and sum it exactly:

$$\mathcal{F} = \sum_{n=0}^{\infty}\mathcal{F}_n = \sum_{n=0}^{\infty}K^n\mathcal{F}_0 = \frac{1}{1-K}\mathcal{F}_0 \tag{3.6}$$

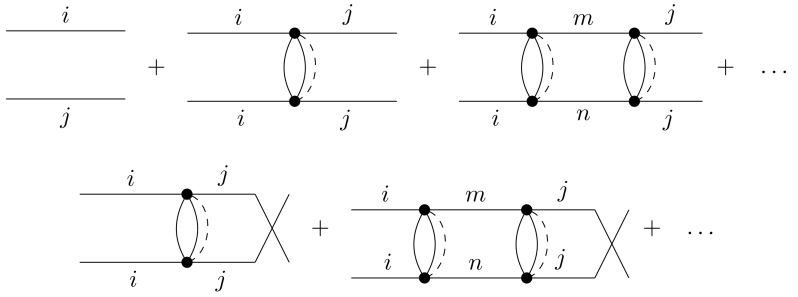

Figure 3.1: First terms of the four point correlator in the case q=4. The diagrams in the second line are the respective of the ones above but with the exchange $\tau_3 \leftrightarrow \tau_4$, which produces a minus sign.

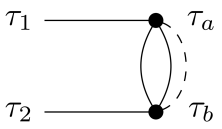

Figure 3.2: The kernel for building the ladder diagrams in the case q=4.

The aim is then to decompose the kernel into a sum of its eigenvalues, and the conformal symmetry will play an essential role in this.

3.1 The SL(2,R) symmetry

The key property that makes it possible to diagonalise the kernel (3.4) is the SL(2,R) symmetry in the strong coupling regime, where we can use expression (1.47) for the propagator to obtain

$$K_c(\tau_1,\tau_2;\tau_3,\tau_4) \equiv -\frac{1}{\alpha_0}\frac{\text{sgn}(\tau_{13})\text{sgn}(\tau_{23})}{|\tau_{13}|^{2\Delta}|\tau_{24}|^{2\Delta}|\tau_{13}|^{2-4\Delta}} \tag{3.7}$$

$$\alpha_0 \equiv \frac{2\pi q}{(q-1)(q-2)\tan\frac{\pi}{q}} = \frac{1}{(q-1)J^2 b^q} \tag{3.8}$$

One can check, in fact, that up to total derivatives τ_3 and τ_4 this commutes with the generators of the algebra

$$\hat{P} = \partial_\tau\,, \quad \hat{D} = -\tau\partial_\tau - \Delta\,, \quad \hat{K} = -\tau^2\partial_\tau + 2\Delta\tau \tag{3.9}$$

which satisfy the commutation relations

$$\left[\hat{D},\hat{P}\right] = \hat{P}\,, \quad \left[\hat{D},\hat{K}\right] = -\hat{K}\,, \quad \left[\hat{P},\hat{K}\right] = -2\hat{D} \tag{3.10}$$

It commutes in the sense that

$$(\hat{D}_1+\hat{D}_2)\,K_c(\tau_1,\tau_2;\tau_3,\tau_4) = K_c(\tau_1,\tau_2;\tau_3,\tau_4)\,(\hat{D}_3+\hat{D}_4) \tag{3.11}$$

This implies that:

- The ladder diagrams can be written as a function of the SL(2,R)-invariant cross-ratio[1] $\chi \equiv \frac{\tau_{12}\,\tau_{34}}{\tau_{13}\,\tau_{24}}$ since the base of the ladder $\mathcal{F}_0$ transforms as a conformal 4-point function and this property is conserved by the action of the kernel K_c. This allows us to work in the space of functions of a single cross-ratio instead of functions of two times. The kernel will then become $K_c(\chi,\tilde{\chi})$

[1] In one dimension there is only one independent cross-ratio of four variables. In $d > 1$ dimensions instead there are $N(N-3)/2$ independent cross ratios for each variable [1].

- The kernel commutes with the Casimir operator of SL(2,R), given by

$$\begin{aligned}\hat{C}_{1+2} &= (\hat{D}_1+\hat{D}_2)^2 - \frac{1}{2}(\hat{K}_1+\hat{K}_2)(\hat{P}_1+\hat{P}_2) - \frac{1}{2}(\hat{P}_1+\hat{P}_2)(\hat{K}_1+\hat{K}_2) \\ &= 2(\Delta^2-\Delta) - \hat{K}_1\hat{P}_2 - \hat{P}_1\hat{K}_2 + 2\hat{D}_1\hat{D}_2\end{aligned} \tag{3.12}$$

  This allows us to decompose the kernel into the sum of its eigenvalues, because the spectrum of the Casimir is nondegenerate, so its eigenfunctions are the same as the one K_c.

3.2 The general procedure

The procedure to compute the four-point function can be summarised in six points, which we report directly from [9]":

1. Understand the properties of $\mathcal{F}$ and $\mathcal{F}_n$ as functions of the cross ratio.
2. Find the eigenfunctions of $\hat{C}_{1+2}$ with these properties. These are particular hypergeometric functions $\Psi_h(\chi)$, related to conformal blocks of weight h.
3. Determine the set of h to have a complete basis of functions. This turns out to be $h = \frac{1}{2} + i\,s$ and $h = 2, 4, 6, 8, \ldots$.
4. Compute $k_c(h)$, the eigenvalue of the kernel K_c as a function of h.
5. Determine the inner products $\langle \Psi_h(\chi), \mathcal{F}_0\rangle$ and $\langle \Psi_h(\chi), \Psi_h(\chi)\rangle$
6. Compute the four-point function as

$$\mathcal{F} = \frac{1}{1-K_c}\mathcal{F}_0 = \sum_h \Psi_h(\chi)\frac{1}{1-k_c(h)}\frac{\langle \Psi_h(\chi), \mathcal{F}_0\rangle}{\langle \Psi_h(\chi), \Psi_h(\chi)\rangle}\text{ ,,} \tag{3.13}$$

To follow the first step, one can write the ladder diagrams as $\mathcal{F}_n(\tau_1,\tau_2,\tau_3,\tau_4) = G_c(\tau_{12})G_c(\tau_{34})\mathcal{F}_n(\chi)$, and then use the SL(2,R) symmetry, the antisymmetry in $\tau_1 \leftrightarrow \tau_2$ and $\tau_3 \leftrightarrow \tau_4$, and the symmetry $(\tau_1,\tau_2) \leftrightarrow (\tau_3,\tau_4)$ to set $\tau_1 = 0$, $\tau_3 = 1$, $\tau_4 = \infty$ and $\tau_2 > 0$ to restrict the cross-ratio $\chi = \tau_2$ to be positive. This allows us to study two separate cases, where the four-point function will have two different analytic expressions: $0 < \chi < 1$ (which is related to the OPE limit $\chi \ll 1$), and $\chi > 1$ (which is related to the OTOC) where the correlator acquires a minus sign due to time ordering. In the latter case, the function $\mathcal{F}$ acquires an additional discrete symmetry, $\chi \to \frac{\chi}{\chi-1}$, which maps between the regions $(1,2]$ and $[2,\infty)$, so that one needs only to study the correlator for $0 < \chi < 2$. This also tells us that $\mathcal{F}$ has a vanishing derivative in $\chi = 2$. Furthermore, the kernel can also be written as a function of cross ratios, so that equation (3.5) can be rewritten as $\mathcal{F}_{n+1}(\chi) = \int_0^2 \frac{d\tilde{\chi}}{\tilde{\chi}^2} K_c(\chi;\tilde{\chi})\mathcal{F}_n(\tilde{\chi})$.

To find the eigenvalues of the Casimir, we have to solve the equation $\mathcal{C}f(\chi) = h(h-1)f(\chi)$ (this parametrization of the eigenvalues is for convenience), where $\mathcal{C}$ is given by

$$C_{1+2}\,\frac{1}{|\tau_{12}|^{2\Delta}}f(\chi) = \frac{1}{|\tau_{12}|^{2\Delta}}\mathcal{C}f(\chi) \tag{3.14}$$

$$\mathcal{C} \equiv \chi^2(1-\chi)\partial_\chi^2 - \chi^2\partial_\chi \tag{3.15}$$

We give a derivation of this in appendix B. The solutions of the equation are then linear combinations of

$$\chi^h\,{}_2F_1(h,h,2h,\chi) \quad \text{and} \quad \chi^{1-h}\,{}_2F_1(1-h,1-h,2-2h,\chi) \tag{3.16}$$

where ${}_2F_1$ are hypergeometric functions. One then needs to impose the following conditions to the eigenfunctions $f(\chi)$:

- the vanishing derivative $f'(2) = 0$

- normalisability with respect to the inner product: $\langle g, f\rangle = \int_0^2 \frac{d\chi}{\chi^2} g^*(\chi) f(\chi)$
- hermiticity of the operator: $\langle g, \mathcal{C} f\rangle = \langle \mathcal{C} g, f\rangle$, which means $\int_0^2 d\chi [g^*(1-\chi) f' - (g^*)'(1-\chi) f]' = 0$.

The last condition requires that $[g^*(1-\chi)f' - (g^*)'(1-\chi)f]$ vanishes for $\chi = 2$ (which is satisfied thanks to $f'(2) = 0$), and for $\chi = 0$ (which, as we will see in a moment, will select the values of h), but since the hypergeometric functions contain a logarithmic divergence in $\chi = 1$[2], so that one needs to match both the logarithmic and the constant term from the left and from the right in order for the boundary to vanish. The solutions with this properties are then

$$\Psi_h = \frac{\Gamma(\frac{1}{2} - \frac{h}{2})\Gamma(\frac{h}{2})}{\sqrt{\pi}} {}_2F_1\left(\frac{h}{2}, \frac{1}{2} - \frac{h}{2}, \frac{1}{2}, \frac{(2-\chi)^2}{\chi^2}\right) \qquad \text{for } \chi > 1 \tag{3.17}$$

$$\Psi_h = A \frac{\Gamma(h)^2}{\Gamma(2h)} \chi^h {}_2F_1(h, h, 2h, \chi) + B \frac{\Gamma(1-h)^2}{\Gamma(2-2h)} {}_2F_1(1-h, 1-h, 2-2h, \chi) \qquad \text{for } \chi < 1 \tag{3.18}$$

with

$$\begin{aligned} A &\equiv \frac{1}{\tan\left(\frac{\pi h}{2}\right)} \frac{\tan(\pi h)}{2} \\ B &\equiv A(1-h) = -\tan\left(\frac{\pi h}{2}\right) \frac{\tan(\pi h)}{2} \end{aligned} \tag{3.19}$$

Furthermore, the hermiticity condition also requires that $\chi^{-\frac{1}{2}} \Psi_h \overset{\chi\to 0}{\longrightarrow} 0$, and this selects two sets of solutions

- the continuous one, $h = \frac{1}{2} + i\, s$, with $s \in \mathbb{R}$, $s > 0$
- the discrete one, $h = 2n$, with $n \in \mathbb{N}_{>0}$.

To find the eigenvalues of the kernel, one could just apply the kernel to the eigenfunctions, or, with simpler calculations, consider the Casimir C_{1+2}, whose eigenfunctions are conformal three-point functions[3] of two fermions and a conformal operator of dimension h

$$\frac{\mathrm{sgn}(\tau_1 - \tau_2)}{|\tau_1 - \tau_0|^h |\tau_2 - \tau_0|^h |\tau_1 - \tau_2|^{2\Delta - h}} \tag{3.20}$$

Using the SL(2,R) symmetry to send $\tau_0 \to \infty$ and applying the kernel one obtains the eigenvalues

$$\begin{aligned} k_c(h) &= \int d\tau d\tau'\, K_c(1, 0; \tau, \tau') \frac{\mathrm{sgn}(\tau - \tau')}{|\tau - \tau'|^{2\Delta - h}} \\ &= -(q-1) \frac{\Gamma\left(\frac{3}{2} - \frac{1}{q}\right)\Gamma\left(1 - \frac{1}{q}\right)}{\Gamma\left(\frac{1}{2} + \frac{1}{q}\right)\Gamma\left(\frac{1}{q}\right)} \frac{\Gamma\left(\frac{1}{q} + \frac{h}{2}\right)}{\Gamma\left(\frac{3}{2} - \frac{1}{q} - \frac{h}{2}\right)} \frac{\Gamma\left(\frac{1}{2} + \frac{1}{q} - \frac{h}{2}\right)}{\Gamma\left(1 - \frac{1}{q} - \frac{h}{2}\right)} \end{aligned} \tag{3.21}$$

which can be rewritten in a more compact way as

$$k_c(h) = -(q-1)\frac{p(h)}{p(0)} = \frac{p(h)}{p(2)}\,, \qquad p(h) \equiv \frac{\Gamma\left(\Delta + \frac{h}{2}\right)\Gamma\left(\Delta + \frac{1-h}{2}\right)}{\Gamma\left(1 - \Delta + \frac{h}{2}\right)\Gamma\left(1 - \Delta + \frac{1-h}{2}\right)} \tag{3.22}$$

(it is easy to show that $p(0)/(1-q) = p(2)$ using the $\Gamma(1+z) = z\Gamma(z)$ property of gamma functions). In particular, for $q = 4$ one has $k_c(h) = -\frac{3}{2}\frac{\tan\left(\frac{\pi}{2}\left(h - \frac{1}{2}\right)\right)}{h - \frac{1}{2}}$, and $k_c(h) \to \frac{2}{h(h-1)}$ for $q \to \infty$. We plotted the continuum and discrete spectrums in figure 3.3.

After computing the normalisation of the eigenfunctions

$$\langle \Psi_h, \Psi'_h \rangle = \begin{cases} \frac{\pi \tan(\pi h)}{4h-2} 2\pi \delta(s - s') & \text{if } h = \frac{1}{2} + i\, s \\ \frac{\pi^2 \delta_{h,h'}}{4h-2} & \text{if } h = 2, 4, 6, \ldots \end{cases} \tag{3.23}$$

[2] In particular, $\lim_{z\to 1^-} \frac{{}_2F_1(a,b,a+b,z)}{-\ln(1-z)} = \frac{\Gamma(a+b)}{\Gamma(a)\Gamma(b)}$. See, for example, equation 15.4.21 of [23]

[3] A similar procedure is used also in reference [13]

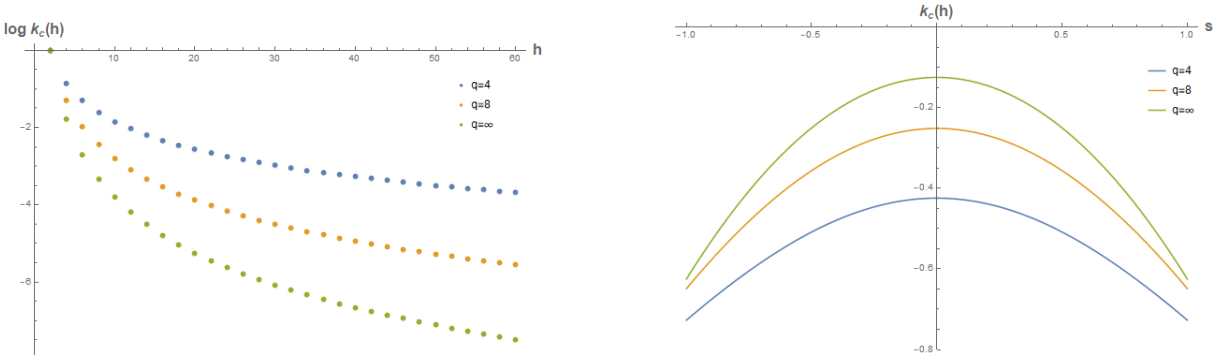

Figure 3.3: Plots of the discrete and continuum parts of the spectrum $k_c(h)$ (without the factor of $-(q-1)$) for the values $q = 4, 8, \infty$. For the discrete spectrum we have plotted the logarithm of $k_c(h)$, while for the continuum part we have plotted k_c as a function of $s = \mathrm{Im}(h)$.

and the product with $\mathcal{F}_0$

$$\langle \Psi_h, \mathcal{F}_0 \rangle = \frac{\alpha_0}{2} k_c(h) \tag{3.24}$$

(where α_0 was defined in (3.8)) we can write a first naive expression for the four point function

$$\begin{aligned} \mathcal{F}(\chi) &= \sum_h \Psi_h(\chi) \frac{1}{1-k_c(h)} \frac{\langle \Psi_h, \mathcal{F}_0 \rangle}{\langle \Psi_h, \Psi_h \rangle} \\ &= \alpha_0 \int_0^\infty \frac{ds}{2\pi} \frac{(2h-1)}{\pi \tan(\pi h)} \frac{k_c(h)}{1-k_c(h)} \Psi_h(\chi) + \alpha_0 \sum_{n=1}^\infty \left[\frac{(2h-1)}{\pi^2} \frac{k_c(h)}{1-k_c(h)} \Psi_h(\chi) \right]_{h=2n} \end{aligned} \tag{3.25}$$

The problem is that this expression has a divergence coming from the eigenvalue $k_c(2) = 1$. This actually comes from the fact that we considered the conformal limit as exact: one should treat the $h = 2$ contribution separately, outside of the conformal limit. This will produce an enhanced contribution which will dominate the four point function, and is the result of the breaking of the reparametrisation invariance. Furthermore, this will also be the contribution responsible for the saturation of the chaos bound.

3.3 The conformal contribution

We first discuss here the finite part in the expression (3.25). Using the identity $\frac{2}{\tan(\pi h)} = \frac{1}{\tan(\pi h/2)} - \frac{1}{\tan(\pi(1-h)/2)}$ to make evident the symmetry in $h \to 1-h$ of the integrand, we can extend the integral over s to the whole axis, obtaining

$$\frac{\mathcal{F}_{h\neq 2}(\chi)}{\alpha_0} = \int_{-\infty}^{+\infty} \frac{ds}{2\pi} \frac{(h-1/2)}{\pi \tan(\pi h/2)} \frac{k_c(h)}{1-k_c(h)} \Psi_h(\chi) + \sum_{n=2}^\infty \left[\frac{(2h-1)}{\pi^2} \frac{k_c(h)}{1-k_c(h)} \Psi_h(\chi) \right]_{h=2n} \tag{3.26}$$

Now we can rewrite the discrete sum as a sum of residues at the poles of $\frac{1}{\tan(\frac{\pi h}{2})}$, so that the whole expression can be written as a single contour integral over the complex plane:

$$\begin{aligned} \frac{\mathcal{F}_{h\neq 2}(\chi)}{\alpha_0} &= \int_{-\infty}^{+\infty} \frac{ds}{2\pi} \frac{(h-1/2)}{\pi \tan(\pi h/2)} \frac{k_c(h)}{1-k_c(h)} \Psi_h(\chi) + \sum_{n=2}^\infty \mathrm{Res} \left[\frac{(h-1/2)}{\pi \tan(\pi h/2)} \frac{k_c(h)}{1-k_c(h)} \Psi_h(\chi) \right]_{h=2n} \\ &= \int_{\mathcal{C}} \frac{dh}{2\pi i} \left(\frac{(h-1/2)}{\pi \tan(\pi h/2)} \frac{k_c(h)}{1-k_c(h)} \Psi_h(\chi) \right) \end{aligned} \tag{3.27}$$

where $\mathcal{C}$ denotes the contour in the imaginary plane made by the $\mathrm{Re}(h) = 1/2$ axis and the residues around the poles in $h = 4, 6, 8, \ldots$ (left side of figure 3.4). Notice that the eigenfunctions Ψ_h have

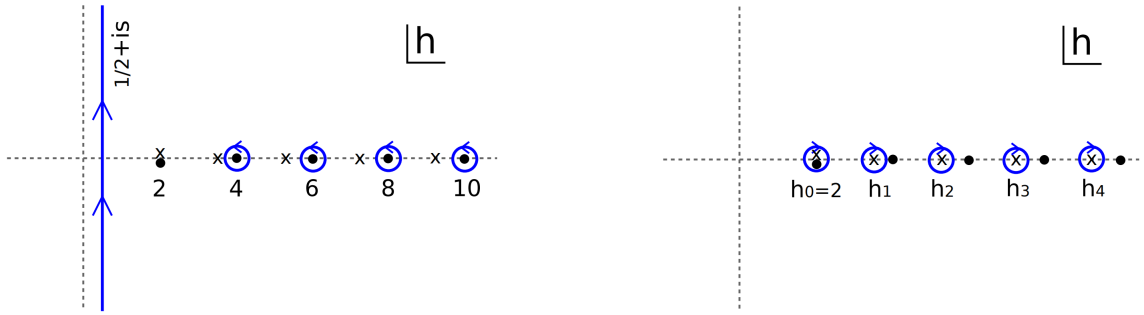

Figure 3.4: Contour integrals for the conformal part of the four-point function. Taken from [9]

poles at $h = 1 + 2n$ which are cancelled by the zeros of $\frac{1}{\tan(\pi h/2)}$. In the case $\chi > 1$, we can move the integral over s towards the right, and one by one we pick up the poles (with a minus sign from the clockwork contour) at the values h_m for which $k_c(h_m) = 1$ (included a double pole at $h = 2$) and cancel the residues at $h = 2n$ (right side of figure 3.4), so that the four-point function becomes

$$\mathcal{F}_{h\neq 2}(\chi) = -\alpha_0 \sum_{m=0}^{\infty} \text{Res}\left[\frac{(h-1/2)}{\pi\tan(\pi h/2)}\frac{k_c(h)}{1-k_c(h)}\frac{\Gamma(\frac{1}{2}-\frac{h}{2})\Gamma(\frac{h}{2})}{\sqrt{\pi}}\,{}_2F_1(\frac{h}{2},\frac{1}{2}-\frac{h}{2},\frac{1}{2},\frac{(2-\chi)^2}{\chi^2})\right]_{h=h_m} \quad \chi > 1 \tag{3.28}$$

In the case $\chi < 1$, one cannot do this directly since we cannot send h to positive infinity in ${}_2F_1(1-h, 1-h, 2-2h, \chi)$, so we use the symmetry under $h \to 1-h$ to write the B term in (3.18) as another copy of the A term inside the integral, and the fact that $\Psi_h = \frac{\Gamma(h)^2}{\Gamma(2h)}\chi^h\,{}_2F_1(h,h,2h,\chi)$ for $h = 2n$, obtaining

$$\begin{aligned}\frac{\mathcal{F}_{h\neq 2}(\chi)}{\alpha_0} = &\int_{-\infty}^{+\infty}\frac{ds}{2\pi}\frac{(h-1/2)}{\pi\tan(\pi h/2)}\frac{k_c(h)}{1-k_c(h)}\frac{\Gamma(h)^2}{\Gamma(2h)}\chi^h\,{}_2F_1(h,h,2h,\chi)\\ &+\sum_{n=2}^{\infty}\text{Res}\left[\frac{(h-1/2)}{\pi\tan(\pi h/2)}\frac{k_c(h)}{1-k_c(h)}\frac{\Gamma(h)^2}{\Gamma(2h)}\chi^h\,{}_2F_1(h,h,2h,\chi)\right]_{h=2n}\end{aligned} \tag{3.29}$$

Now we can push the contour towards the right as before, thus

$$\mathcal{F}_{h\neq 2}(\chi) = -\alpha_0 \sum_{m=0}^{\infty} \text{Res}\left[\frac{(h-1/2)}{\pi\tan(\pi h/2)}\frac{k_c(h)}{1-k_c(h)}\frac{\Gamma(h)^2}{\Gamma(2h)}\chi^h\,{}_2F_1(h,h,2h,\chi)\right]_{h=h_m} \quad , \chi < 1 \tag{3.30}$$

3.4 The h=2 contribution

Since the divergence of this contribution comes from consider the conformal symmetry as exact, we must move away from that limit and consider the first order correction to the kernel in the limit of strong coupling, in other words we need to consider contributions of order $\delta K \sim (\beta J)^{-1}$. This way we will obtain an eigenvalue of the kernel close but not exactly equal to one, and in turn the contribution to the four-point function will be parametrically large, of order βJ. As the reparametrisation symmetry is now broken, we can no longer work in the euclidean line and must consider, instead, the finite-temperature circle, that we parametrise with the angular coordinate $\theta = 2\pi\tau/\beta$, with $\theta \in [0, 2\pi)$. It is also convenient to use the symmetric kernel

$$\tilde{K}(\theta_1,\theta_2;\theta_3,\theta_4) \equiv -(q-1)J^2|G(\theta_{12})|^{\frac{q-2}{2}}G(\theta_{13})G(\theta_{24})|G(\theta_{34})|^{\frac{q-2}{2}} \tag{3.31}$$

We use the Fourier index n to parametrise the "center-of-mass" coordinate $\frac{\theta_1+\theta_2}{2}$ of the antisymmetric eigenfunctions $\Psi^{exact}_{h,n}(\theta_1,\theta_2)$, and consider the inner product

$$\langle\Psi,\Phi\rangle = \int_0^{2\pi} d\theta_1 d\theta_2 \Psi^*(\theta_1,\theta_2)\Phi(\theta_1,\theta_2) \tag{3.32}$$

Then we write $\mathcal{F}_0$ as the kernel acting on the antisymmetric identity

$$I(\theta_1,\dots,\theta_4)=\frac{1}{2}\left(\delta(\theta_{14})\delta(\theta_{23})-\delta(\theta_{13})\delta(\theta_{24})\right)=-\sum_{h,n}\Psi^{exact}_{h,n}(\theta_1,\theta_2)\Psi^{exact*}_{h,n}(\theta_3,\theta_4) \tag{3.33}$$

so that now

$$\left[(q-1)J^2|G(\theta_{12})|^{\frac{q-2}{2}}|G(\theta_{34})|^{\frac{q-2}{2}}\right]\mathcal{F}(\theta_1,\theta_2,\theta_3,\theta_4)=2\sum_{h,n}\frac{k(h,n)}{1-k(h,n)}\Psi^{exact}_{h,n}(\theta_1,\theta_2)\Psi^{exact*}_{h,n}(\theta_3,\theta_4) \tag{3.34}$$

where $k(h,n)$ are the eigenvalues of $\tilde{K}$. Notice that this expression is valid for any value of βJ, and if we take the limit $\beta J\ll 1$ we recover the original eigenfunctions of the Casimir C_{1+2} and the eigenvalues $k_c(h)$. In fact, we can do it for any value of h except $h=2$, where the eigenvalue would be one, and we have to take into account corrections of order $1/(\beta J)$.

Let's consider now the Schwinger-Dyson equations in the conformal limit, which are reparametrisation invariant, and a linearised reparametrisation $\theta\to\theta+\epsilon(\theta)$. Under this transformation, the variation of the conformal two-point function is

$$\delta_\epsilon G_c=\left[\Delta\epsilon'(\theta_1)+\Delta\epsilon'(\theta_2)+\epsilon(\theta_1)\partial_{\theta_1}+\epsilon(\theta_2)\partial_{\theta_2}\right]G_c(\theta_1,\theta_2) \tag{3.35}$$

Since $G_c+\delta_\epsilon G_c$ must also solve the SD equations in the conformal limit, we take the variation of the generalisation of equations (1.27) to q interacting fermions, obtaining

$$\begin{aligned}0&=\delta_\epsilon G_c*\Sigma_c+G_c*\delta\Sigma_c\\ \xrightarrow{*G_c}\ 0&=\delta_\epsilon G_c+G_c*\left[(q-1)J^2G_c^{q-2}\delta_\epsilon G_c\right]*G_c\\ &=(1-K_c)\delta_\epsilon G_c\end{aligned} \tag{3.36}$$

where the $*$ product means $F*G=\int dt' F(t,t')G(t',t'')$. We deduce then that the variations $\delta_\epsilon G_c$ are eigenfunctions of K_c with eigenvalue equal to one. To get the eigenvalue one of the symmetric kernel $\tilde{K}$ we must consider instead $|G_c^{\frac{q-2}{q}}|\delta_\epsilon G_c$. We choose for the functions ϵ a convenient Fourier basis $\epsilon(\theta)=\sum_n\epsilon_n e^{-in\theta}$, then use the finite temperature conformal correlator $G_c(\tau)=b\left[\frac{\pi}{\beta\sin\frac{\pi\tau}{\beta}}\right]^{2\Delta}\mathrm{sgn}(\tau)$ to evaluate (3.35).

As a preliminary step, assuming for simplicity $\theta_1>\theta_2$ (the other case is identical), we use the following redefinitions:

$$\begin{aligned}&G_c(\theta_1,\theta_2)=a\frac{1}{\sin^{2\Delta}\left(\frac{x}{2}\right)}\\ &a\equiv b\left(\frac{\pi}{\beta}\right)^{2\Delta}\qquad x\equiv\theta_1-\theta_2\qquad y\equiv\frac{\theta_1+\theta_2}{2}\ .\end{aligned} \tag{3.37}$$

We have that

$$\begin{aligned}\partial_{\theta_1}G_c(\theta_1,\theta_2)&=-\Delta\cot\left(\frac{x}{2}\right)G_c(\theta_1,\theta_2)=-\partial_{\theta_2}G_c(\theta_1,\theta_2)\\ |G_c^{\frac{q-2}{q}}|G_c&=\frac{a^{q/2}}{\sin\left(\frac{x}{2}\right)}\ ,\end{aligned} \tag{3.38}$$

and inserting everything in (3.35) we get

$$\begin{aligned}\frac{|G_c^{\frac{q-2}{q}}|\delta_\epsilon G_c}{a^{q/2}\Delta}&=\sum_n\epsilon_n\left[-in(e^{-in\theta_1}+e^{-in\theta_2})-\cot\left(\frac{x}{2}\right)(e^{-in\theta_1}-e^{-in\theta_2})\right]\frac{1}{\sin\left(\frac{x}{2}\right)}\\ &=\sum_n\epsilon_n\,2i\frac{e^{-iny}}{\sin\left(\frac{x}{2}\right)}\underbrace{\left[\frac{\sin\left(\frac{nx}{2}\right)}{\tan\left(\frac{x}{2}\right)}-n\cos\left(\frac{x}{2}\right)\right]}_{\equiv f_n(x)}\end{aligned} \tag{3.39}$$

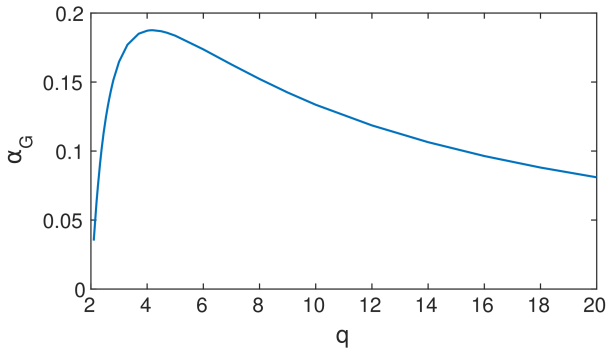

Figure 3.5: Numerical plot of α_G from [9].

Notice that $f_n(x)$ is identically zero for $n = -1, 0, 1$: this is because the $G_c(\theta_1, \theta_2)$ is invariant under SL(2,R) transformations. We then then normalise this eigenfunctions with respect to the inner product (3.32):

$$\begin{aligned}\frac{|G_c^{\frac{q-2}{q}}|\delta_\epsilon G_c \cdot |G_c^{\frac{q-2}{q}}|\delta_\epsilon G_c}{16a^q\Delta^2} &= \sum_{n,m}\epsilon_m^*\epsilon_n\frac{1}{2}\int_0^{2\pi}dx\int_0^{2\pi}dy\frac{e^{-iy(n-m)}}{4\sin^2\left(\frac{x}{2}\right)}f_m(x)f_n(x)\\ &= \pi\sum_n|\epsilon_n|^2\int_0^{2\pi}dx\frac{1}{4\sin^2\left(\frac{x}{2}\right)}(f_n(x))^2\\ &= \frac{\pi^2}{3}\sum_n|\epsilon_n|^2|n|(n^2-1)\,,\end{aligned} \tag{3.40}$$

where we have used the periodicity in $\theta_{1,2}$ to factorise the integrals in x and y. Dividing by this normalisation factor we get

$$\begin{aligned}\Psi_{2,n} &= \gamma_n\frac{e^{-iny}}{2\sin\frac{x}{2}}\left(\frac{\sin\frac{nx}{2}}{\tan\frac{x}{2}} - n\cos\frac{nx}{2}\right)\\ \gamma_n^2 &\equiv \frac{\pi^2|n|(n^2-1)}{3}\end{aligned} \tag{3.41}$$

These are then the eigenfunctions of $\tilde{K}$ with eigenvalue one, and the eigenfunctions of C_{1+2} with $h = 2$. They are defined only for $|n| \geq 2$.

To evaluate the shift in the eigenvalue when we move away from the conformal limit, we apply first-order perturbation theory and compute $\langle\Psi_{2,n}, \delta\tilde{K}\,\Psi_{2,n}\rangle$, where $\delta\tilde{K}$ is the leading correction to the conformal kernel, which is obtained by substituting $G_c + \delta G$ to G_c, and δG is the leading correction to the propagator. This correction, however, can be found analytically only in the limit of large q [4], where it is proportional to the function $f_0(\theta) \equiv 2 + \frac{\pi-|\theta|}{\tan\frac{\theta}{2}}$. For general q, one finds that

$$\frac{\delta G}{G_c} = -\frac{\alpha_G}{\beta\mathcal{J}}f_0 \tag{3.42}$$

where $\mathcal{J} \equiv \frac{\sqrt{q}}{2^{\frac{q-1}{2}}}J$, and α_G is found by numerically solving the SD equations (see figure 3.5), and in the limit of large q it behaves like $2/q$. Computing the shift in the eigenvalue then requires some involved calculations, and for brevity we report only the result

$$\begin{aligned}k(2,n) &= 1 - \frac{\alpha_K}{\beta\mathcal{J}}|n| + \dots\\ \alpha_K &\equiv -qk_c'(2)\alpha_G\end{aligned} \tag{3.43}$$

[4] In this limit the model simplifies considerably, and one can find the solutions to the SD equations at any temperature by perturbing in $1/q$.

Finally, we can compute the enhanced non-conformal contribution, and from (3.34) one obtains

$$\frac{\mathcal{F}_{h=2}(\theta_1,\theta_2,\theta_3,\theta_4)}{G(\theta_{12})G(\theta_{34})} = \frac{6\alpha_0}{\pi^2\alpha_K}\beta\mathcal{J}\sum_{|n|\geq 2}\frac{e^{in(y'-y)}}{n^2(n^2-1)}\left[\frac{\sin\frac{nx}{2}}{\tan\frac{x}{2}} - n\cos\frac{nx}{2}\right]\left[\frac{\sin\frac{nx'}{2}}{\tan\frac{x'}{2}} - n\cos\frac{nx'}{2}\right] \tag{3.44}$$
$$x=\theta_{12},\quad x'=\theta_{34},\quad y=\frac{\theta_1+\theta_2}{2},\quad y'=\frac{\theta_3+\theta_4}{2}$$

As we said earlier, this contribution is proportional to βJ, and so it is parametrically large with respect to the other contribution $\mathcal{F}_{h\neq 2}$, and it also violates the conformal invariance. Furthermore, the sum over n gives a particularly simple expression in the case where one is in the "ijij" configuration (i.e. the correlator is of the form $\langle\chi_i\chi_j\chi_i\chi_j\rangle$) and one sets two of the times at opposite angles in the circle, for example $\theta_3=0$ and $\theta_4=\pi$, which gives

$$\frac{\mathcal{F}_{h=2}(\theta_1,\theta_2,0,\pi)}{G(\theta_{12})G(\pi)} = -\frac{6\alpha_0}{\pi^2\alpha_K}\beta\mathcal{J}\left(\frac{\theta_{12}}{2\tan\frac{\theta_{12}}{2}} - 1 - \pi\frac{\sin\frac{\theta_1}{2}\sin\frac{\theta_2}{2}}{|\sin\frac{\theta_{12}}{2}|}\right) \tag{3.45}$$

This is the appropriate configuration for computing the correlation function (2.11), since the pairs of equal operators are alternating in the thermal circle. One can analytically continue this expression to the values $\theta_2=\frac{\pi}{2}-\frac{2\pi i}{\beta}t$ and $\theta_1=\theta_2-\pi$, finding

$$\frac{\mathcal{F}_{OTOC}(t)}{G(\theta_\pi)G(\pi)} = \frac{6\alpha_0}{\pi^2\alpha_K}\beta\mathcal{J}\left(1-\frac{\pi}{2}\cosh\frac{2\pi t}{\beta}\right) \tag{3.46}$$

After an initial time $\sim\frac{\beta}{2\pi}$, the hyperbolic cosine can be approximated with an exponential, and the expression (3.46) saturates the chaos bound (2.17), since the t-dependent part is $e^{\frac{2\pi t}{\beta}}$, therefore the system has a maximal Lyapunov exponent.

3.5 The Schwarzian action

In this section we derive the effective action that describes the reparametrisation modes, which are responsible for the dominant contribution of the four-point functions and the saturation of the scrambling time. We start by recalling the effective action in the bilocal fields that we derived in 1.2.2, generalised to the q-body interaction:

$$\frac{S_{eff}}{N} \equiv -\frac{1}{2}\operatorname{tr}\log\left(\partial_\tau-\tilde{\Sigma}\right)+\frac{1}{2}\int d\tau_1 d\tau_2\left(\tilde{\Sigma}(\tau_1,\tau_2)\tilde{G}(\tau_1,\tau_2)-\frac{J^2}{q}\tilde{G}(\tau_1,\tau_2)^q\right). \tag{3.47}$$

We expand it to up to second order by defining the fluctuations g and σ by $\tilde{G}\equiv G+\delta G = G+|G|^{\frac{q-2}{2}}g$ $\tilde{\Sigma}\equiv\Sigma+\delta\tilde{\Sigma}=\Sigma+|G|^{\frac{q-2}{2}}\sigma$, where G and Σ are the solutions of the saddle point equations

$$G(i\omega)^{-1} = i\omega-\Sigma(i\omega) \tag{3.48}$$
$$\Sigma(\tau_1,\tau_2) = J^2\,G(\tau_1,\tau_2)^q \tag{3.49}$$

For the expansion of the trace term, we obtain

$$\begin{aligned}
&\operatorname{tr}\log\left(\partial_\tau-\tilde{\Sigma}\right) = \\
&= \operatorname{tr}\log(\partial_\tau-\Sigma)+\operatorname{tr}\left(-(\partial_\tau-\Sigma)^{-1}*\delta\tilde{\Sigma}\right)-\frac{1}{2}\operatorname{tr}\left((\partial_\tau-\Sigma)^{-1}*\delta\tilde{\Sigma}*(\partial_\tau-\Sigma)^{-1}*\delta\tilde{\Sigma}\right)+\mathcal{O}(\sigma^3) \\
&\approx\cdots+\int d\tau_1\,d\tau_2\,d\tau_4\,d\tau_3\;G(\tau_{13})\,\delta\tilde{\Sigma}(\tau_{12})G(\tau_{24})\delta\tilde{\Sigma}(\tau_{43}) \\
&= \cdots+\int d\tau_1\,d\tau_2\,d\tau_4\,d\tau_3\;\sigma(\tau_{12})|G(\tau_{12})|^{\frac{q-2}{2}}G(\tau_{13})G(\tau_{24})|G(\tau_{43})|^{\frac{q-2}{2}}\sigma(\tau_{43}) \\
&= \cdots-\frac{(q-1)}{J^2}\int d\tau_1\,d\tau_2\,d\tau_3\,d\tau_4\;\sigma(\tau_{12})\tilde{K}(\tau_1,\tau_2;\tau_3,\tau_4)\sigma(\tau_{34})\,,
\end{aligned} \tag{3.50}$$

where the dots denote the zeroth and first order terms. In the third line we used $G = (\partial_\tau - \Sigma)^{-1}$, and in the last line we used the antisymmetry in the times of G and σ to relabel $\tau_3 \leftrightarrow \tau_4$ and the definition of the symmetric kernel

$$\tilde{K}(\tau_1, \ldots, \tau_4) \equiv -J^2(q-1)|G(\tau_{12})|^{\frac{q-2}{2}} G(\tau_{13})G(\tau_{24})|G(\tau_{34})|^{\frac{q-2}{2}} \ . \tag{3.51}$$

For the remaining terms, one straightforwardly obtains (using again $G = (\partial_\tau - \Sigma)^{-1}$)

$$\begin{aligned} &\int d\tau_1 d\tau_2 \left[\tilde{\Sigma}(\tau_1,\tau_2)\tilde{G}(\tau_1,\tau_2) - \frac{J^2}{q}\tilde{G}(\tau_1,\tau_2)^q\right] \\ &= \cdots + \int d\tau_1 d\tau_2 \left[\sigma(\tau_1,\tau_2)g(\tau_1,\tau_2) - J^2(q-1)g(\tau_1,\tau_2)^2\right] + \text{higher order terms} \end{aligned} \tag{3.52}$$

Discarding the constant terms (which do not matter), and the linear terms (which cancel against each other by the saddle-point equations), we are left with the quadratic action

$$\begin{aligned} \frac{S_{eff}}{N} = &-\frac{1}{4J^2(q-1)} \int d\tau_1 \ldots d\tau_4 \sigma(\tau_1,\tau_2)\tilde{K}(\tau_1,\ldots,\tau_4)\sigma(\tau_3,\tau_4) \\ &+ \frac{1}{2}\int d\tau_1 d\tau_2 \left[g(\tau_1,\tau_2)\sigma(\tau_1,\tau_2) - \frac{1}{2}J^2(q-1)g(\tau_1,\tau_2)^2\right] \ . \end{aligned} \tag{3.53}$$

Noticing that the integration measure is left invariant, $D\tilde{\Sigma}\, D\tilde{G} = D\sigma\, Dg$, we integrate over the σ fields to obtain

$$\begin{aligned} \frac{S_{eff}}{N} &= \frac{J^2(q-1)}{4}\int d\tau_1 d\tau_2 d\tau_3 d\tau_4 \ g(\tau_1,\tau_2)(\tilde{K}^{-1}(\tau_1,\ldots,\tau_4) - \delta(\tau_{13})\delta(\tau_{24}))g(\tau_3,\tau_4) \\ &= \frac{J^2(q-1)}{4}\,\langle g|\,\tilde{K}^{-1} - 1\,|g\rangle \end{aligned} \tag{3.54}$$

One can derive the four-point function by evaluating

$$\begin{aligned} &\frac{1}{N^2}\sum_{i,j}\langle\chi_i(\tau_1)\chi_i(\tau_2)\chi_j(\tau_3)\chi_j(\tau_4)\rangle = \int D\tilde{\Sigma}\, D\tilde{G}\, e^{-S_{eff}}\tilde{G}(\tau_1,\tau_2)\tilde{G}(\tau_3,\tau_4) \\ &= \int D\sigma\, Dg\, e^{-S_{eff}}|G(\tau_{12})|^{\frac{2-q}{q}} g(\tau_1,\tau_2)|G(\tau_{34})|^{\frac{2-q}{q}} g(\tau_3,\tau_4) \end{aligned} \tag{3.55}$$

Evaluating this gaussian integral with the appropriate contour gives back the expression (3.34) that we derived from a diagrammatic approach.

The analysis done so far is valid at any temperature, but now we go to the strong coupling limit $\beta J \gg 1$ where we can use the explicit expression of the saddle-point solution G_c in eq. (1.30). If we naively substitute G_c into the kernel, as we discussed earlier, the quadratic action in the fluctuations completely vanishes, due to the fact that the fluctuations of G_c under reparametrisations are eigenfunctions of the kernel with eigenvalue one. This is because in the IR limit we can drop the ∂_τ in the action (3.47) and it becomes invariant under reparametrisations. The Green's function G_c, however, is invariant only under the subgroup $SL(2,R)$. This means that, as we go towards the infrared, the action acquires an emergent reparametrisation invariance which is spontaneouly broken into $SL(2,R)$ by the saddle-point solution, and this generates an infinite number of Nambu-Goldstone modes, which are responsible for the dominant contribution to the four-point function.

To study the four-point function in the conformal limit, then, one needs to derive an effective action for these reparametrisation modes. One can do it by considering small reparametrisations $\tau \to \tau + \epsilon(\tau)$, to evaluate the fluctuations $\delta_\epsilon G_c$, which are eigenfunctions of $\tilde{K}$ with eigenvalue one, and substitute them in (3.54). We already derived this fluctuations in the last section, where we chose to decompose the reparametrisations in a Fourier basis and normalised them, arriving to the eigenfunctions (3.41).

Notice that in deriving (3.54) we have used $\delta_\epsilon G_c = |G|^{\frac{2-q}{2}} g$, so $g = |G|^{\frac{2-q}{2}} \delta_\epsilon G_c$ is an eigenfunction of the symmetric kernel $\tilde{K}$, but this time it is not normalised. Keeping the first correction in $1/(\beta J)$ to the eigenvalue, $\delta k(n) = -\frac{\alpha_K}{\beta \mathcal{J}}|n|$, we get

$$\begin{aligned} \frac{S_s}{N} &= \frac{J^2(q-1)}{4}(-\delta k)\langle g|g\rangle \\ &= \frac{J^2(q-1)}{4}\frac{\alpha_K}{\beta\mathcal{J}}\frac{16\pi^2}{3} b^q \left(\frac{\pi}{\beta}\right)^2 \sum_n n^2(n^2-1)|\epsilon_n|^2 \\ &= \frac{\alpha_s}{\mathcal{J}}\frac{8\pi}{\beta^3}\sum_n n^2(n^2-1)|\epsilon_n|^2 \,, \\ \alpha_s &\equiv \frac{\alpha_K}{6q^2\alpha_0} \end{aligned} \tag{3.56}$$

(α_0 was defined in (3.8)). Now we do the inverse Fourier transform of the n-dependent piece, which gives

$$\begin{aligned} &\sum_n n^2(n^2-1)|\epsilon_n|^2 = \sum_n \int \frac{d\theta_1 d\theta_2}{(2\pi)^2}\epsilon(\theta_1)\epsilon(\theta_2)e^{-in(\theta_1-\theta_2)}n^2(n^2-1) \\ &= \int \frac{d\theta_1 d\theta_2}{(2\pi)^2}\sum_n \epsilon(\theta_1)e^{-in\theta_1}\epsilon(\theta_2)\partial_{\theta_2}^2(\partial_{\theta_2}^2+1)e^{in\theta_2} \\ &= \int \frac{d\theta_1 d\theta_2}{(2\pi)^2}\underbrace{\sum_n e^{-in(\theta_1-\theta_2)}}_{2\pi\delta(\theta_1-\theta_2)}\epsilon(\theta_1)\partial_{\theta_2}^2(\partial_{\theta_2}^2+1)\epsilon(\theta_2) \\ &= \int_0^{2\pi}\frac{d\theta}{2\pi}[(\partial_\theta^2\epsilon)^2 - (\partial_\theta\epsilon)^2] \\ &= \left(\frac{\beta}{2\pi}\right)^3\int_0^\beta \frac{d\tau}{2\pi}\left[(\epsilon''(\tau))^2 - \left(\frac{2\pi}{\beta}\right)(\epsilon'(\tau))^2\right] . \end{aligned} \tag{3.57}$$

Putting everything together we obtain the action for infinitesimal reparametrisations:

$$\frac{S_s}{N} = \frac{\alpha_s}{\mathcal{J}}\frac{1}{2}\int_0^\beta d\tau\left[(\epsilon'')^2 - \left(\frac{2\pi}{\beta}\right)^2(\epsilon')^2\right] . \tag{3.58}$$

To generalise this action to finite reparametrisations $\tau \to f(\tau)$, let's start with the euclidean line. Since τ corresponds to small reparametrisations of the correlator (which is a power of f), let's consider a small deviation of τ from the origin

$$f(\tau) = f(0) + f'(0)\left(\tau + \frac{1}{2}\frac{f''(0)}{f'(0)}\tau^2 + \dots\right) \tag{3.59}$$

and compare it with $\tau+\epsilon(\tau)$. For small τ, then, we have a small reparametrisation with $\epsilon' = 0$ $\epsilon'' = \frac{f''}{f'}$, together with a scaling of f' and a translation of f, but this last transformations are not relevant since they belong to the $SL(2,R)$ group. Up to a total derivative, the action (3.58) then becomes

$$\begin{aligned} \frac{S_s}{N} &= \frac{\alpha_s}{\mathcal{J}}\int d\tau\,\mathrm{Sch}[f,\tau] \\ \mathrm{Sch}[f,\tau] &\equiv \frac{f'''}{f'} - \frac{3}{2}\left(\frac{f''}{f'}\right)^2 \end{aligned} \tag{3.60}$$

where we used $\frac{d}{d\tau}\left(\frac{f''}{f'}\right) = \mathrm{Sch}[f,\tau] + \frac{1}{2}\left(\frac{f''}{f'}\right)^2$. To get the action on the temperature circle one can just use $f(\tau) = \tan\left(\frac{\pi\tau}{\beta}\right)$. Notice that the Schwarzian $\mathrm{Sch}[f,\tau]$ is invariant under the SL(2,R) symmetry

$f \to \frac{af+b}{cf+d}$. The action (3.60), in fact, is the action with the minimum number of derivatives which is invariant under these transformations.

Another way to derive this action is by isolating the conformally-invariant part of the action (3.47) from the rest. To do this, we redefine the Lagrange multiplier $\tilde{\Sigma}$ with $\tilde{\Sigma} \to \tilde{\Sigma} - \partial_\tau = \tilde{\Sigma} - G_0^{-1}$, getting $S_{eff} = S_{CFT} + S_s$, with

$$\frac{S_{CFT}}{N} \equiv -\frac{1}{2}\operatorname{tr}\log\left(-\tilde{\Sigma}\right) + \frac{1}{2}\int d\tau_1 d\tau_2 \left(\tilde{\Sigma}(\tau_1,\tau_2)\tilde{G}(\tau_1,\tau_2) - \frac{J^2}{q}\tilde{G}(\tau_1,\tau_2)^q\right) \tag{3.61}$$

$$\frac{S_s}{N} \equiv -\frac{1}{2}\int d\tau_1 d\tau_2\, G_0^{-1}(\tau_1,\tau_2)\tilde{G}(\tau_1,\tau_2)\,. \tag{3.62}$$

S_{CFT} in fact is the reparametrisation-invariant part (recall that the SD equations gained this invariance when we dropped the $i\omega$ term), while the UV part S_s (which picks up small-times contributions since it contains a delta function) explicitly breaks this symmetry. Thus, to derive the reparametrisations effective action (in the low temperature limit), let's recall the transformation of $G_c(\tau_1,\tau_2) = \frac{b}{|\tau_{12}|^{2\Delta}}\mathrm{sng}(\tau_{12})$

$$G_c(\tau_1,\tau_2) \to [f'(\tau_1)f'(\tau_2)]^\Delta G_c(f(\tau_1),f(\tau_2)) \tag{3.63}$$

and expand it around $\tau \equiv \frac{\tau_1+\tau_2}{2}$ up to second order in powers of τ_{12}. One has

$$[f'(\tau_1)]^\Delta = f'(\tau)^\Delta + \Delta(f')^{\Delta-1}f''\frac{\tau_{12}}{2} + \frac{1}{2}\Delta(f')^{\Delta-2}[(\Delta-1)(f'')^2 + f'''\,f']\left(\frac{\tau_{12}}{2}\right)^2 + \dots \tag{3.64}$$

$$[f'(\tau_1)f'(\tau_2)]^\Delta = (f')^{2\Delta-2}\left\{(f')^2 + \Delta\left[-(f'')^2 + f'''\,f'\right]\left(\frac{\tau_{12}}{2}\right)^2\right\} + \dots \tag{3.65}$$

$$|f(\tau_1) - f(\tau_2)|^{-2\Delta} = |\tau_{12}|^{-2\Delta}|f'|^{-2\Delta}\left(1 - \frac{\Delta}{3}\frac{f'''}{f'}\left(\frac{\tau_{12}}{2}\right)^2 + \dots\right) \tag{3.66}$$

Putting all together we obtain

$$G_c(\tau_1,\tau_2) \to G_c(\tau_1,\tau_2)\left[1 + \frac{\Delta}{6}\mathrm{Sch}[f,\tau]\,\tau_{12}^2 + \mathcal{O}(\tau_{12}^3)\right]\,. \tag{3.67}$$

Then we finally insert this into the action (3.62) to get:

$$\begin{aligned}\frac{\delta S_s}{N} &= -\frac{1}{2}\int d\tau d\tau_{12}\, G_0(\tau_{12})^{-1}\delta\tilde{G}(\tau_{12})\left[\frac{\Delta}{6}\mathrm{Sch}[f,\tau]\,\tau_{12}^2 + \mathcal{O}(\tau_{12}^3)\right] \\ &\approx -\frac{\Delta}{12}\underbrace{\int d\tau_{12}\delta(\tau_{12})\partial_{\tau_{12}}(\tau_{12}^2\tilde{G}(\tau_{12}))}_{C}\int d\tau\,\mathrm{Sch}[f,\tau]\end{aligned} \tag{3.68}$$

The integral for the coefficient C, however, is indefinite, since

$$C \underset{\eta\equiv J\tau_{12}}{\propto} \int d\eta\,\delta(\eta)\partial_\eta(\eta^2\mathrm{sgn}(\eta)|\eta|^{-2\Delta}) \tag{3.69}$$

which contains products of functions that are divergent and other that are null for $\eta = 0$. To get a reasonable coefficient one should replace G_0 (which gives the delta function) with a smooth source and introduce UV and IR cutoffs as was done in [17], whose result agrees with (3.60).

Chapter 4

The holographic duality

We give here a very concise introduction to some concepts of quantum holography, as there is a great amount of literature on the subject, and to enter into the details is beyond the scope of this work. We will mainly follow the reference [7]. The holographic duality, or AdS/CFT correspondence, is the duality between quantum field theory in $d+1$ dimensions and general relativity in a $d+2$ dimensional spacetime[1]. The two theories are dual in the same way that particles and waves are dual through a Fourier transform. Here the correspondence revolves around the fact that the evolution of a QFT under the change of the energy scale (the Renormalisation Group flow) becomes, instead, an additional *geometric* dimension (often called the "radial direction") in the gravity dual. The main reason why this works is the "holographic principle", that states that the number of degrees of freedom of a gravitational system behaves as quantum field theory in a space with one dimension fewer (originating from the famous result of Bekenstein-Hawking entropy). In general, the correspondence relates stringy quantum gravity to quantum field theories, but the quantum gravity side is still mysterious, so we can only apply it in a specific limit where the theory becomes classical. The AdS/CFT duality, in fact, is a "weak-strong" duality, which relates strongly interacting QFTs with a large number of degrees of freedom to perturbative classical general-relativity. As an example, the AdS/CFT correspondence was first discovered by Maldacena by applying the so called "open/closed string duality" to $\mathcal{N} = 4$ supersymmetric $U(N)$ Yang-Mills theory and type IIB superstring theory in $AdS_5 \times S^5$, and the latter involves *classical* gravity in the limit where the first is at strong 't Hooft coupling, $Ng_{YM}^2 \gg 1$.

The theories belonging to this family of dual couples are then quite interesting, since they provide a common ground between two fundamental areas of physics that were previously incompatible with each other: quantum field theory and general relativity. Although the correspondence is still at the conjecture level, there are strong mathematical arguments in favour of it, and it already provided a lot of cross-fertilisation and unexpected new insights in different areas of physics, in particular in condensed-matter physics (where it takes the name "AdS/CMT"). We will now see a few basic concepts that will help to give an idea of how the holographic formalism works, and even though the AdS/CFT correspondence originates in the context of string theory, it can be applied without the use of any string-theoretical formalism.

4.1 AdS/CFT

The name "AdS/CFT" comes from the particular setting in which it was first discovered. To have an intuitive picture, one can imagine the set of theories obtained under the RG flow of a particular d+1 dimensional QFT in a flat Minkowski spacetime, with metric $ds^2 = \eta_{\mu\nu}\, dx^\mu dx^\nu = -dt^2 + d\vec{x}^2$ ($\mu, \nu = 0, \ldots, d$). Now let's "stack them together" along an additional direction r, corresponding to the energy scale, effectively creating a d+2 dimensional spacetime. If the QFT is invariant under

[1] Hence the name "quantum holography", in analogy with an optical hologram, where a 3D image is encoded on a 2D surface.

conformal transformations (which is the set of transformations that preserve the angles), hence a CFT, it is in particular invariant under scale transformations, $x^\mu \to \lambda x^\mu$ [2]. Since our starting theory is Poincaré-invariant, we already know that the metric of the d+2 dimensional spacetime must be of the form

$$ds^2 = f(r)\eta_{\mu\nu}\, dx^\mu dx^\nu + g(r)dr^2 \tag{4.1}$$

The fact that it is also invariant under scale transformations, under which $r \to \frac{r}{\lambda}$ (since we set r equal to the energy scale) restricts the metric to the form

$$ds^2 = \frac{r^2}{L^2}\eta_{\mu\nu}\, dx^\mu dx^\nu + \frac{L^2}{r^2}dr^2 \tag{4.2}$$

where L is a length scale called "AdS radius". This, in fact, is exactly the metric of a d+2 dimensional anti-de Sitter space. We notice now that the AdS metric is not only invariant under Lorentz and scale transformations, but under the full $SO(d+1,2)$ group, which corresponds to the conformal group. A characteristic of AdS space is that, although being formally infinite, objects propagating at the speed of light reach the edges of spacetime in a finite time. This means that the gravitational theory must be provided with specific boundary conditions. Since the boundary is $d+1$ dimensional, one can guess that it corresponds to the original QFT, and this intuition is indeed correct. To summarise the whole picture, we start from a CFT "living" in the boundary of an AdS space (which corresponds to the "UV"); as we integrate out the short-scale degrees of freedom, the theory "moves" towards the interior (which corresponds to the "IR"), and the whole process is encoded by the geometry of the bulk [3]. What field theory do we put in the gravitational part? The answer is not trivial, and in the next section we will see a few mathematical rules that will help to clear some aspects.

4.2 The mathematical rules

As an introductory example, let's see a somewhat heuristic arguments that relates two-point functions to the mass of the fields in the gravity dual. Let's consider the two point function of a "bare" (UV) scalar operator of a CFT. The conformal symmetry constraints it to be of the form

$$\langle O(x)O(0)\rangle = \frac{c}{|x|^{2\Delta}} \tag{4.3}$$

where Δ is the scaling dimension of the operator, c is a constant that depends on the normalisation, and $|x|$ is the euclidean distance $\sqrt{c^2\tau^2 + \vec{x}^2}$. Going to Fourier space, and Wick rotating to real time, we obtain the correlation function

$$\langle O(\omega,\vec{k})O(0)\rangle \sim k^{2\Delta-d-1} \sim (-\omega^2/c^2 + \vec{k}^2)^{\Delta-\frac{d}{2}-\frac{1}{2}} \tag{4.4}$$

Since we considered a scalar operator for the CFT, let's now introduce a scalar field in the AdS space, keeping in mind that the boundary should correspond to our starting field theory. We then consider the quadratic action

$$S[\phi] = \int d^{d+2}x\,\sqrt{-g}\left(-\frac{1}{2}g^{\mu\nu}\partial_\mu\phi\partial_\nu\phi - \frac{1}{2}m^2\phi^2\right) \tag{4.5}$$

which gives the equations of motion

$$\frac{1}{\sqrt{-g}}\partial_\mu\left(\sqrt{-g}g^{\mu\nu}\partial_\nu\phi\right) = 0 \tag{4.6}$$

Fourier-transforming the boundary coordinates, so that

$$\phi(x^\mu, r) = \int \frac{d\omega d^d\vec{k}}{(2\pi)^{d+1}} f_k(r) e^{ik^\mu x_\mu}\ , \tag{4.7}$$

[2] It is also conjectured the opposite, that is, if a unitary, Lorentz-invariant QFT is invariant under scale transformations, it must also be invariant under conformal transformations. At the moment this has been proven only in two dimensions.

[3] As Kitaev said [6][5], one can think of the curved metric as a "linear filter" that reproduces the same correlation functions.

and using the metric (4.2), one obtains the following equation for the radial components:

$$\left[\frac{\partial^2}{\partial r^2} + \frac{d+2}{r}\frac{\partial}{\partial r} - \left(\frac{k^2L^4}{r^4} + \frac{m^2L^4}{r^2}\right)\right] f_k(r) = 0 \tag{4.8}$$

Noticing that the solution should be a function of the ratio r/k, and assuming a power-law behaviour near the boundary ($r \to \infty$) we find

$$f_k(r) = r^{-d-1+\Delta}\left(A(k) + \mathcal{O}(k/r)\right) + r^{-\Delta}\left(B(k) + \mathcal{O}(k/r)\right) \tag{4.9}$$

where $A(k) = a\,k^{d+1-\Delta}$, $B(k) = b\,k^{\Delta}$, and

$$\Delta = \frac{d+1}{2} + \sqrt{\frac{(d+1)^2}{4} + m^2L^2} \tag{4.10}$$

To reconnect with the CFT result, since the boundary field theory should not be related to the "unphysical" dimension r, the information must be contained in the coefficients $A(k)$ and $B(k)$, which have a simple algebraic dependence in k. Given that the constants a and b are undetermined, and that the overall normalization should not matter, this suggests to consider the ratio

$$\frac{B(k)}{A(k)} = \frac{b}{a}k^{2\Delta-d-1}\ , \tag{4.11}$$

which has the same power-law in k of (4.4) (it can be shown, in fact, that generally $A(k)$ is proportional to the source of the field, and $B(k)$ to the response, so their ratio is related to the correlation function (4.4) by linear response theory). We see, then, that the scaling dimension of the original operator is related to the mass of the scalar field by equation (4.10). By a similar argument, one can also relate the stress-energy tensor $T_{\mu\nu}$, which generates global spacetime transformations in the CFT, to the metric tensor $g_{\mu\nu}(x)$, which instead is the gauge field related to this symmetries. This in fact is another deep feature AdS/CFT: *global* symmetries in the boundary field theory correspond to *local* gauge symmetries in the bulk.

The previous heuristic argument can actually be made in a rigorous way, and the set of mathematical rules that regulates the correspondence was developed by Gubser, Klebanov, Polyakov, and independently by Witten. At the heart of it, there is the GKPW rule, which allows us to apply the duality quantitatively:

$$Z_{CFT}(N) = \int D\phi\, \mathrm{e}^{iS_{AdS}} \tag{4.12}$$

where in the right-hand side the action depends on N in such a way that the integral reduces to its saddle-point in the limit $N \to \infty$. This equates the two partition functions of the theory, but it also applies in the presence of a source term, where the (more general) rule becomes

$$\langle e^{\int d^{d+1}x\, J(x)O(x)}\rangle_{QFT} = \int D\phi\, e^{iS_{bulk}[\phi(x,r)]_{|\phi(x,r=\infty)=J(x)}} \tag{4.13}$$

which equates the source J of the QFT to the boundary value of the field in the gravity dual. One can use it to derive correlation functions such as (4.3).

We conclude by stressing the fact that the large N limit of the theory is essential in order to have a classical theory in the gravity sector, which would be otherwise intractable.

4.3 Holography and the SYK model

The SYK model particularly interesting because it is, at the moment, the simplest "interesting" model of quantum holography that we know of [9]. Previously, there were two main families of large-N models: vector models and matrix models. The first one are particularly simple, since at

large N the self-energy is made of bubble diagrams which just shift the mass, and the mean-field theory describes a free system; large-N matrix models, instead, are composed of planar diagrams, which produce a much richer interaction, but they are difficult to solve. The SYK model, instead, still produces an interesting interaction while being solvable thanks to its peculiar structure. The model, however, is not actually a CFT, since the symmetry gets only approximated in the infrared limit, and the term "NCFT$_1$/NAdS$_2$" has been in coined [9] to describe one dimensional theories with an approximate conformal symmetry that are dual to an approximate anti-de Sitter space. The spontaneous breaking of the reparametrisation invariance in SYK produces a divergent four-point function in the low-temperature limit, and one must consider corrections of the order $(\beta J)^{-1}$ that explicitly break the symmetry. This corrections give rise to the dominant contribution of the four-point function and saturate the chaos bound. The same mechanism happens in AdS$_2$ dilaton gravity, where the conformal symmetry of the AdS space is broken by the presence of the dilaton field, and this gives rise to an effective action for the reparametrisation modes which has the same form as (3.60).

Contrary to the examples from string theory, the bulk theory of the gravitational dual is still unknown[4]. There are a few proposals, but for now we are still in the dark. There are, however, many things that we know about the bulk dual, and in principle one could compute all of its couplings order by order [14], even though the complete theory would remain unknown. The first things that one can say is that, since the four-point function of chapter 3 is made of an infinite series of conformal blocks with dimension h_m, in the bulk dual there is an infinite tower of scalar operators with mass given by the relation (4.10): their two-point function is given by $\langle O_m(x)O_m(0)\rangle = \frac{C_m}{|x|^{2h_m}}$. Their dual operators in the SYK models have the structure $\sum_i \chi_i \partial_\tau^{1+2m}\chi$ (this is a symbolic expression, since the derivatives have to be distributed between left and right in such a way that the operator is primary). The cubic couplings of these operators has been derived from the six-point function in [15].

[4]AdS/CFT examples from string theory, in fact, follow *top-down* approach where the two theories are known from the start, since they come from the "open/closed string" duality. The construction of holographic theories like the SYK model, instead, is called *bottom-up*, since one has to "engineer" the duality from a given QFT.

Chapter 5

NLO corrections

5.1 Coloured SYK

In this section we review the rules for generating higher order corrections in the 1/N expansion of the coloured SYK model following the derivation of [12]. In this case the action is given by

$$S[\chi] = \int \mathrm{d}t \left(\frac{1}{2} \sum_{a=1}^{f} \sum_{i_a=1}^{N} i\hbar \chi^a_{i_a} \frac{d}{dt} \chi^a_{i_a} + \frac{i^{f/2}}{f!} \sum_{i_1,\ldots,i_f} J_{i_1,\ldots,i_f} \chi^1_{i_1} \cdots \chi^f_{i_f} \right) \tag{5.1}$$

where the χ's are Majorana fermions and f is the number of colours/flavours. The $J_{i_1,\ldots,i_f}$ are random coupling with zero mean and covariance

$$\langle J_{i_1,\ldots,i_f} J_{l_1,\ldots,l_f} \rangle = \frac{J^2}{N^{f-1}} \prod_{a=1}^{f} \delta_{i_a,l_a} \tag{5.2}$$

The diagrams are then f-regular edge-coloured graphs: each colour is incident once and only once on each vertex. The disorder-average can be represented, as usual, with a dashed line, to which we assign the additional colour 0. For now we consider only vacuum diagrams, since the diagrams for 2p-points correlation functions can be obtained from vacuum graphs by cutting edges. Following the terminology from [12], we call "faces" the cycles[1] of a graph G alternating the colours 0 and i, and denote them with $F_{0i}(G)$, so that their total number in a graph G is

$$F_0(G) = \sum_{i=1}^{f} F_{0i}(G) \tag{5.3}$$

One can see that for each of this cycles the diagrams receives a factor of N given by the sum over the index. The reason is that whenever a disorder line connects the endpoints of edges with the same index it does not produce any additional constraint: the Kronecker delta produced by the disorder average is made redundant by the one contained in the propagator(s), and we are free to sum over that index. Thus the resulting power of N of the graph is

$$\chi_0(G) = F_0(G) - (f-1)E_0(G) \tag{5.4}$$

where $E_0(G)$ is the number of edges of colour 0.

We then construct a new graph $G_{/0}$ by contracting the edges of colour 0 in the graph G. Each vertex then has exactly two incident edges of the same colour for each colour, and the faces $F_{0i}(G)$ become single-coloured cycles $l_i(G_{/0})$. The number of vertices is now equal to $E_0(G)$, and the total number of independent loops is

$$L(G_{/0}) = (f-1)E_0(G) + 1 \tag{5.5}$$

[1] In this section by "cycles" we refer only to the *independent* cycles of the graph.

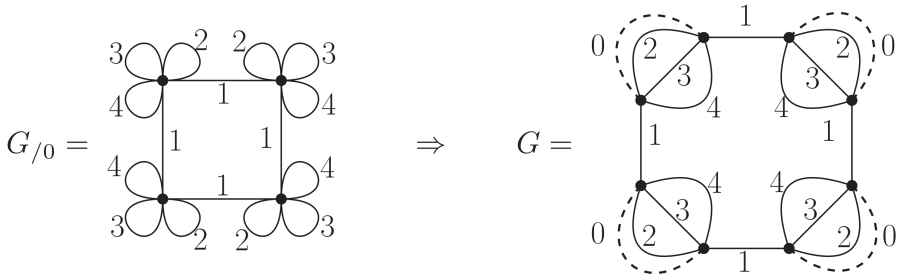

Figure 5.1: Example of LO vacuum graph and its contracted version. Taken from [12].

where we exploited the Euler's graph formula and the fact that we have a total of $f\,E_0(G)$ edges. This, together with 5.4, gives us

$$\chi_0(G) = \sum_{i=1}^{f} l_i(G_{/0}) - L(G_{/0}) + 1 \tag{5.6}$$

Since the sum in this equation gives the total number of single-coloured cycles we obtain

$$\chi_0(G) = -l_m(G_{/0}) + 1 \tag{5.7}$$

where $l_m(G_{/0})$ is the number of multicoloured cycles. We then see that at leading order we only have vacuum graphs with no multicoloured cycles, and that they are proportional to N, while at next-to-leading order there is one multicoloured cycle and the vacuum graphs' amplitudes are independent of N.

5.2 Generalised SYK model

We now extend the previous result to the generalised version of the SYK model proposed by Gross and Rosenhaus in [13], in which the action is

$$S\left[\chi\right] = \int \mathrm{d}t \left(\frac{1}{2} \sum_{a=1}^{f} \sum_{i=1}^{N_a} i\hbar\, \chi_i^a \frac{d}{dt} \chi_i^a + \frac{i^{q/2}}{\prod_{a=1}^{f} q_a!} \sum_I J_I \left(\chi_{i_1}^1 \dots \chi_{i_{q_1}}^1\right) \dots \left(\chi_{j_1}^f \dots \chi_{j_{q_f}}^f\right) \right) \tag{5.8}$$

where $I = i_1, \dots, i_{q_1}, \dots, j_1, \dots, j_{q_f}$ is a collective index. For simplicity, however, we will restrict to the case where $N_a = N$ for each a. Both the coloured SYK model and the "original" one constitute a particular case of this generalisation: the first corresponds to the case where $q_a = 1$ for each a, while the latter corresponds to the case $f = 1$.

The structure of the graphs is now the same, except for the fact that now we have multiple colours attached to each vertex, but we can apply the same reasoning if we consider the particle index i_{q_a} instead of the colour. The random couplings J_I, in fact, are totally antisymmetric, so that each vertex is connected only to edges with different particle indices. Therefore, we can say that the power of N of each graph G is given by (5.4), but $F_0(G)$ is now the total number of cycles which are composed by disorder lines and fermion lines with the same index. Following the same reasoning of the previous section, we can say that

$$\chi_0(G) = -l_m(G_{/0}) + 1 \tag{5.9}$$

where now $l_m(G_{/0})$ is the number of independent cycles composed of different particles. The presence of colour of the previous model is made redundant by the fact that the disorder average forces not only the colour to be equal, but also the particle index. We are able, then, to neglect the first and consider only the latter.

The reason why we can apply the same rules for the graphs of the coloured model to the generalised Gross-Rosenhaus model is simple. Consider for simplicity the original $\mathrm{SYK_q}$ model (which is the Gross-Rosenhaus one with $f = 1$). In the previous derivation we never used any assumption on the total number of fermions N, and we can lower it down to the limit case where $N = q$ (where the hamiltonian has only one interaction term). This is equivalent to considering a coloured SYK model with q colours and $N = 1$ fermions for each colour. This means that the diagrams of the $\mathrm{SYK_q}$ model are the same of a coloured SYK model with q colours, independently of N (and thus they have a chromatic index[2] equal to q). In the case of the Gross-Rosenhaus model, they are simply equal to the diagrams of a coloured model with $q_{tot} = \sum_{a=1}^{f} q_a$ colours. We can see that the diagrams of the generalised version have chromatic index q because they can be divided in two sets (see for example figure 5.4): the first set is made of bipartite graphs, which are known to have the minimum possible chromatic index, the other set is made of diagrams that can made bipartite by exchanging the ends of two fermion lines with the same index, so it still has the same chromatic index (in the limit of minimum N, colours and indices are the same).

5.3 NLO diagrams

We now focus on the vacuum diagrams contributing at NLO in the 1/N expansion. From (5.9) we see that these must have exactly one cycle made with different particle indices. We will assume each solid edge to be a fully dressed LO propagator. Both in the original and in the coloured version, then, these diagrams are characterised only by the "length" n of the multi-particle cycle. In the generalised version, however, we should also account for all the possible combinations of flavours with which we can construct the cycle. Figure 5.2 shows an example of a NLO vacuum graph in the case of $f = 4$ flavours and $q_a = 1$. By varying the number of fermions in the interaction and the number of flavours one can vary the number of "ears" attached to each vertex and the flavours of the fermions running in the main loop. As an example, in figure 5.3 we drew a multiparticle circle of length 4 in the case of 3 flavours (red, green and blue), $q_a = 1$ for red and green, and $q_a = 2$ for blue. When we restore the disorder lines, there are multiple ways to connected the edges, and this leads to the two families of graphs represented in figure 5.4: if there is an even number of crossings the graph belongs to the family on the left otherwise to the family on the right.

It has been shown in [18] that, for the coloured SYK model, also at NLO the conformal invariance (in the strong coupling regime) of the two-point function is preserved. Since the the structure of the diagrams is the same also for the Gross-Rosenhaus generalisation of the model, it follows that the conformality is preserved also for this generalisation. For the following orders, instead, this still remains to be checked, and it should be noted that at higher order in the large N expansion there are other contribution that we did not account for, namely possible replica off-diagonal contributions and corrections from the non-gaussianity of the probability distribution of the couplings.

5.4 Handlebody interpretation

In [17] Kitaev proposed an alternative visualisation for the counting of the power of N of the diagrams. For simplicity, let's restrict ourselves to the original q=4 model, and consider only vacuum diagrams. As we saw previously, the power of N is given by the the number of fermion indices minus (q-1) times

[2]The chromatic index of a graph is the minimum number of colours needed so that no edges with the same colour are incident to the same vertex.

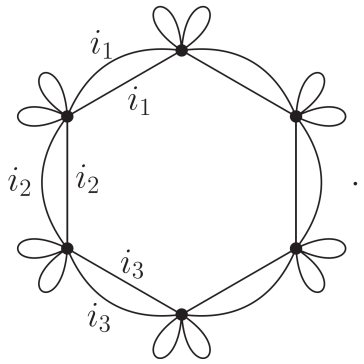

Figure 5.2: Example of a NLO vacuum graph's contracted version. Taken from [12].

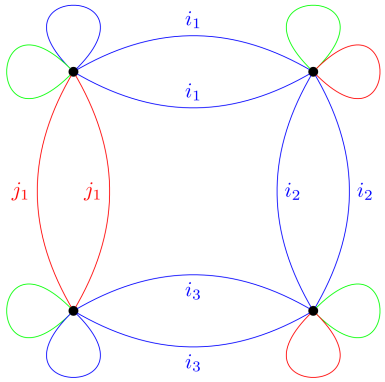

Figure 5.3: Example of a NLO vacuum graph's after the contraction of the disorder lines in the generalized version. Here the degree of interaction is 1 for the flavours red green, and 2 for the flavour blue.

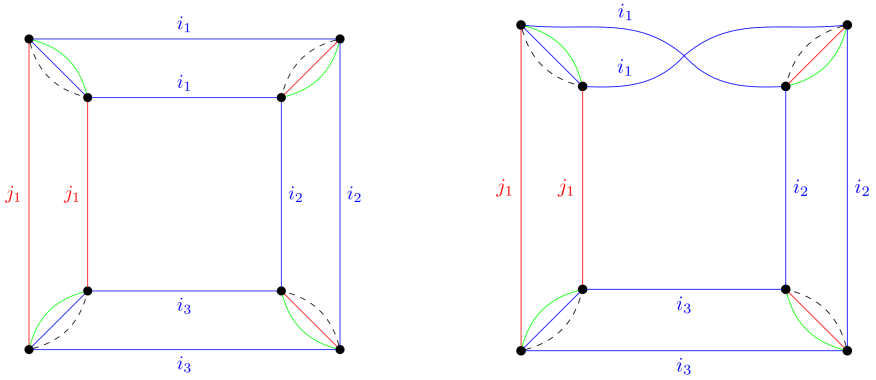

Figure 5.4: The two families of graphs coming from 5.3.

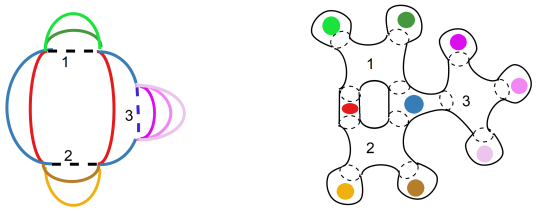

Figure 5.5: Next-to-leading order vacuum diagram and its corresponding handlebody of genus one. The dotted lines correspond to the 1-handles. Figure adapted from [17].

the number of disorder averages, so that

$$\begin{aligned}\text{power of N} &= (1-q)(\#\text{ of disorder avg.}) + (\#\text{ of indices}) \\ &= \underbrace{(\#\text{ of disorder avg.})}_{\frac{V}{2}} - \underbrace{(\#\text{ of times a line connects to a vertex})}_{=q\cdot\#\text{ of disorder avg.}=\frac{E}{2}} + \underbrace{(\#\text{ of indices})}_{\frac{F}{2}} \\ &= 1-g\end{aligned} \tag{5.10}$$

The notation under the brackets refers to the Euler counting of a corresponding multigraph, and in fact in the last line we obtained half of the the Euler characteristic $\chi = 2-2g$ of this multigraph. g is a quantity called "genus", which corresponds pictorially to the minimum number of "holes" of a 3D manyfold on which we can embed the graph so that none of the lines cross with each other (e.g. $g=0$ for a sphere, $g=1$ for a torus, and so on). The genus corresponding to each diagram can be seen more easily by constructing a related three-dimensional "handlebody". We build it by associating each fermion index and each pair of vertices joined by a disorder average to a 3-ball, and if a fermion index is connected to a vertex we connect the corresponding 3-balls with a 1-handle (see figure 5.5).

There is yet another interpretation of this counting, and it comes from the diagrammatic expansion of $\log\overline{\mathcal{Z}}$ related to the effective bilocal action (1.22). It contains a main part

$$-S_{eff,0}[\tilde{G},\tilde{\Sigma}] = -\frac{N}{2}\int d\tau d\tau' \tilde{\Sigma}(\tau,\tau')\tilde{G}(\tau,\tau') \tag{5.11}$$

and two perturbation terms, containing $\log\det\left(\partial_\tau - \tilde{\Sigma}\right)$ and $\tilde{G}^4$. The expectation value of $\tilde{\Sigma}\tilde{G}$ with respect to the main part of the action is easily obtained

$$\langle\tilde{\Sigma}(\tau_1,\tau_2)\tilde{G}(\tau_3,\tau_4)\rangle_0 = \frac{1}{N}(\delta(\tau_1-\tau_3)\delta(\tau_2-\tau_4) - \delta(\tau_1-\tau_4)\delta(\tau_2-\tau_3)) \tag{5.12}$$

The perturbative expansion of the log term, instead, gives[3]

$$N\log\frac{\det\partial_\tau - \tilde{\Sigma}}{\det\partial_\tau} = -N\left(\frac{1}{2}\operatorname{tr}\left(\hat{G}_b\tilde{\Sigma}\right) + \frac{1}{4}\operatorname{tr}\left(\hat{G}_b\tilde{\Sigma}\right)^2 + \frac{1}{6}\operatorname{tr}\left(\hat{G}_b\tilde{\Sigma}\right)^3 + \dots\right) \tag{5.13}$$

where $\hat{G}_b \equiv \partial_\tau^{-1}$. Since $\tilde{\Sigma}$ is a bilocal field, it must be represented not as a single line but as a surface (that we will call "sheet"). Each of these terms in this expansion can be depicted as a single sheet, contoured by n solid lines, corresponding to the n powers of $\hat{G}_b$, so that there are $2n$ endpoints of solid lines and n open ends of the sheet. These open ends are then connected by four-fold "seams" corresponding to the interaction term $\frac{NJ^2}{4}\tilde{G}(\tau,\tau')^4$. These seams carry combinatorial factor of 4! for the number of ways in which they can connect, and a factor of N^{-4} due to (5.12) taken four times, so overall we obtain a prefactor $\frac{3!J^2}{N^3}$. Finally, the overall sign of the diagram is determined by orienting each sheet and seam, and counting a factor of minus one for each connection where the orientation do

[3]The denominator is introduced to regularise the UV-divergence. The different sign in front of ∂_τ is due to a different definition of $\tilde{\Sigma}$.

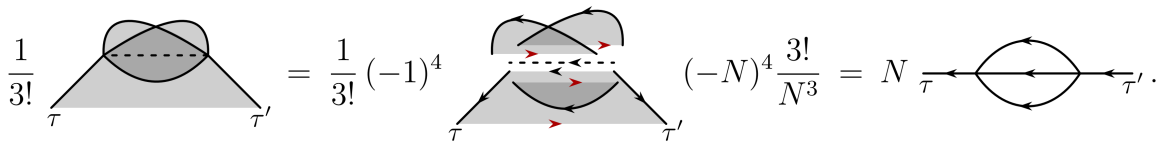

Figure 5.6: Example of LO diagram for the two-point function in the bilocal fields formulation. Taken from [17].

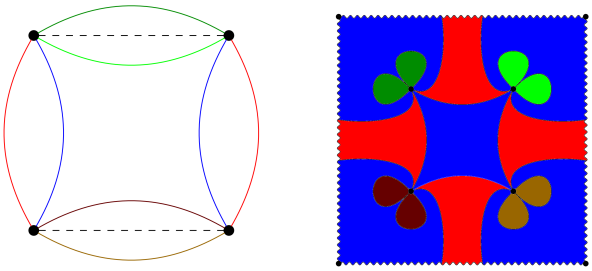

Figure 5.7: Simplest next-to-leading order diagram (left) and a related multigraph of genus one (right) with V=4, E=16, F=12 (each colour corresponds to a fermion index). The multigraph on the right should be seen on a torus obtained by gluing the top boundary with the bottom one and the left one with the right one.

not match (see figure 5.6). Finally, the three dimensional handlebody corresponding to each diagram can be seen as a tubular neighbourhood of the diagram made with sheets and seems.

Notice also that a similar counting of the powers of N in relation with the genus is was first implemented for large N matrix models (e.g. see paragraph 4.2.2 of [7]), in which case it lead to the conclusion that the diagrams contributing at leading order where planar diagrams, so that one had to consider each possible tiling of a surface at each order. Here we have a similar situation where the possible "tilings" of the surface are restricted at each order by the power of N, but we only have one kind of vertex.

Chapter 6

Generalisations in the disorder

It has been shown in [19] that the SYK model, in the limit of $N \to \infty$, retains its characteristics even in the case of a non-gaussian distribution of the couplings (with very few conditions). The proof is based on the idea that if the probability distribution of the couplings can be written as

$$P(\mathbf{J}) \propto \exp\left(-\frac{N^{q-1}}{\sigma^2}\mathbf{J}\mathbf{J} - V_N(\mathbf{J})\right) \tag{6.1}$$

where V_N is an analytic and O(N)-invariant potential, one can write a Polchinski-like flow equation which shows that in the large N limit the quadratic term dominates over the rest.

The intuitive idea behind this universal behaviour is that, with a mean-field approach in mind, one can consider the each fermion χ_i as immersed in a "thermal bath" made of all the remaining degrees of freedom,

$$\underbrace{\sum_{j,k,l=1}^{N} J_{ijkl}\chi_j\chi_k\chi_l}_{\text{thermal bath } \Sigma_i} \quad \chi_i \tag{6.2}$$

and when $N \to \infty$ the probability distribution of Σ_i will converge to a gaussian by the central limit theorem.

6.1 The uniform distribution

As an example, we choose compute the disorder-averaged partition function in the case of a uniform distribution for the $q = 4$ model. More precisely, assuming $J > 0$,

$$P\left[J_{ijkl}\right] = \theta\left(\frac{J^2}{N^3} - J_{ijkl}^2\right) \tag{6.3}$$

where here θ is the Heaviside step function, and the $1/N^3$ was introduced so that the variance scales with N as in the gaussian case. We then proceed as in section 1.2.2, replicating the action and averaging over the disorder, so that

$$\begin{aligned}
\overline{\mathcal{Z}^M} &= \int dJ_{ijkl}\, P[J_{ijkl}]\mathcal{Z}[J]^M \\
&= \int D\chi_i^\alpha \int_{-J/N^{3/2}}^{+J/N^{3/2}} dJ_{ijkl} \exp\left[-\sum_{\alpha=1}^{M}\int d\tau \left(\frac{1}{2}\sum_{i=1}^{N}\chi_i^\alpha\frac{d}{d\tau}\chi_i^\alpha + \frac{1}{4!}\sum_{i,j,k,l} J_{ijkl}\chi_i^\alpha\chi_j^\alpha\chi_k^\alpha\chi_l^\alpha\right)\right] \\
&= \int D\chi_i^\alpha \exp\left\{-\sum_{\alpha=1}^{M}\int d\tau \frac{1}{2}\sum_{i=1}^{N}\chi_i^\alpha\frac{d}{d\tau}\chi_i^\alpha - \sum_{i,j,k,l}\log\left(\sum_{\alpha=1}^{M}\int d\tau \frac{2\,4!\,\sinh\left(\frac{J}{N^{3/2}}\chi_i^\alpha\chi_j^\alpha\chi_k^\alpha\chi_l^\alpha\right)}{\chi_i^\alpha\chi_j^\alpha\chi_k^\alpha\chi_l^\alpha}\right)\right\}
\end{aligned} \tag{6.4}$$

In the large N limit we can expand both the hyperbolic sine and the logarithm, using

$$\log\left(\frac{\sinh x}{x}\right) = \log\left(\frac{1}{x}\sum_{n=0}^{\infty}\frac{x^{2n+1}}{(2n+1)!}\right) = \log\left(1+\sum_{n=1}^{\infty}\frac{x^{2n}}{(2n+1)!}\right) \overset{x\ll 1}{\approx} \frac{x^2}{3!} + \mathcal{O}(x^3) \tag{6.5}$$

and neglect the $2\,4!$ factor, obtaining

$$\overline{\mathcal{Z}^M} = \int D\chi_i \exp\left[-\frac{1}{2}\sum_{\alpha=1}^{M}\sum_{i=1}^{N}\int d\tau \chi_i^\alpha \frac{d}{d\tau}\chi_i^\alpha + \frac{J^2}{3!\,N^3}\int d\tau_1 d\tau_2 \sum_{\alpha,\beta}\left(\sum_{i=1}^{N}\chi_i^\alpha(\tau_1)\chi_i^\beta(\tau_2)\right)^4\right] \tag{6.6}$$

which is the same as the last line of (1.16) (although with a different numerical prefactor due to our definition of the edges of the uniform distribution), so we recover the original SYK model.

6.2 Correlations in the disorder

We will now attempt to slightly generalise the SYK_q model by introducing small "non-diagonal" correlations between the couplings. Up to now, in fact, we assumed that the couplings were completely uncorrelated with each other, so that

$$\langle J_{i_1,\dots,i_q} J_{i'_1,\dots,i'_q}\rangle = \frac{(q-1)!\,J^2}{N^{q-1}}\prod_{a=1}^{q}\delta_{i_a,i'_a} \tag{6.7}$$

We try instead to consider a more general version, where, for example[1]

$$\langle J_{a,i_2,\dots,i_q} J_{b,i'_2,\dots,i'_q}\rangle = \frac{(q-1)!\,J^2}{N^{q-1}}\lambda_{ab}\prod_{a=2}^{q}\delta_{i_a,i'_a} \tag{6.8}$$

with $|\lambda_{ab}-\delta_{ab}| \sim \epsilon \ll 1$ and $\lambda_{ab} = \lambda_{ba}$. To do this, let's consider, for example, a probability distribution

$$\begin{aligned} P_c(J_I) &= \frac{1}{\mathcal{N}}\exp\left[-\frac{1}{2\sigma^2}\left(\sum_{\substack{a,b,\\ i_2,\dots,i_q}}\lambda_{ab}\,J_{a,i_2,\dots,i_q}\,J_{b,i_2,\dots,i_q}\right)\right] \\ &= \frac{1}{\mathcal{N}}\exp\left[-\frac{1}{2\sigma^2}\left(\sum_I J_I^2 \;-\; \sum_{\substack{a,b,\\ i_2,\dots,i_q}}(\lambda_{ab}-\delta_{a,b})\,J_{a,i_2,\dots,i_q}\,J_{b,i_2,\dots,i_q}\right)\right] \end{aligned} \tag{6.9}$$

where $I \equiv i_1,\dots,i_q$ is a collective index, and $\sigma^2 \equiv \frac{(q-1)!\,J^2}{N^{q-1}}$. As a check, for $c \neq d$, let's compute

$$\begin{aligned} &\langle J_{c,i_2,\dots,i_q} J_{d,i_2,\dots,i_q}\rangle = \int DJ J_{c,i_2,\dots,i_q} J_{d,i_2,\dots,i_q} P_c(J_I) \\ &= \frac{1}{\mathcal{N}}\int DJ J_{c,i_2,\dots,i_q} J_{d,i_2,\dots,i_q} e^{-\frac{\sum_I J_I^2}{2\sigma^2}}\left(1-\frac{1}{2\sigma^2}\sum_{a,b}\lambda_{ab}(1-\delta_{a,b})J_{a,i_2,\dots,i_q}J_{b,i_2,\dots,i_q}+\mathcal{O}(\epsilon^2)\right) \\ &\approx -\frac{\lambda_{cd}}{\mathcal{N}\sigma^2}\int DJ J^2_{c,i_2,\dots,i_q} J^2_{d,i_2,\dots,i_q} e^{-\frac{1}{2\sigma^2}(\sum_I J_I^2)} \\ &\approx -\lambda_{cd}\,\sigma^2 = -\lambda_{cd}\frac{(q-1)!\,J^2}{N^{q-1}} \end{aligned} \tag{6.10}$$

[1] This section is to be taken just as a preliminary step for the next section, where we consider non-diagonal corrections in all q indices.

Before trying to compute the disorder-averaged partition function, we rewrite the probability distribution as

$$\begin{aligned} P_c(J_I) &\propto \exp\left[-\frac{1}{2\sigma^2}\left(\sum_{\substack{a,b,\\ i_2,\dots,i_q}} \lambda_{ab}\, J_{a,i_2,\dots,i_q}\, J_{b,i_2,\dots,i_q}\right)\right] \\ &= \exp\left[-\frac{1}{2\sigma^2}\left(\sum_{\substack{a,b,\\ i_2,\dots,i_q}} \underbrace{\sum_{j,k} P_{ja}\, P_{kb} D_j\, \delta_{jk}}_{\lambda_{ab}}\; J_{a,i_2,\dots,i_q}\, J_{b,i_2,\dots,i_q}\right)\right] \\ &= \exp\left[-\frac{1}{2\sigma^2}\left(\sum_{i_1,\dots,i_q} D_{i_1}\, \tilde{J}^2_{i_1,\dots,i_q}\right)\right] \end{aligned} \tag{6.11}$$

where P_{ij} are the elements of the matrix that diagonalises λ (since it is symmetric), D_j are the eigenvalues (in other words $P^T\lambda P = D$), and we defined $\tilde{J}_{i_1,\dots,i_q} \equiv \sum_a P_{i_1 a} J_{a,i_2,\dots,i_q}$. Now we try to compute the disorder averaged partition function following the approach of section 1.2.2. We have

$$\begin{aligned} \overline{\mathcal{Z}^M} &= \int D\chi DJ_I \exp\Big[-\frac{1}{2\sigma^2}\sum_{i_1,\dots,i_q} D_{i_1}\, \tilde{J}^2_{i_1,\dots,i_q} - \sum_{\alpha=1}^{M}\int d\tau\Big(\frac{1}{2}\sum_i \chi_i^\alpha \partial_\tau \chi_i^\alpha + \\ &+ \frac{1}{q!}\sum_{i_1,\dots,i_q} \tilde{J}_{i_1,\dots,i_q}\left(\sum_k P_{ki_1}\chi_k^\alpha\right)\chi_{i_2}^\alpha\cdots\chi_{i_q}^\alpha\Big)\Big] \\ &= \int D\chi \exp\left[-\sum_{\alpha=1}^{M}\int d\tau \frac{1}{2}\sum_i \chi_i^\alpha\partial_\tau\chi_i^\alpha + \frac{\sigma^2}{2q!}\sum_{i_1,\dots,i_q}\frac{1}{D_{i_1}}\left(\sum_\alpha\int d\tau\left(\sum_k P_{ki_1}\chi_k^\alpha\right)\chi_{i_2}^\alpha\cdots\chi_{i_q}^\alpha\right)^2\right] \\ &= \int D\chi \exp\Big[-\sum_{\alpha=1}^{M}\int d\tau\frac{1}{2}\sum_i\chi_i^\alpha\partial_\tau\chi_i^\alpha + \\ &+ \frac{\sigma^2}{2q!}\sum_{\alpha,\beta}\int d\tau_1\, d\tau_2 \sum_{i_1}\sum_{k,l}\frac{P_{ki_1}P_{li_1}}{D_{i_1}}\chi_k^\alpha(\tau_1)\chi_l^\beta(\tau_2)\left(\sum_i \chi_i^\alpha(\tau_1)\chi_i^\beta(\tau_2)\right)^{q-1}\Big] \end{aligned} \tag{6.12}$$

Notice that, if $D_j = D_k \equiv D\ \forall j,k$, we recover the original SYK with an additional factor of D in the interaction (and since we assumed λ to be close to the identity then $|D-1| \sim \epsilon \ll 1$). If instead they are different, the $O(N)$ symmetry would be explicitly broken by the disorder average, and we would obtain mixing terms in the S.D. equations. Here and in the original model this symmetry was explicitly broken in the individual realisations, but in the original model it was restored after the disorder average since the variance of the couplings was the same for each site. We then showed that, if we maintain the same symmetries, the behaviour of the model is not changed by this deviations. In this calculations, however, we assumed parametrically small correlations, so the next step would be to find for which value of this correlations the model starts to behave differently.

6.3 With q indices

Now let's consider the appropriate generalisation to the case where

$$\langle J_{i_1,\dots,i_q} J_{i'_1,\dots,i'_q}\rangle = \frac{(q-1)!\, J^2}{N^{q-1}}\prod_{a=1}^{q}\lambda_{i_a,i'_a} \tag{6.13}$$

with $\lambda_{ab} = \lambda_{ba} \equiv \delta_{ab} + \epsilon_{ab}$, $|\epsilon_{ab} \ll 1|$. To do this, let's consider as probability distribution

$$\begin{aligned} P_c(J_I) &= \frac{1}{\mathcal{N}} \exp\left[-\frac{1}{2\sigma^2} \left(\sum_{\substack{i_1,\dots,i_q \\ i'_1,\dots,i'_q}} \lambda_{i_1 i'_1} \dots \lambda_{i_q i'_q} J_{i_1,\dots,i_q} J_{i'_1,\dots,i'_q} \right) \right] \\ &= \frac{1}{\mathcal{N}} \exp\left[-\frac{1}{2\sigma^2} \left(\sum_{\substack{i_1,\dots,i_q \\ i'_1,\dots,i'_q}} \left(\sum_{j_1} P_{i_1 j_1} P_{i'_1 j_1} D_{j_1} \right) \dots \left(\sum_{j_1} P_{i_q j_q} P_{i'_q j_q} D_{j_q} \right) J_{i_1,\dots,i_q} J_{i'_1,\dots,i'_q} \right) \right] \\ &= \exp\left[-\frac{1}{2\sigma^2} \left(\sum_{j_1,\dots,j_q} D_{j_1} \dots D_{j_q} \tilde{J}^2_{j_1,\dots,j_q} \right) \right] \end{aligned} \tag{6.14}$$

where in the second line we have diagonalised the λ matrices with $\lambda_{ab} = \sum_{j,k} P_{aj} P_{bk} D_j \delta_{jk} = \sum_j P_{aj} P_{bj} D_j$, and in the last line we defined $\tilde{J}_{j_1,\dots,j_q} \equiv \sum_{i_1,\dots,i_q} P_{i_1 j_1} \dots P_{i_q j_q} J_{i_1,\dots,i_q}$. The averaged partition function becomes

$$\begin{aligned} \overline{\mathcal{Z}^M} &= \int D\chi DJ \exp\Bigg[-\frac{1}{2\sigma^2} \sum_{i_1,\dots,i_q} D_{j_1} \dots D_{j_q} \tilde{J}^2_{j_1,\dots,j_q} - \sum_{\alpha=1}^{M} \int d\tau \Bigg(\frac{1}{2} \sum_i \chi_i^\alpha \partial_\tau \chi_i^\alpha + \\ &+ \frac{1}{q!} \sum_{j_1,\dots,j_q} \tilde{J}_{j_1,\dots,j_q} \left(\sum_{i_1} P_{j_1 i_1} \chi^\alpha_{i_1} \right) \dots \left(\sum_{i_q} P_{j_q i_q} \chi^\alpha_{i_q} \right) \Bigg) \Bigg] \\ &= \int D\chi \exp\Bigg[-\sum_{\alpha=1}^{M} \int d\tau \frac{1}{2} \sum_i \chi_i^\alpha \partial_\tau \chi_i^\alpha \\ &+ \frac{\sigma^2}{2q!} \sum_{j_1,\dots,j_q} \frac{1}{D_{j_1} \dots D_{j_q}} \left(\sum_\alpha \int d\tau \left(\sum_{i_1} P_{j_1 i_1} \chi^\alpha_{i_1} \right) \dots \left(\sum_{i_q} P_{j_q i_q} \chi^\alpha_{i_q} \right) \right)^2 \Bigg] \\ &= \int D\chi \exp\left[-\sum_{\alpha=1}^{M} \int d\tau \frac{1}{2} \sum_i \chi_i^\alpha \partial_\tau \chi_i^\alpha + + \frac{\sigma^2}{2q!} \sum_{\alpha,\beta} \int d\tau_1 \, d\tau_2 \left(\sum_j \sum_{k,l} \frac{P_{jk} P_{jl}}{D_j} \chi^\alpha_k(\tau_1) \chi^\beta_l(\tau_2) \right)^q \right] \\ &= \int D\tilde{\chi} \exp\left[-\sum_{\alpha=1}^{M} \int d\tau \frac{1}{2} \sum_i \tilde{\chi}_i^\alpha \partial_\tau \tilde{\chi}_i^\alpha + + \frac{\sigma^2}{2q!} \sum_{\alpha,\beta} \int d\tau_1 \, d\tau_2 \left(\sum_j \frac{1}{D_j} \tilde{\chi}^\alpha_j(\tau_1) \tilde{\chi}^\beta_j(\tau_2) \right)^q \right] \end{aligned} \tag{6.15}$$

where in the last line we have redefined the fields as $\tilde{\chi}_i^\alpha(\tau) \equiv \sum_k P_{ik} \chi_k^\alpha(\tau)$, which does not change the measure. Following the same approach of section 1.2.2, we define the collective fields

$$\tilde{G}^{\alpha,\beta}(\tau_1, \tau_2) = \frac{1}{N} \sum_{i=1}^{N} \frac{1}{D_i} \chi_i^\alpha(\tau_1) \chi_i^\beta(\tau_2) \tag{6.16}$$

with the insertion of a delta function

$$\begin{aligned} &\delta\left(\tilde{G}^{\alpha,\beta}(\tau_1, \tau_2) - \frac{1}{N} \sum_{i=1}^{N} \frac{1}{D_i} \tilde{\chi}_i^\alpha(\tau_1) \tilde{\chi}_i^\beta(\tau_2) \right) \propto \\ &\propto \int D\tilde{\Sigma}^{\alpha,\beta}(\tau_1, \tau_2) \exp\left[-\frac{N}{2} \tilde{\Sigma}^{\alpha,\beta}(\tau_1, \tau_2) \left(\tilde{G}^{\alpha,\beta}(\tau_1, \tau_2) - \frac{1}{N} \sum_{i=1}^{N} \frac{1}{D_i} \tilde{\chi}_i^\alpha(\tau_1) \tilde{\chi}_i^\beta(\tau_2) \right) \right] \end{aligned} \tag{6.17}$$

and the bilocal effective action now becomes

$$\overline{\mathcal{Z}^M} = \int D\chi_i D\tilde{G}^{\alpha,\beta} D\tilde{\Sigma}^{\alpha,\beta} \exp\Big[-\frac{1}{2}\sum_{\alpha,\beta}\sum_{i=1}^{N}\int d\tau_1 d\tau_2\, \chi_i^{\alpha}(\tau_1)\left(\delta_{\alpha,\beta}\delta(\tau_{12})\frac{d}{d\tau_2} - \frac{1}{D_i}\tilde{\Sigma}^{\alpha,\beta}(\tau_1,\tau_2)\right)\chi_i^{\beta}(\tau_2) - \frac{N}{2}\sum_{\alpha,\beta}\int d\tau_1 d\tau_2\,\left(\tilde{\Sigma}^{\alpha,\beta}(\tau_1,\tau_2)\tilde{G}^{\alpha,\beta}(\tau_1,\tau_2) - \frac{J^2}{q}\tilde{G}^{\alpha,\beta}(\tau_1,\tau_2)^q\right)\Big] \tag{6.18}$$

We saw that in the original case we can assume replica-diagonal solutions for reasonable temperatures, and we do the same here (since we considered small deviations), with $\tilde{G}^{\alpha,\beta} \equiv \tilde{G}\delta_{\alpha\beta}$, in order to factorise the partition functions and take the limit $M \to 0$. If we integrate over the fermions, we obtain

$$\begin{aligned} \overline{\mathcal{Z}} &= \int D\tilde{G} D\tilde{\Sigma} \exp\left[-S_{eff,N}\right] \\ S_{eff,N} &\equiv -\frac{1}{2}\sum_{i=1}^{N}\operatorname{tr}\log\left(\partial_\tau - \frac{1}{D_i}\tilde{\Sigma}\right) + \frac{N}{2}\int d\tau_1 d\tau_2\left(\tilde{\Sigma}(\tau_1,\tau_2)\,\tilde{G}(\tau_1,\tau_2) - \frac{J^2}{q}\tilde{G}(\tau_1,\tau_2)^q\right) \end{aligned} \tag{6.19}$$

We see here more explicitly that, in the case where $D_j = D_k \equiv D\ \forall j,k$, we restore the $O(N)$ symmetry of the original model and we obtain the same S.D. equations. Here, instead, we cannot factorise the kinetic term and take the limit $N \to \infty$, which allowed us to consider only the solutions of the saddle-point equations. However, since we assumed small deviations, we can still assume that these solutions will be the main contribution. The equations we obtain are

$$\begin{aligned} &\Sigma(\tau) = J^2 G(\tau)^{q-1} \\ &\sum_{i=1}^{N}\frac{1}{i\omega_n - D_i^{-1}\Sigma(i\omega)} = G(i\omega) \end{aligned} \tag{6.20}$$

In the usual low energy limit $\omega_n \ll J$, they become

$$\begin{aligned} &\Sigma(\tau) = J^2 G(\tau)^{q-1} \\ &\Sigma(i\omega)\,G(i\omega)\left(\sum_{i=1}^{N} D_i\right)^{-1} = -1 \end{aligned} \tag{6.21}$$

so the model still exhibits an approximate conformal symmetry. More precisely, since the at the beginning we assumed $|\lambda_{ab} - \delta_{ab}| \ll 1$, the eigenvalues will be of the form $D_i = 1 + s_i$ with $|s_i| \ll 1$, so that the difference between this action and the one of the original model is

$$\begin{aligned} &\sum_{i=1}^{N}\operatorname{tr}\log\left(\partial_\tau - D_i^{-1}\tilde{\Sigma}\right) - N\operatorname{tr}\log\left(\partial_\tau - \tilde{\Sigma}\right) = \sum_{i=1}^{N}\operatorname{tr}\log\left(\frac{\partial_\tau - D_i^{-1}\tilde{\Sigma}}{\partial_\tau - \tilde{\Sigma}}\right) \\ &\approx \sum_{i=1}^{N}\operatorname{tr}\log\left(1 + s_i\frac{\tilde{\Sigma}}{\partial_\tau - \tilde{\Sigma}}\right) \approx \operatorname{tr}\log\left(\frac{\tilde{\Sigma}}{\partial_\tau - \tilde{\Sigma}}\right)\left(\sum_{i=1}^{N} s_i\right) \end{aligned} \tag{6.22}$$

Then we can rewrite the action as $\overline{\mathcal{Z}} = \int D\tilde{G} D\tilde{\Sigma} \exp\left[-N\,S_{eff}\right]$, with

$$\begin{aligned} S_{eff} \equiv &-\frac{1}{2}\operatorname{tr}\log\left(\partial_\tau - \tilde{\Sigma}\right) + \frac{1}{2}\int d\tau_1 d\tau_2\left(\tilde{\Sigma}(\tau_1,\tau_2)\,\tilde{G}(\tau_1,\tau_2) - \frac{J^2}{q}\tilde{G}(\tau_1,\tau_2)^q\right) + \\ &+ \left(\frac{1}{N}\sum_{i=1}^{N} s_i\right)\operatorname{tr}\log\left(\frac{\tilde{\Sigma}}{\partial_\tau - \tilde{\Sigma}}\right) \end{aligned} \tag{6.23}$$

so we can take the limit $N \to \infty$ and consider only the saddle-point equations since $\frac{1}{N}\sum_{i=1}^{N} s_i$ is small given our assumptions.

There are two things to take into consideration in the previous analysis. The first one is that we considered a specific form for the correlations in the couplings, and the fact that it was factorised in the couples of indices allowed us to switch to a diagonal basis of the fields where the equivalence to the original model is manifest. If one were to take the two-point correlation of the couplings to have a generic tensor form, the analysis is sure to be less trivial. The second thing is that the requirement of the couplings to be identically distributed is crucial in order for the free energy to be self-energy, and this is why it is reasonable to consider the previous eigenvalues D_i to be equal. If, instead, the probability distribution of the couplings was strongly dependent on the single sites involved, the thermodynamic limit of large N would no longer make sense, and each system would behave differently depending on the set of sites considered (so that one would then have to study a different theory for every single example).

Chapter 7

Sparse SYK

The attempts at producing an experimental realisation of the SYK model have been hampered by the huge amount of interaction terms in the hamiltonian, which is $\binom{N}{q} \underset{N\gg 1}{\approx} \frac{N^q}{q!}$. This problem has been drastically reduced by a variation called "sparse SYK" [21]. The idea behind it is that the peculiar properties of the SYK model, in particular the saturation of the chaos bound, derive from the high degree of connectivity between its components: the high number of interaction terms, combined with the strong coupling limit, makes so that the information of any perturbation introduced in the system gets "scrambled" as fast as possible across all the degrees of freedom, as we mentioned in chapter 2.

Except for some special phenomena like Anderson localisation, the scrambling time of a system is mainly determined by its geometry. Consider, for example, a hamiltonian defined on a d dimensional lattice with N sites and a nearest-neighbour interaction. Suppose, also, that the local dynamics of this system are characterised by a single timescale τ. If we perturb one of the sites, the perturbation will propagate ballistically (i.e. as if it is carried by quasiparticles), and it will take a time $t_* \sim N^{\frac{1}{d}}$ to affect the totality of the sites. The dimension of the space is then heavily tied to the size-scaling of the scrambling time. In the limit of d going to infinity the scrambling time becomes, instead, of order $\log N$. This result is not straightforward, since the couplings must be normalised in a specific in a specific N-dependent way, and one obtains the scrambling time only after some non-trivial calculations, as we saw for the SYK model. A similar result can be obtained, for example, if the N sites are arranged in a tree-like structure, since the maximum distance between any two vertices of a tree-graph is of order $\log N$. Another example is if they form a uniform tiling of a hyperbolic space, with a nearest-neighbour interaction: since the volume grows exponentially with the radius, information with ballistic propagation will cover a sphere of radius t/τ after a time t, and if the volume of the system is proportional to the number of sites, it will be covered in a time $\sim \tau \log N$.

The behaviour of all this examples can be characterised by considering the graph-structure of each of these hamiltonians, where each of the sites is represented by a vertex, and each couple of vertices is connected by an edge if the hamiltonian contains an interaction term between the corresponding sites. It turn out that lattices are a very particular kind of graph, while trees are more general. In fact, if one considers a connected graph of bounded degree[1] and with N randomly connected vertices, in the limit of N large, the local structure of the graph resembles a tree with high probability. In particular, the is a wide class of graphs, called "expander graphs" that will allow to reach the same scrambling time as the SYK model but with much fewer interaction terms. In the next section we present a simple argument, given in [21], that explains the powerful idea behind the choice of this kind of graphs. Since the following paragraphs involve some simple graph theory, we have added a list of necessary notions in appendix C (both for the unfamiliar reader, and to avoid ambiguity in the definitions).

[1] The degree of a graph is the maximum number of edges connected to a vertex.

7.1 Expander graphs

Consider a simple graph made of N vertices and with bounded degree. If one vertices is given a piece of information at $t = 0$, and this information takes a time λ^{-1} to be transmitted from one vertex to the adjacent ones, the time it takes for the information to spread to all vertices can be estimated in the continuum limit by

$$\frac{d|S_t|}{dt} = \lambda|\partial S_t| \tag{7.1}$$

where $|S_t|$ is the number of vertices that "know" the information at time t, and $|\partial S_t|$ is the number of unaffected vertices that are adjacent to the one the ones which have already been affected. This dynamic stops at the time t_* (the "scrambling" time) when all the vertices have been affected, and we can estimate it if we know the relation between $|S|$ and $|\partial S|$. For a lattice graph for a lattice graph of dimension/degree d, we have $|\partial S| \sim |S|^{1-\frac{1}{d}}$, and then $t_* \sim N^{\frac{1}{d}}$. Lattice graph are actually "sparse", since the number of edges is proportional to N, and one could just shorten the scrambling time by increasing the number of interactions, as in all-to-all model, where instead the number of interaction terms scales much faster. Expander graphs, instead, posses a much stronger connectivity than lattices while still having a number of edges proportional to N. In fact, for an expander graph G, each subgraph S containing less than half of the total number of vertices has a number of neighbouring vertices proportional to its size. This means that

$$|\partial S| \propto |S| \quad \forall\, S \text{ s.t. } |S| < \frac{|G|}{2}\,, \tag{7.2}$$

and inserting this in equation (7.1) we obtain a scrambling time $t_* \sim \log N$. In fact, while the diameter (i.e. the maximum number of edges that it takes to go from a vertex to another) of lattices is of order $N^{\frac{1}{d}}$, the diameter of an expander graph is of order $\log N$.

One could expect that such graphs must obey some particular construction, but it turns out that expander graphs are instead rather generic. In fact, it is known that random graphs where each vertex has the same degree, called random regular graphs, belong to this class. Even more, we could start with an complete graph (with all possible edges), and then randomly select the edges with a probability $p = \frac{2k}{N}$ (deleting the others), so that on average we remain with kN edges, and the degree of each vertex follows the Poisson distribution $P(2k)$. If $k > \frac{1}{2}$, the resulting graph (called "sparse random graph") will contain some disconnected components (to be discarded) and one *giant connected component* with a number of vertices of order N. This component, for large enough k, will be with high probability an expander graph. A visual comparison of these kinds of graphs is given in figure 7.1.

To apply the previous reasoning to the SYK model, we need to translate the hamiltonian into the corresponding graph. If the hamiltonian is 2-local, i.e. it contains interaction terms only between pairs of sites, one can construct a simple graph by translating sites into vertices and connecting them with an edge if and only if there is an interaction term between them. The $q = 2$ SYK model, however, is not an interacting model, therefore it cannot exhibit fast scrambling behaviour. We need to consider $q \geq 4$ model, which are translated to hypergraphs[2]. We can, though, consider the related interaction graphs, and if these are expanders, we can expect the model to exhibit fast scrambling.

7.2 Sparse SYK from random pruning

A first way to build the SYK model on expander graphs is by random pruning: we delete each interaction term (each hyperege) in the complete hamiltonian (1.44) with a probability $1 - p$, so that we are left, on average, with $L = p\binom{N}{q} \approx p\frac{N^q}{q!}$ terms (hyperedges). We also need to normalise the

[2]See appendix C

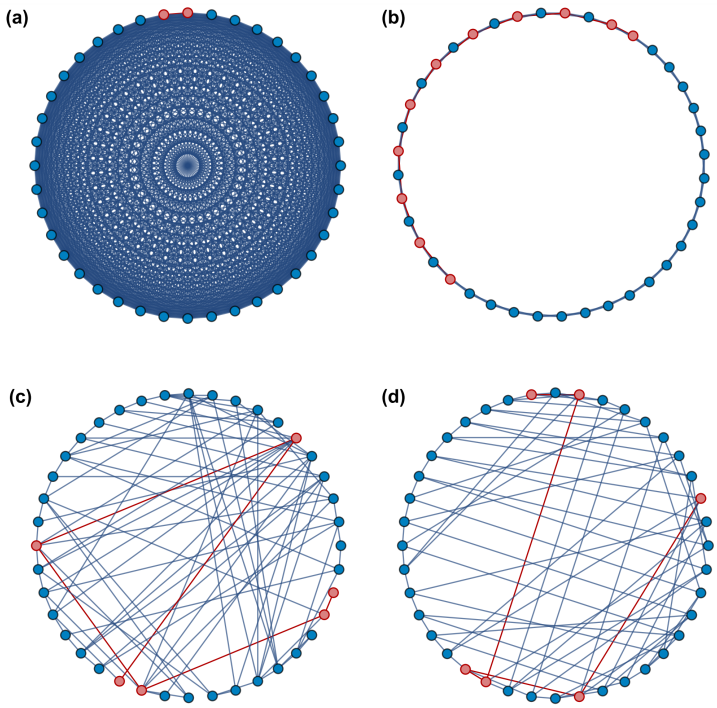

Figure 7.1: An complete graph (a), a one-dimensional lattice (b), a random graph (c) and a random regular graph (d). The diameter of each graph is highlighted in red. Taken from [21].

variance of the couplings as

$$\langle J^2_{i_1,\dots,i_q}\rangle = \frac{(q-1)!J^2}{N^{q-1}}\frac{1}{p}\,, \tag{7.3}$$

so that the energy remains the same. To see this, consider for example the basic melon diagram 1.2, which, for the complete case $p = 1$, gives a factor of

$$\frac{1}{2}\times\frac{1}{(q!)^2}\times\frac{(q-1)!J^2}{N^{q-1}}\times 2\times q\times q!\times N^{q-1} = J^2\,. \tag{7.4}$$

The origin of this factors is as follows: $\frac{1}{2}$ from second order expansion in perturbation theory, a $\frac{1}{q!}$ for each vertex from the prefactor in the hamiltonian, $\frac{(q-1)!J^2}{N^{q-1}}$ is the variance of the couplings, 2 is the permutation of vertices, q is the number of ways to connect the incoming line to the vertex, $q!$ for the number of ways to connect the two vertices, and N^{q-1} for the summation over internal indices. When $p < 1$, instead, the number of possible configurations gets multiplied by a factor of p, which cancels against the one we put in the variance. We also want the average number of remaining interactions to be proportional to N, i.e. $L = kN$, therefore the pruning probability must be

$$p = kN\binom{N}{q}^{-1} \approx \frac{kq!}{N^{q-1}}\,, \tag{7.5}$$

and k to be a positive constant.

One key difference with respect to the complete model, is that now we not only have a an expansion in the parameter $1/N$, but also in $1/(kq)$. One way to see this is to consider a series of two melon diagrams, as in figure 7.2. If the indices $j'k'l'$ in the second melon are a permutations of the jkl indices in the first, which happens in $\frac{3!}{N^3}$ terms for the $q = 4$ case or $\frac{(q-1)!}{N^{q-1}}$ in general, this contribution gets cancelled all together by the pruning of the corresponding interaction term. This means that we get a correction of

$$\delta = p\times\frac{(q-1)!}{N^{q-1}}\times\frac{1}{p^2} = \frac{(q-1)!}{pN^{q-1}}\,. \tag{7.6}$$

The first term is the probability of the corresponding coupling to be cancelled, the second is the number of term involved, and the last is the correction we introduced in the coupling variance. Moreover, using

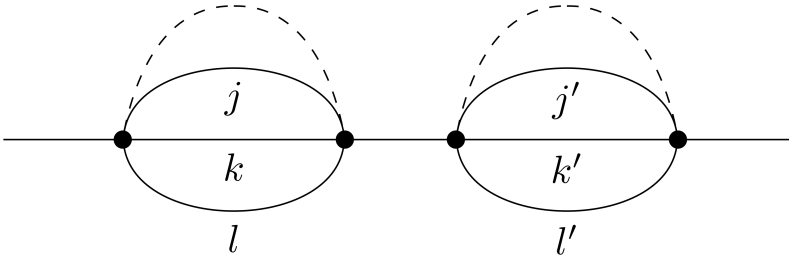

Figure 7.2: Diagrammatic contribution to the two point function in the case $q = 4$.

(7.5), we find that this correction approaches $\delta \approx \frac{1}{kq}$. Besides the factor of q, which is due to the chances of a fermion appearing in each interaction term, we see that in the $k >> 1$ limit we recover the diagrammatics of the complete model. If we take $N \to \infty$ and keep k finite, instead, we still have corrections organised in a $1/k$ expansion.

7.3 Sparse SYK from random regular hypergraphs

The above method, while generally easy to implement, contains a few inconvenience: the possible creation of disconnected clusters, and the fluctuations in the connectivity of the single fermions. One can avoid this issues by considering regular random hypergraphs, where we impose each vertex to have the same degree. If we want the total number of interaction terms to be $L = kN$, this degree must be equal to kq. To construct our model we define then the random variables $x_{i_1 \dots i_q} \in 0, 1$, with $i_a = 1, \dots, N$, and impose that

$$\frac{1}{(q-1)!} \sum_{i_2,\dots,i_q} x_{i_1 \dots i_q} = kq \quad \forall i_1 \ . \tag{7.7}$$

The hamiltonian of the sparse-SYK is then

$$H_S = \frac{i^{\frac{q}{2}}}{q!} \sum_{i_1,\dots,i_q} x_{i_1 \dots i_q} J_{i_1 \dots i_q} \chi_{i_1} \cdots \chi_{i_q} \tag{7.8}$$

where now the couplings have the variance

$$\langle J^2_{i_1 \dots i_q} \rangle = \frac{J^2}{kq} \ . \tag{7.9}$$

Notice that the variables $x_{i_1 \dots i_q}$ are symmetric under permutations of the indices. The same form of the hamiltonian can be used also for the random-pruning case if we consider the $x_{i_1 \dots i_q}$ to be random independent variables without the restriction (7.7) and with $\Pr\big(x_{i_1 \dots i_q} = 1\big) = p$.

7.4 Disorder-averaged partition function

In this section we apply the disorder average through the usual replica trick, however, before proceeding, we mention that in this case it must be applied more carefully, since the free energy is no longer self-averaging. To simplify the notations we introduce the collective index $I \equiv i_1 \dots i_q$ and the notation $\Phi^\alpha_I \equiv \chi^\alpha_{i_1} \dots \chi^\alpha_{i_q}$ ($\alpha = 1, \dots, m$ is the usual replica index). We obtain (averaging only on the

couplings, not on the pruning variables $x_{i_1\dots i_q}$)

$$\begin{aligned}\overline{\mathcal{Z}^m} &= \int d\mathbf{J} P(\mathbf{J}))\mathcal{Z}^m \\ &= \int d\mathbf{J} D\chi_i^\alpha \exp\left[-\frac{kq}{2J^2}\sum_I J_I^2 - \sum_{\alpha=1}^m \int d\tau \left(\frac{1}{2}\sum_{i=1}^N \chi_i^\alpha \partial_\tau \chi_i^\alpha + \frac{i^{\frac{q}{2}}}{q!}\sum_I x_I J_I \Phi_I^\alpha\right)\right] \\ &= \int D\chi_i^\alpha \exp\left[-\sum_{\alpha=1}^m \int d\tau \left(\frac{1}{2}\sum_{i=1}^N \chi_i^\alpha \partial_\tau \chi_i^\alpha\right) + \frac{\langle J_I^2\rangle}{2q!}\sum_{\alpha,\beta}\int d\tau_1 d\tau_2 \sum_I x_I \Phi_I^\alpha(\tau_1)\Phi_I^\beta(\tau_2)\right] .\end{aligned} \tag{7.10}$$

Since the presence of the x_I explicitly breaks the O(N) symmetry, this time we define the bilocal fields as

$$G_i^{\alpha\beta}(\tau_1,\tau_2) = \chi_i^\alpha(\tau_1)\chi_i^\beta(\tau_2) \tag{7.11}$$

by inserting the delta function

$$\delta\left(G_i^{\alpha\beta}(\tau_1,\tau_2) - \chi_i^\alpha(\tau_1)\chi_i^\beta(\tau_2)\right) \propto \int D\Sigma_i^{\alpha\beta}(\tau_1,\tau_2)\exp\left[-\frac{1}{2}\Sigma_i^{\alpha\beta}\left(G_i^{\alpha\beta}(\tau_1,\tau_2) - \chi_i^\alpha(\tau_1)\chi_i^\beta(\tau_2)\right)\right] . \tag{7.12}$$

After integrating out the fermions, we are left with a familiar effective action

$$S_{eff}[\Sigma,G] = -\frac{1}{2}\sum_i \log\det\left(\delta^{\alpha\beta}\partial_\tau - \Sigma_i^{\alpha\beta}\right) + \frac{1}{2}\sum_{\alpha,\beta}\int d\tau_1 d\tau_2 \left(\sum_i \Sigma_i^{\alpha\beta}G_i^{\alpha\beta} - \frac{\langle J_I^2\rangle}{q!}\sum_I x_I G_{i_1}^{\alpha\beta}\dots G_{i_q}^{\alpha\beta}\right) \tag{7.13}$$

where this time we have purposely kept the replica dependence. The equations of motions coming from this action are

$$G_i^{\alpha\beta}(\omega)^{-1} = i\omega - \Sigma_i^{\alpha\beta}(\omega) \tag{7.14}$$

$$\Sigma_{i_1}^{\alpha\beta} = \langle J_I^2\rangle \sum_{i_2<\dots<i_q} x_{i_1 i_2\dots i_q} G_{i_2}^{\alpha\beta}\dots G_{i_q}^{\alpha\beta} \tag{7.15}$$

In this case, however, we cannot take the limit $N\to\infty$ (since the action does not depend explicitly on N): this means that the fluctuations around the saddle point may be an important contribution to consider.

7.5 Regular graphs and fluctuations

In this section we study the fluctuations around a replica diagonal saddle-point for the case of random regular hypergraphs. Non-diagonal saddle solutions do exist even in the complete case, but they are subleading in the large N limit for any reasonable temperature (e.g see appendix A.2). In the sparse case, we see from (7.14) that, if the solutions are uniform in the site index (independently of i), they obey the same equations of motions of the fully connected case (as long as the couplings obey $\langle J_I^2\rangle = \frac{J^2}{kq}$, as we mentioned earlier). We can see from (7.7) that there are indeed uniform solutions to the sparse E.O.M.s, and by analogy with the complete case we expect this solutions to be dominated by the replica-diagonal ones. The problem is that, contrary to the original model, the fluctuations of the sparse model give a relevant contribution at leading-order in N. This fluctuations, however, are suppressed by $1/(kq)$, while the saddle-point is not, so if k is large enough we can still expect the saddle-point contribution to be dominant.

After considering the ansatz of a uniform and replica-diagonal saddle point, we proceed to study the fluctuations around it. To do it, we follow again the approach of [9] for the complete model, though

his time we have kept the replica and site dependence. Let's follow again the steps of section 3.5, but with a bit more attention to the interaction term, that gives

$$\begin{aligned}
&-\frac{J^2}{kq}\frac{1}{2q!}\sum_{\alpha,\beta}\sum_{i_1,\dots,i_q} x_{i_1\dots i_q}(G_s+\delta\tilde{G}^{\alpha\beta}_{i_1})\dots(G_s+\delta\tilde{G}^{\alpha\beta}_{i_q})\\
&=\dots-\frac{J^2}{kq}\frac{1}{2q!}G_s^{q-2}\sum_{\alpha,\beta}\sum_{i_1,\dots,i_q} x_{i_1\dots i_q}\left(\delta\tilde{G}^{\alpha\beta}_{i_1}\delta\tilde{G}^{\alpha\beta}_{i_2}+\text{all other pairs}\right)+\mathcal{O}(\delta G^3)\\
&\approx\dots-\frac{J^2}{kq}\frac{1}{2q!}\frac{q(q-1)}{2}G_s^{q-2}\sum_{\alpha,\beta}\sum_{i,j,i_3,\dots,i_q} x_{iji_3\dots i_q}\,\delta\tilde{G}^{\alpha\beta}_{i}\delta\tilde{G}^{\alpha\beta}_{j}\\
&=\dots-\frac{J^2}{kq}\frac{1}{4(q-2)!}G_s^{q-2}\sum_{\alpha,\beta}\sum_{i,j,i_3,\dots,i_q} x_{iji_3\dots i_q}\,\delta\tilde{G}^{\alpha\beta}_{i}\delta\tilde{G}^{\alpha\beta}_{j}\\
&=\dots-\frac{J^2(q-1)}{4}G_s^{q-2}\sum_{\alpha,\beta}\sum_{i,j}M_{ij}\,\delta\tilde{G}^{\alpha\beta}_{i}\delta\tilde{G}^{\alpha\beta}_{j}
\end{aligned}\tag{7.16}$$

where the dots denote zeroth and first order terms, G_s is the uniform saddle-point solution, and M_{ij} is a rescaled adjacency matrix defined by

$$M_{ij}=\frac{1}{kq(q-1)}\sum_{i_3<\dots<i_q} x_{iji_3\dots i_q}\,. \tag{7.17}$$

In fact, $\sum_{i_3<\dots<i_q} x_{iji_3\dots i_q}$ counts the number of interaction terms between between the sites i and j. We then obtain a quadratic action in the fluctuations

$$\begin{aligned}
\delta S_{eff}=&\frac{1}{4}\sum_{\alpha,\beta}\sum_{i}\int d\tau_1\dots d\tau_4\,\delta\tilde{\Sigma}^{\alpha\beta}_i(\tau_1,\tau_2)G_s(\tau_1,\tau_3)G_s(\tau_2,\tau_4)\delta\tilde{\Sigma}^{\alpha\beta}_i(\tau_3,\tau_4)\\
&+\frac{1}{2}\sum_{\alpha,\beta}\sum_{i}\int d\tau_1 d\tau_2\left(\delta\tilde{\Sigma}^{\alpha\beta}_i(\tau_1,\tau_2)\delta\tilde{G}^{\alpha\beta}_i(\tau_1,\tau_2)\right)\\
&-\frac{J^2(q-1)}{4}\sum_{\alpha,\beta}\sum_{i,j}\int d\tau_1 d\tau_2\left(M_{ij}G_s^{q-2}(\tau_1,\tau_2)\delta\tilde{G}^{\alpha\beta}_i(\tau_1,\tau_2)\delta\tilde{G}^{\alpha\beta}_j(\tau_1,\tau_2)\right)
\end{aligned}\tag{7.18}$$

We then split the fluctuations into a replica diagonal and an off-diagonal part,

$$\begin{aligned}
\delta\tilde{G}^{\alpha\beta}&=g_d\,\delta^{\alpha\beta}+g^{\alpha\beta}_{nd}\\
\delta\tilde{\Sigma}^{\alpha\beta}&=\sigma_d\,\delta^{\alpha\beta}+\sigma^{\alpha\beta}_{nd}
\end{aligned}\tag{7.19}$$

and we also assume them to be replica symmetric, so that $g^{\alpha\beta}_{nd}\equiv g_{nd}\ \forall\alpha\neq\beta$ (and the same for σ). The quadratic action then decouples into two parts, since $g_d\delta^{\alpha\beta}\,g^{\alpha\beta}_{nd}=0$, and the interaction part contributes only to the diagonal action. The interaction contributes can contribute to the off-diagonal part only at order q or higher because at lower orders there is at least one factor of $G_s\delta^{\alpha\beta}$ (since we expanded the action around a replica diagonal saddle point). Therefore we can write $\delta S_{eff}=m\delta S_{eff,d}+m(m-1)\delta S_{eff,nd}$, where

$$\delta S_{eff,d}=\frac{1}{4}\sum_i\int d^4\tau\,\sigma_{i,d}G_sG_s\sigma_{i,d}+\frac{1}{2}\sum_i\int d^2\tau\sigma_{i,d}g_{i,d}-\frac{J^2(q-1)}{4}\sum_{i,j}\int d^2\tau M_{ij}G_s^{q-2}g_{i,d}g_{j,d} \tag{7.20}$$

$$\delta S_{eff,nd}=\frac{1}{4}\sum_i\int d^4\tau\,\sigma_{i,nd}G_sG_s\sigma_{i,nd}+\frac{1}{2}\sum_i\int d^2\tau\,(\sigma_{i,nd}g_{i,nd}) \tag{7.21}$$

(we omitted the time dependences to lighten the notation). We then rescale the fluctuations as in section 3.5, $g \to |G_s|^{\frac{2-q}{2}} g$ and $\sigma \to |G_s|^{\frac{q-2}{2}} \sigma$, and do the gaussian gaussian integral over the σ fields, which gives

$$\delta S_{eff,d} = \frac{J^2(q-1)}{4} \sum_l \tilde{g}_{d,l} (\tilde{K}^{-1} - \lambda_l) \tilde{g}_{d,l} + \frac{N}{2} \log\det \tilde{K} \ , \qquad \tilde{g}_{d,l} = \sum_i P_{il} g_{d,i} \tag{7.22}$$

$$\delta S_{eff,nd} = \frac{J^2(q-1)}{4} \sum_i g_{nd,i} \, \tilde{K}^{-1} \, g_{nd,i} + \frac{N}{2} \log\det \tilde{K} \tag{7.23}$$

where λ_l eigenvalue of M, P is the matrix to diagonalise it, $\tilde{K}$ is the usual symmetric kernel of the complete model.

We then restrict the analysis to the low temperature case, where the spectrum of K^{-1} is known thanks to the conformal symmetry. (see chapter 3). The eigenvalues of K^{-1} start at one for the discrete case $h = 2, 4, 6, \dots$, and have a negative upper bound for the continuum case $h = \frac{1}{2} + is$ (we will discuss this more precisely in section 7.7). As consequence, all the modes of the off-diagonal fluctuations are gapped, independently of the interaction graph (as long as k is large enough). The diagonal part, instead, depends on the eigenvalues of the adjacency matrix. To study these eigenvalues, let's compare this analysis with the complete case of the original model. To obtain the adjacency matrix for the complete case, we replace the kq in the normalisation of the coupling variance with the original $\frac{N^{q-1}}{(q-1)!}$, and set all the x_I to one, obtaining

$$M_{ij}^{complete} = \frac{(q-1)!}{N^{q-1}} \frac{1}{(q-1)!} \sum_{i_3,\dots,i_q} 1 = \frac{1}{N} \quad \forall i \neq j \tag{7.24}$$

(the diagonal elements are all zero). This matrix has one eigenvalue equal to $\frac{N-1}{N} \approx 1$, corresponding to the uniform vector $(1, 1, 1, \dots)$, while the rest of the eigenvalues are equal to $-1/N \approx 0$ (for the corresponding eigenvectors one can choose $N-1$ vectors with zeroes everywhere except -1 for the first component and 1 in the i-th component, with $i = 2, \dots, N$).

In the case of a random regular graph, the matrix M has one eigenvalue equal to one, corresponding again to the uniform mode (which is always the maximum eigenvalue for regular graphs); this can be seen from equation (7.7), which implies $\sum_j M_{ij} = 1$. In general, all the the other eigenvalues are not zero, but they still obey certain helpful bounds. One can, in fact, write the adjacency matrix as

$$M = \frac{1}{kq(q-1)} (AA^T - kq\mathbb{I}) \tag{7.25}$$

where A is the incidence matrix of the hypergraph, and this ensures that the eigenvalues are bounded below by $-1/(q-1)$ (so that there is a gap between them and the continuum spectrum of K). Furthermore, for regular graphs [21], the eigenvalues below the maximum one[3] obey

$$\max(0, \sqrt{kq-1} - \sqrt{q-1})^2 - kq \leq kq(q-1)\lambda_l \leq 2\sqrt{kq-1}\sqrt{q-1} + q - 2 \tag{7.26}$$

which ensures that the corresponding modes are also gapped. We then separate the uniform mode, which we call $\tilde{g}_0 \equiv \frac{1}{\sqrt{N}} \sum_i g_{d,i}$, from all the others, obtaining

$$\delta S_{eff,d} = \frac{J^2(q-1)}{4} \tilde{g}_0 (\tilde{K}^{-1} - 1) \tilde{g}_0 + \frac{J^2(q-1)}{4} \sum_l \tilde{g}_{d,l} (\tilde{K}^{-1} - \lambda_l) \tilde{g}_{d,l} + \frac{N}{2} \log\det \tilde{K} \tag{7.27}$$

Since the uniform mode is gapless, we expect the system to exhibit a similar dynamic to the original model (the enhanced contribution to the four-point function due to the symmetry breaking of the emergent conformal symmetry, described by the Schwarzian action of section 3.5). If there are other gapless modes, these would also contribute to the low-energy dynamics, and this case has yet to be studied.

[3] Except for the uniform mode eigenvector, the matrix M can have another eigenvalue equal to one if the graph is disconnected, or if it has a translational symmetry (i.e. it forms a lattice).

7.6 Random hypergraphs

In this section we relax the conditions on the interaction graph and consider random hypergraphs where the degree of the vertices is no longer fixed. From the application of a random pruning as we discussed in section 7.2, the degrees now follow a Poisson distribution with average and variance equal to kq, and the saddle-point equations no longer admit a uniform solution (because equation (7.7) is no longer valid). In the strong coupling limit, however, the equations of motion still obey the same reparametrisation symmetry, so the solutions will have the same form but with different coefficients. In fact we can parametrise the solutions as

$$G_i(\tau) = \gamma_i \, b \frac{\mathrm{sgn}(\tau)}{|\tau|^{2\Delta}} \equiv \gamma_i G(\tau) \tag{7.28}$$

$$\Sigma_i(\tau) = \frac{J^2}{kq} \sum_{i_2,\ldots,i_q} x_{i,i_2,\ldots,i_q} \gamma_{i_2} \ldots \gamma_{i_q} G^{q-1}(\tau) \equiv \frac{\Sigma(\tau)}{\gamma_i} \ , \tag{7.29}$$

where the coefficients γ_i are positive constants that satisfy

$$\frac{1}{kq} \sum_{i_1,\ldots,i_q} x_{i_1,\ldots,i_q} \gamma_{i_1} \ldots \gamma_{i_q} = 1 \ . \tag{7.30}$$

They can be considered as a site-dependent normalisation which compensates for the fluctuations in the degree of the vertices. The quadratic action for the replica-diagonal fluctuations around the saddle point now becomes

$$\begin{aligned} \delta S_{eff,d} = & \frac{1}{4} \sum_i \gamma_i^2 \int d\tau_1 \ldots d\tau_4 \, \delta\tilde{\Sigma}_i(\tau_1,\tau_2) G_s(\tau_1,\tau_3) G_s(\tau_2,\tau_4) \delta\tilde{\Sigma}_i(\tau_3,\tau_4) \\ & + \frac{1}{2} \sum_i \int d\tau_1 d\tau_2 \left(\delta\tilde{\Sigma}_i(\tau_1,\tau_2) \delta\tilde{G}_i(\tau_1,\tau_2) \right) \\ & - \frac{J^2(q-1)}{4} \sum_{i,j} \int d\tau_1 d\tau_2 \left(M_{ij} G_s^{q-2}(\tau_1,\tau_2) \gamma_i^{-1} \gamma_j^{-1} \delta\tilde{G}_i(\tau_1,\tau_2) \delta\tilde{G}_j(\tau_1,\tau_2) \right) \end{aligned} \tag{7.31}$$

where the matrix M_{ij} is now defined by

$$M_{ij} = \frac{1}{kq(q-1)} \sum_{i_3 < \cdots < i_q} x_{iji_3\ldots i_q} \gamma_i \gamma_j \gamma_{i_2} \ldots \gamma_{i_q} \ . \tag{7.32}$$

We then rescale the fluctuations similarly to the usual way, $\delta\tilde{G}_i = \gamma_i |G_s|^{\frac{2-q}{q}} g_i$ and $\delta\tilde{\Sigma}_i = \gamma_i |G_s|^{\frac{q-2}{q}} \sigma_i$ and integrate over the σ_i, obtaining

$$\delta S_{eff,d} = \frac{J^2(q-1)}{4} \sum_{ij} g_i (\tilde{K}^{-1} - M_{ij}) g_j \tag{7.33}$$

so again one has to study the interplay between the spectrum of $\tilde{K}^{-1}$ and the matrix M. Thanks to the condition (7.30), this matrix still has an eigenvalue equal to one related to the uniform mode, and the other eigenvalues still have the same lower bound as before since one can write M as

$$M = \frac{1}{kq(q-1)} (A \Gamma A^T - kq \mathbb{I}) \tag{7.34}$$

where Γ is a diagonal matrix with elements $\Gamma_j = \gamma_{i_1} \ldots \gamma_{i_q}$, where $i_1, \ldots, i_q$ are the vertices connected by the hyperedge j. For the other eigenvalues, however, we no longer have an upper bound because of the unknown coefficients γ_i, but we can still expect them to resemble the results of regular graphs as the parameter kq becomes large (since the degrees follow the Poisson distribution), and the numerical results of [21] confirm this.

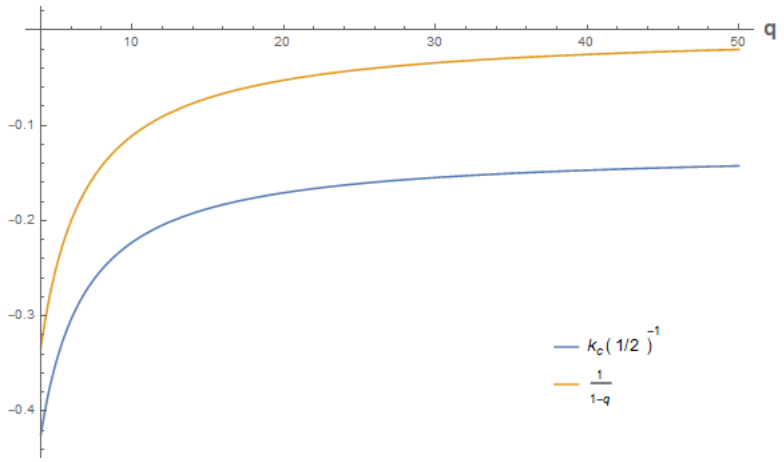

Figure 7.3: Comparison (as a function of q) between the maximum value of $k_c(h)^{-1}$ for the $h = \frac{1}{2} + is$ spectrum, and the lower bound for the eigenvalues λ of the adjacency matrix.

7.7 Comments on the spectra of K and M

In this section we discuss the statement that we made previously on the bounds of the eigenvalues of $\tilde{K}^{-1}$, starting from the discrete case. The equations to find the extrema $k_c'(h) = 0$ are not analytically solvable, however one can see from numerical computations (e.g. see figure 3.3) that the eigenvalues $k_c(h)$, for $h = 2, 4, 6, \ldots$, have a minimum maximum in $h = 2$ for the first few values of q. When q start to become large, we can approximate $k_c(h) \underset{q\gg 1}{\approx} \frac{2}{h(h-1)}$, which is clearly decreasing.

For the continuous spectrum, instead, we simply use the fact that the gamma function and its derivatives have zeroes and poles only on the real axis, therefore if there is an extremum it must be for $s = 0$ (as one can see from the plot), where we have

$$k_c\left(\frac{1}{2}\right) = \frac{\Gamma\left(\Delta + \frac{1}{4}\right)^2}{\Gamma\left(\Delta + \frac{5}{4}\right)^2} \frac{\Gamma(2-\Delta)\Gamma\left(\frac{1}{2} - \Delta\right)}{\Gamma(1+\Delta)\Gamma\left(\Delta - \frac{1}{2}\right)} \underset{q\gg 1}{\approx} -8 \tag{7.35}$$

and we can see (see figure 7.3) that its inverse is always inferior to the lower bound for the eigenvalues of the adjacency matrix.

Regarding the upper bound on the eigenvalues λ_l of the , instead, we have

$$\lambda_l \leq \frac{2\sqrt{kq-1}\sqrt{q-1} + q - 2}{kq(q-1)} \equiv f_u(k, q) \ . \tag{7.36}$$

This function is always decreasing in k for $k > 2/q$, so we have $\lambda_l \leq f_u(1, q)$, and it is simple to see that $f_u(1, q)$ is always decreasing in q for $q > 4$, so we obtain $\lambda_l \leq f_u(1, 4) = \frac{2}{3}$, so there is always a gap between λ_l and the eigenvalue $k_c(2) = 1$.

Chapter 8

Conclusions

8.1 Main properties

In this work we have discussed the basic properties of the Sachdev-Ye-Kitaev model, in particular the two- and four-point functions in the limit of strong coupling. Systems that are solvable in this limit are rare, but this model exhibits many other interesting properties, first of all the approximate conformal symmetry. We saw that in the limit of $\beta J \gg 1$ the equations of motion are invariant under time-reparametrisations, and that this symmetry is both spontaneously broken to the SL(2,R) subgroup by the saddle-point solutions and explicitly broken by the corrections in the parameter $1/(\beta J)$. In the study of the two-point function, we saw that, thanks to the large N limit and the disorder average, it is dominated by an infinite sum diagrams which contain any number of melonic insertions at any point. This recursive procedure leads to simple Schwinger-Dyson equations. This equations were derived also by employing a dynamic mean-field technique, which produced an effective action in two bilocal fields, whose saddle-point solutions correspond to the large N limit of the Green's function and the self-energy. In this effective action, in fact, the role of the Planck constant is replaced by the parameter 1/N. We also discussed the role of quenched disorder in the model, and how to compute quantities independently of the single realisations of the disorder. Thanks to the replica-trick, we were able to show that we could compute the free energy as in the annealed case, since the differences are subleading in the large N limit.

The four-point function, instead, was dominated by an infinite sum of ladder diagrams. This infinite sum correspond to a geometric series in the kernel K, which is the building block of this ladder. To perform this sum explicitly, we considered the kernel as an operator in the space of functions of two times, and we exploited the fact that in the conformal limit it is covariant under SL(2,R) transformations. Since it commutes with the Casimir operator, in fact, the eigenfunctions are the same, and we expressed the eigenvalues of the kernel as a function of the parameter h. The spectrum is divided into a discrete part, with $h = 2, 4, 6, \ldots$, and a continuum part, $h = \frac{1}{2} + is$. The $h = 2$ contribution, however, produces an eigenvalues $k_c(2) = 1$, which gives a divergence of the four-point function. One has to regularise this divergence by considering first order corrections in $1/(\beta J)$, which produces an enhanced contribution. The divergence is caused by the spontaneous symmetry breaking from the reparametrisation symmetry down to the SL(2,R) group, which produces an infinite number of Goldstone-modes. We then derived an explicit action for these reparametrisation modes, which contains the Schwarzian derivative of the reparametrisation function.

The $h = 2$ mode (and equivalently the Schwarzian action) are responsible for another interesting property of the model, perhaps the main one, which is the saturation of the chaos bound. Many-body systems can, at most, scramble information in an exponentially fast way, and the exponent (which is the quantum analogue of the Lyapunov exponent) can be at most equal to $\frac{2\pi}{\beta}$ (where β is the inverse of the temperature). We saw that the SYK model saturates this bound, which means that it belongs to the class of "fast scramblers": any perturbation of the systems gets spread across its large number

of degrees of freedom in the fastest possible way, and the main objects that belongs to this class are black holes.

This leads us to another point of view on the model, which is quantum holography. This conjecture states that any quantum field theory which exhibits conformal symmetry can has a one-to-one correspondence to a classical theory of general relativity in an anti-de Sitter spacetime with an additional spatial dimension (which represents the Renormalisation Group flow). Contrary to the context of string theory, however, the complete gravitational dual of the SYK model is unknown, although one can derive its correlation functions order-by-order. The interesting thing about this model is that it can be studied in a finite temperature setting, which translates in the presence of a black hole with the same temperature in the AdS space. This makes possible to study information scrambling and related phenomena through the holographic duality.

8.2 Generalisations

In this work we have presented some of the many generalisations of the SYK model, in particular the Gross-Rosenhaus version in which the Majorana fermions are can have multiple flavours, and the coloured SYK, which is a particular case. For these models, we have discussed the rules which determine the power of N related to general diagrams, in such a way that one can generate the diagrams for higher order correlations in the expansion in 1/N according to this criteria. We have seen that the power of N of each vacuum diagrams is determined by the number of cycles with multiple particle indices, and one can generate the diagrams of $2n$-point correlation functions by cutting n propagators in the vacuum diagrams of the corresponding order. There is also an equivalent criterion for the power counting of N, which is particularly well suited for the diagrammatic expansion of the bilocal effective action. Since the fields are bilocal, the Feynman diagrams are constructed with sheets and seams instead of lines and vertices, and the criterion consists in counting the genus of the 3-dimensional body created by considering a tubular neighbourhood of such diagrams.

We then discussed possible generalisations to the probability distribution of the couplings, which at the beginning was considered to be gaussian. As long as the first and second momenta stay the same, the model shows no differences in the limit of N going to infinity, and we showed this explicitly in for the case of a uniform distribution. We also considered the possibility of small correlations among different interaction terms, although in the case we considered the correlations were factorised, and the case in which they have a tensorial form remains to be studied.

Finally, we have discussed the sparse SYK model, which is a modification of the model which makes much easier the experimental realisation of this model with quantum computers. The idea behind this model is to drastically reduce the number of interaction terms in the hamiltonian, which becomes proportional to N instead of N^q, while maintaining its chaotic property of information-scrambling. This is possible by selecting a number of interaction terms which form an expander graph, that is a graph in which any subset of vertices (smaller than half the total system) has a number of neighbours proportional to itself. In particular, if the remaining interactions form a regular connected graph, we are guaranteed to have an expander graph. The dynamic of this model is not identical to the original model, since we saw that there are differences in the diagrammatic expansion. However, if the previously mentioned conditions are satisfied, the low temperature dynamics are dominated by the same uniform mode which is responsible for the chaotic behaviour of the original SYK model.

In conclusion, we have seen that the interesting properties of the SYK model are related to few of its characteristics: the high number of fermionic degrees of freedom, the disorder in the interaction, and the high-connectivity between its components. There are many aspects of the model that we did not analyse in detail, and other versions that we did not take into consideration, but we tried to give different points of view for the mechanisms behind its peculiar properties.

In future works, it would be interesting to study more accurately higher order corrections in the large N expansion, taking into account also the replica off-diagonal contributions. Furthermore, for finite

N one should expect a transition to a spin-glass phase at low temperatures, and there has been low interest in the study of this transition since most of the focus is towards the holographic duality features. Another thing which is not well understood is how different probability distributions of the disorder affect the model, (beyond the fact that symmetric distributions are equivalent to a gaussian in the large N limit). For example, we have not found any analysis (up to now) on how a nonzero average of the couplings would affect the model. Finally, there have been some discussions (see e.g. [17]) on how there could be unitarity problems for the model, since the "average of a quantum system is not really a quantum system", and this lead to the search of model which show the same characteristics of SYK but without quantum disorder (e.g. [16]).

Acknowledgements

I want to thank professor Luca Dell'Anna for introducing me to this fascinating topic and for the useful and interesting discussions. A huge thanks goes to my family and friends for the support during my years as a student.

Appendix A

Assumptions of the model

A.1 One dimensional Majorana fermions

To build a consistent and straightforward quantisation of our Majorana fermions, let's restrict ourselves to an even number N=2K. In this case one can define a set of K Dirac fermions as

$$c_i \equiv \frac{\chi_{2i} - i\chi_{2i+1}}{\sqrt{2}} \qquad c_i^\dagger \equiv \frac{\chi_{2i} + i\chi_{2i+1}}{\sqrt{2}}\,, \qquad i = 1, \dots, K \tag{A.1}$$

which satisfy the usual anticommutation relations $\left\{c_i, c_j^\dagger\right\} = \delta_{i,j}$ and $\{c_i, c_j\} = \left\{c_i^\dagger, c_j^\dagger\right\} = 0$. Then we define the free vacuum state as the state which is annihilated by all the c_i operators:

$$c_i \left|0\right\rangle \equiv 0 \quad \forall\, i = 1, \dots, K \tag{A.2}$$

Notice that this implies that the Hilbert space of the SYK model is made of $2^{N/2}$ states. Let's compute the finite temperature Green's function:

$$\begin{aligned} \left\langle T\left(\chi_i(\tau)\chi_j(0)\right)\right\rangle_\beta = \frac{\operatorname{tr}\left[e^{-\beta H_0} T\left(\chi_i(\tau)\chi_j(0)\right)\right]}{\operatorname{tr}\left[e^{-\beta H_0}\right]} = \frac{\operatorname{tr}\left[T\left(\chi_i(\tau)\chi_j(0)\right)\right]}{\operatorname{tr}\left[1\right]} = \\ = \theta(\tau)\frac{\operatorname{tr}\left[\chi_i\chi_j\right]}{\operatorname{tr}\left[1\right]} - \theta(-\tau)\frac{\operatorname{tr}\left[\chi_j\chi_i\right]}{\operatorname{tr}\left[1\right]} \end{aligned} \tag{A.3}$$

We compute separately the traces for i, j equal or different, but keeping $|i-j| \leq 1$, otherwise the trace would contain different annihilation operators which anticommute:

$$\operatorname{tr}\left[\chi_{2l}\chi_{2l}\right] = \operatorname{tr}\left[\chi_{2l+1}\chi_{2l+1}\right] = \frac{1}{2}\operatorname{tr}\left[c_l c_l^\dagger + c_l^\dagger c_l\right] = \frac{1}{2}2^{K-1}\left(\left\langle 0\right| c_l c_l^\dagger + c_l^\dagger c_l \left|0\right\rangle + \left\langle l\right| c_l c_l^\dagger + c_l^\dagger c_l \left|l\right\rangle\right) = 2^{K-1} \tag{A.4}$$

$$\operatorname{tr}\left[\chi_{2l}\chi_{2l+1}\right] = -\operatorname{tr}\left[\chi_{2l+1}\chi_{2l}\right] = \frac{i}{2}\operatorname{tr}\left[c_l^\dagger c_l - c_l c_l^\dagger\right] = \frac{1}{2}2^{K-1}\left(\left\langle 0\right| c_l^\dagger c_l - c_l c_l^\dagger \left|0\right\rangle + \left\langle l\right| c_l^\dagger c_l - c_l c_l^\dagger \left|l\right\rangle\right) = 0 \tag{A.5}$$

Putting all together we obtain

$$\left\langle T\left(\chi_i(\tau)\chi_j(0)\right)\right\rangle_\beta = \frac{1}{2}\mathrm{sgn}(\tau)\delta_{ij} \tag{A.6}$$

Using this definition of the χ_i, also the path integral formulation becomes consistent, as the measure is given by

$$D\chi_{2i}\, D\chi_{2i+1} = Dc_i\, D\overline{c_i} \tag{A.7}$$

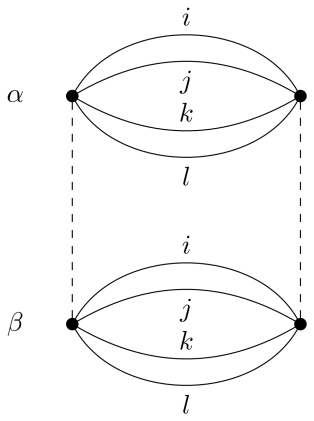

Figure A.1: Example of non-diagonal contribution to the free energy. The fermion lines in the upper part belong to the replica α while the ones in the lower part belong to the replica β.

A.2 Non-diagonal contributions

The use of the replica-diagonal ansatz (1.20) is equivalent to considering $\log \overline{\mathcal{Z}}$, which given by the sum of all connected diagrams (they can be connected also through disorder-average lines), while $\overline{\log \mathcal{Z}}$ is given, instead, by the sum of diagrams connected along fermionic lines. For example, $\log \overline{\mathcal{Z}}$, contains also contributions as the diagram in figure A.1, but as we can see it contains two disorder-averages and four fermion indices, so it is proportional to N^{-2}, while we free energy, at leading order in N, is proportional to N. This agrees with the argument that we made at the end of section 1.1.

Through this work, additionally, we have assumed the solutions to be replica-symmetric. This is justified since the Sachdev-Ye model (which is formally similar to the SYK model) does not exhibit any spin-glass behaviour for temperatures above $T_{glass} \sim Je^{-\sqrt{N}}$ [3][17], so we it is safe to neglect any replica symmetry breaking since we worked in the limit of N large. It was argued in [2] that it is the fermionic nature of the degrees of freedom that is responsible for this.

Appendix B

The Casimir eigenvalue equation

In this section we want to check the statement that

$$C_{1+2}\,\frac{1}{|\tau_{12}|^{2\Delta}}f(\chi)=\frac{1}{|\tau_{12}|^{2\Delta}}\mathcal{C}f(\chi) \tag{B.1}$$

$$\mathcal{C}\equiv\chi^2(1-\chi)\partial_\chi^2-\chi^2\partial_\chi \qquad \chi\equiv\frac{\tau_{12}\,\tau_{34}}{\tau_{13}\,\tau_{24}} \tag{B.2}$$

Using the explicit definitions

$$\hat{P}=\partial_\tau\,,\quad \hat{D}=-\tau\partial_\tau-\Delta\,,\quad \hat{K}=-\tau^2\partial_\tau+2\Delta\tau \tag{B.3}$$

from which $\hat{D}^2=\hat{K}\hat{P}-\hat{D}+\Delta^2-\Delta$, we have that

$$\begin{aligned}\hat{C}_{1+2}&=(\hat{D}_1+\hat{D}_2)^2-\frac{1}{2}(\hat{K}_1+\hat{K}_2)(\hat{P}_1+\hat{P}_2)-\frac{1}{2}(\hat{P}_1+\hat{P}_2)(\hat{K}_1+\hat{K}_2)\\&=2(\Delta^2-\Delta)-\hat{K}_1\hat{P}_2-\hat{P}_1\hat{K}_2+2\hat{D}_1\hat{D}_2\end{aligned} \tag{B.4}$$

We find that

$$\begin{aligned}\hat{C}_{1+2}&=2(\Delta^2-\Delta)+2(\tau_1\partial_1+\Delta)(\tau_2\partial_2+\Delta)-(\tau_1^2\partial_1+2\tau_1\Delta)\partial_2-\partial_1(\tau_2^2\partial_2+2\tau_2\Delta)\\&=-\tau_{12}^2\partial_1\partial_1+2\Delta\tau_{12}(\partial_1-\partial_2)+4\Delta^2-2\Delta\end{aligned} \tag{B.5}$$

Now, for the partial derivatives, we have that (assuming $\tau_1>\tau_2$ since the other case is analogous)

$$\begin{aligned}\partial_1\left(\frac{f(\chi)}{\tau_{12}^{2\Delta}}\right)&=\frac{1}{\tau_{12}^{2\Delta}}\left(\partial_1-\frac{2\Delta}{\tau_{12}}\right)f(\chi)\\\partial_2\left(\frac{f(\chi)}{\tau_{12}^{2\Delta}}\right)&=\frac{1}{\tau_{12}^{2\Delta}}\left(\partial_2+\frac{2\Delta}{\tau_{12}}\right)f(\chi)\\\partial_1\partial_2\left(\frac{f(\chi)}{\tau_{12}^{2\Delta}}\right)&=\frac{1}{\tau_{12}^{2\Delta}}\left(\partial_1\partial_2+\frac{2\Delta}{\tau_{12}}(\partial_1-\partial_2)-\frac{2\Delta(2\Delta+1)}{\tau_{12}^2}\right)f(\chi)\end{aligned} \tag{B.6}$$

Using this together with (B.5) in (B.1) we find that

$$C_{1+2}\,\frac{1}{\tau_{12}^{2\Delta}}f(\chi)=\frac{1}{\tau_{12}^{2\Delta}}(-\tau_{12}^2\partial_1\partial_2)f(\chi) \tag{B.7}$$

Furthermore,

$$\begin{aligned}\partial_1\partial_2 f(\chi)&=\partial_1\left(\frac{\partial\chi}{\partial\tau_2}\partial_\chi f\right)=-\partial_1\left(\frac{\tau_{14}\,\tau_{34}}{\tau_{13}\,\tau_{24}^2}\,\partial_\chi f\right)\\&=\frac{\chi^2}{\tau_{12}^2}-\left(\frac{\tau_{14}\,\tau_{34}}{\tau_{13}\,\tau_{24}^2}\right)\frac{\partial\chi}{\partial\tau_2}\partial_\chi^2 f=\frac{\chi^2}{\tau_{12}^2}\partial_\chi f-\frac{\chi^2(1-\chi)}{\tau_{12}^2}\partial_\chi^2 f\end{aligned} \tag{B.8}$$

where we used the fact that $\frac{\tau_{14}\,\tau_{23}}{\tau_{13}\,\tau_{24}}=1-\chi$, and so equation (B.1) is verified.

Appendix C

Graph theory notions

In this appendix we recall some simple notions of graph theory that were mainly used in chapter 7:

- A *graph* is a collection of N vertices (also called sites) which are connected in pairs by a number of edges (also called) links. Two vertices are *adjacent* if they are linked by one or more edges. A *simple* graph is a graph where there is at most one edge that connects two vertices, while *multigraphs* can have more than one edge connecting two vertices, and can also contain *loops*, which are edges that connect a vertex to itself.
- A *hypergraph* is a graph where a single edge (also called *hyperedge*) connects more than two vertices. One can, however, consider the corresponding *interaction graph*, i.e. the a graph with the same number of vertices and a simple edge between two vertices if and only if they are linked in the original hypergraph. In general, different hyperedges in the same hypergraph can connect different number of vertices; if they always connect the same number of vertices q, the hypergraph is said to be *q-uniform*. Since we consider only this kind of hypergraphs, we omit this term.
- The *degree* of a vertex is the number of edges attached to that vertex. The degree of a graph is the maximum degree among its vertices. A graph is called *d-regular* if all of its vertices have the same degree d.
- A *complete* graph is a graph where each vertex is connected to every other vertex.
- The *diameter* of a graph is the maximum distance (the minimum number of edges for a path to connect two vertices) between two vertices.
- The *adjacency matrix* A is a $N \times N$ symmetric matrix (where N is the number of vertices) whose matrix elements A_{ij} are equal to the number of edges connecting the vertices i and j. For simple graphs, then, the diagonal elements are zero, and the off-diagonal can be either zero or one.
- The *degree matrix* D is a diagonal matrix whose diagonal elements are equal to the degree of each vertex.
- The *laplacian matrix* is the matrix $L = D - A$. It is simple to prove that this matrix has at least an eigenvalue $\lambda_1 = 0$ by taking a vector whose elements are all equal. This is also the minimum amongst all the eigenvalues of L If the graph is regular, the degree matrix D is proportional to the identity, thus A has a maximum eigenvalue equal to the degree of the graph.
- The *incidence* matrix B is an $m \times n$ matrix (where m is the number of vertices and n the number of edges) whose matrix elements are

$$B_{ij} = \begin{cases} 1 & \text{if the j-th edge contains the vertex i} \\ 0 & \text{otherwise} \end{cases} \tag{C.1}$$

Bibliography

[1] Paul Ginsparg. "Applied Conformal Field Theory". In: (1991). DOI: 10.48550/ARXIV.HEP-TH/9108028. URL: https://arxiv.org/abs/hep-th/9108028.

[2] Subir Sachdev and Jinwu Ye. "Gapless spin-fluid ground state in a random quantum Heisenberg magnet". In: *Phys. Rev. Lett.* 70 (21 May 1993), pp. 3339–3342. DOI: 10.1103/PhysRevLett.70.3339.

[3] A. Georges, O. Parcollet, and S. Sachdev. "Quantum fluctuations of a nearly critical Heisenberg spin glass". In: *Phys. Rev. B* 63 (13 Mar. 2001), p. 134406. DOI: 10.1103/PhysRevB.63.134406.

[4] Yasuhiro Sekino and L. Susskind. "Fast scramblers". In: *Journal of High Energy Physics* 2008.10 (Oct. 2008), p. 065. DOI: 10.1088/1126-6708/2008/10/065.

[5] Kitaev, Alexei. *A simple model of quantum holography.* http://online.kitp.ucsb.edu/online/entangled15/kitaev/ and http://online.kitp.ucsb.edu/online/entangled15/kitaev2/. Apr. 2015.

[6] Kitaev, Alexei. *Hidden correlations in the Hawking radiation and thermal noise.* https://online.kitp.ucsb.edu/online/joint98/kitaev/. Feb. 2015.

[7] Jan Zaanen et al. *Holographic Duality in Condensed Matter Physics.* Cambridge University Press, 2015. DOI: 10.1017/CBO9781139942492.

[8] Juan Maldacena, Stephen H. Shenker, and Douglas Stanford. "A bound on chaos". In: *Journal of High Energy Physics* 2016.8 (Aug. 2016), p. 106. ISSN: 1029-8479. DOI: 10.1007/JHEP08(2016)106.

[9] Juan Maldacena and Douglas Stanford. "Remarks on the Sachdev-Ye-Kitaev model". In: *Phys. Rev. D* 94 (10 Nov. 2016), p. 106002. DOI: 10.1103/PhysRevD.94.106002.

[10] Ben Michel et al. "Four-point function in the IOP matrix model". In: *Journal of High Energy Physics* 2016.5 (May 2016), p. 48. ISSN: 1029-8479. DOI: 10.1007/JHEP05(2016)048.

[11] Joseph Polchinski and Vladimir Rosenhaus. "The spectrum in the Sachdev-Ye-Kitaev model". In: *Journal of High Energy Physics* 2016.4 (Apr. 2016), p. 1. ISSN: 1029-8479. DOI: 10.1007/JHEP04(2016)001.

[12] Valentin Bonzom, Luca Lionni, and Adrian Tanasa. "Diagrammatics of a colored SYK model and of an SYK-like tensor model, leading and next-to-leading orders". In: *Journal of Mathematical Physics* 58.5 (2017), p. 052301. DOI: 10.1063/1.4983562. eprint: https://doi.org/10.1063/1.4983562.

[13] David J. Gross and Vladimir Rosenhaus. "A generalization of Sachdev-Ye-Kitaev". In: *Journal of High Energy Physics* 2017.2 (Feb. 2017), p. 93. ISSN: 1029-8479. DOI: 10.1007/JHEP02(2017)093.

[14] David J. Gross and Vladimir Rosenhaus. "All point correlation functions in SYK". In: *Journal of High Energy Physics* 2017.12 (Dec. 2017), p. 148. ISSN: 1029-8479. DOI: 10.1007/JHEP12(2017)148.

[15] David J. Gross and Vladimir Rosenhaus. "The bulk dual of SYK: cubic couplings". In: *Journal of High Energy Physics* 2017.5 (May 2017), p. 92. ISSN: 1029-8479. DOI: 10.1007/JHEP05(2017)092.

[16] Razvan Gurau. "The complete 1/N expansion of a SYK–like tensor model". In: *Nuclear Physics B* 916 (2017), pp. 386–401. ISSN: 0550-3213. DOI: https://doi.org/10.1016/j.nuclphysb.2017.01.015.

[17] Alexei Kitaev and S. Josephine Suh. "The soft mode in the Sachdev-Ye-Kitaev model and its gravity dual". In: *Journal of High Energy Physics* 2018.5 (May 2018), p. 183. ISSN: 1029-8479. DOI: 10.1007/JHEP05(2018)183.

[18] Stéphane Dartois, Harold Erbin, and Swapnamay Mondal. "Conformality of $1/N$ corrections in Sachdev-Ye-Kitaev-like models". In: *Phys. Rev. D* 100 (12 Dec. 2019), p. 125005. DOI: 10.1103/PhysRevD.100.125005.

[19] T. Krajewski et al. "Non-Gaussian disorder average in the Sachdev-Ye-Kitaev model". In: *Phys. Rev. D* 99 (12 June 2019), p. 126014. DOI: 10.1103/PhysRevD.99.126014.

[20] Vladimir Rosenhaus. "An introduction to the SYK model". In: *Journal of Physics A: Mathematical and Theoretical* 52.32 (July 2019), p. 323001. DOI: 10.1088/1751-8121/ab2ce1.

[21] Shenglong Xu et al. *A Sparse Model of Quantum Holography*. 2020. DOI: 10.48550/ARXIV.2008.02303.

[22] Daniel Jafferis et al. "Traversable wormhole dynamics on a quantum processor". In: *Nature* 612.7938 (Dec. 2022), pp. 51–55. ISSN: 1476-4687. DOI: 10.1038/s41586-022-05424-3.

[23] *NIST Digital Library of Mathematical Functions*. http://dlmf.nist.gov/, Release 1.1.8 of 2022-12-15. F. W. J. Olver, A. B. Olde Daalhuis, D. W. Lozier, B. I. Schneider, R. F. Boisvert, C. W. Clark, B. R. Miller, B. V. Saunders, H. S. Cohl, and M. A. McClain, eds. URL: http://dlmf.nist.gov/.